The University of Manitoba

FILTERING AND RADIATION CHARACTERISTICS OF ANNULAR SLOT ARRAY STRUCTURES

By

BAHMAN AZARBAR

A Thesis
Submitted To The Faculty Of Graduate Studies
In Partial Fulfillment Of The Requirements For The
Degree Of Doctor Of Philosophy

DEPARTMENT OF ELECTRICAL ENGINEERING

Winnipeg, Manitoba
Canada

October 1978

FILTERING AND RADIATION CHARACTERISTICS OF ANNULAR SLOT ARRAY STRUCTURES

BY

BAHMAN AZARBAR

A dissertation submitted to the Faculty of Graduate Studies of the University of Manitoba in partial fulfillment of the requirements of the degree of

DOCTOR OF PHILOSOPHY

To the memory of

MONEER NAGHAVI KAMAL

for all her love and devotion

ABSTRACT

A method is established which gives field solutions inside two radial waveguides coupled by an array of annular slots on the common boundary. The cases of electromagnetic penetration into half space as well as cylindrical cavity regions are also treated. For the half space problem, the thickness of one of the waveguide regions is allowed to approach infinity. Whereas, for the cylindrical cavity case, the radial waveguide is terminated at an appropriate place by a cylindrical short circuit. Since the analysis is based on the response of the system to azimuthal current rings, the appropriate Green's functions for electric current rings are obtained in a similar manner as those of magnetic type. Therefore, the method can be extended to the geometries involving annular or cylindrical type conducting bodies as well as aperture-type geometrical discontinuities.

The solution is obtained by constructing the impulse response of the system and expressing the induced current distribution over the slots and the conducting bodies in terms of a suitable set of basis functions with complex coefficients. These constants are then obtained by an application of the boundary conditions on the discontinuity surfaces. The method is applied to three different geometries, namely, two radial waveguides coupled by an array of annular slots on the common boundary, an annular slot array antenna fed by a radial waveguide and the cavity backed annular slot antenna. Graphical results for selected cases are presented to substantiate the applicability of the models in the design of microwave filtering devices as well as highly directive antenna systems.

It is also shown that, in general, higher order modes excited by the discontinuities can have significant effect on the solution and for a precise evaluation of the fields in the respective regions, their contribution must also be included. A method of generating the desired incident mode or modes is suggested which uses simple vertically oriented arrays of thin probes.

ACKNOWLEDGEMENTS

The author wishes to express his sincere appreciation to Dr. L. Shafai of the Electrical Engineering Department, University of Manitoba, for his guidance, constant encouragement and constructive criticism, throughout all phases of this work.

The valuable review of the entire manuscript by my wife, Mrs. Elaheh Kamal Azarbar, led to a number of clarifications and other improvements. Her understanding and forebearance throughout the years made this work possible. To Ms. M. Tyler, the author expresses his special gratitude for her cheerful and patient efforts in an excellent typing job and editorial assistance throughout the several drafts of this dissertation.

It is a pleasure to thank Professor E. Bridges for his many helpful suggestions. The author is also indebted to Mr. A. McKay, Electronics Technologist and Mr. A. Symmons, Machining Technologist of the Electrical Engineering Department who have made various contributions in the fabrication process of the antenna model. Drafting facilities provided by Mr. H.H. Weiss of the Central Drafting Office and secretarial assistance by Mrs. L. Ramsay is appreciated.

Thanks are also due to my colleagues, Mr. H. Kunkel for his help in the early stages of the research project and Mr. A. Ittipiboon and Mr. M. Jullian for their assistance in the experimental phase of this work.

The financial support by the National Research Council of Canada in the form of Post-graduate Scholarship and the Operating Grant A7702 and also through the University of Manitoba in the form of University Fellowship is appreciated.

TABLE OF CONTENTS

LIST OF FIGURES

LIST OF SYMBOLS

Unless otherwise stated, the symbols most commonly used in this thesis have the following meaning:

GREEK ALPHABET:

ε	Dielectric constant of a medium.
ε_o	Dielectric constant of free space.
μ_o	Permeability of free space.
(ρ, ϕ, z) , (ρ', ϕ', z')	Cylindrical coordinate variables, prime denotes source coordinates.
(r, ϕ, θ)	Spherical coordinate variables.
ρ_i	Average radius of the ith slot.
η_o	Intrinsic wave impedance of free space.
τ	Ratio of the radii of the edges of an annular slot.
λ	Intrinsic wavelength of a region.
λ_o	Free space wavelength.
(ρ_s, ϕ_s)	Coordinates of the feeding probe.
ε_r	Relative dielectric constant of a medium with respect to free space.
δ_m	Width of the mth slot.
$\hat{\rho}, \hat{\phi}, \hat{\theta}$	Unit coordinate vectors of the respective variables.
ε_n	Neumann constant.
ω	Angular frequency.
ψ^e, ψ^h	Green's functions or wave functions of TM and TE types, respectively.
Φ_n^e, Φ_n^h	Angular dependent part of the nth mode functions of TM and TE types, respectively.

GREEK ALPHABET:

ψ_a^e, ψ_a^h	Auxiliary Green's functions of TM and TE types, respectively.
$\delta(\cdot)$	Delta function.
$\psi_{pq}^{e\ inc}$	Incident pq mode of TM type.
$\overset{+}{\rho}_m$, $\overset{-}{\rho}_m$	Radii of the outer and the inner edges of the mth annular slot.
$\bar{\psi}^e$, $\bar{\psi}^h$	Hankel transforms of ψ^e and ψ^h, respectively.
γ	Complex propagation constant in the z direction for the spacial frequency domain.
α	Complex variable of the spacial frequency domain.

LATIN ALPHABET:

a, b	Height of radial waveguides.
a_n, b_n	Fourier coefficients in the expansions of the angular dependent part of the current rings and the aperture fields.
c	Radius of a cylindrical cavity.
$C_n^{J,H,N}(\alpha\rho')$	Integrals of the respective Bessel functions with respect to ρ'.
dB, db	Decibel.
E_{in}	Electric field strength of the nth mode over the ith cell.
E_a, H_a, J_a	Auxiliary fields and their source.
$H_n^{(2)}(\cdot)$, $H_n^{(2)\prime}(\cdot)$	Second kind Hankel function of order n and its derivative.
$\|H\|_n(\cdot)$	Struve function of order n.
I^e, I^h	Infinite integrals associated with half-space Green's functions of TM and TE types, respectively.
$I_m(\cdot)$	Imaginary part of a complex number.

LATIN ALPHABET:

$J_n(\cdot)$, $J_n'(\cdot)$	Bessel function of order n and its derivative.
J, J_m	Electric and magnetic current densities, respectively.
$k_{\rho m}$	Radial propagation constant of the mth mode.
k	Wave number of a region.
k_o	Free space wave number.
$\ell_n(\cdot)$	Natural logarithm.
$P_i(\rho' - \rho'_i)$	Unit pulse function of the ith cell.
$R_n(\rho')$	Radial dependent part of the aperture electric field of the nth mode.
$Re(\cdot)$	Real part of a complex number.
S_1, S_2	Arbitrary cylindrical surfaces in regions I and II, respectively.
S'	Source plane.
TEM	Transverse electromagnetic field to z axis.
TE(h)	Transverse electric to z (h waves).
TM(e)	Transverse magnetic to z (e waves).
TM_{mn}	Transverse magnetic field of the (mn)th mode.
U^e_{mn}, V^e_{mn}, U^h_{mn}	Coefficients of the (mn)th mode of radial waveguide and cavity Green's functions of TM and TE types, respectively for $\rho > \rho'$
u^e_{mn}, u^h_{mn}	Coefficients of the (mn)th mode of radial waveguide and cavity Green's functions of TM and TE types, respectively for $\rho < \rho'$
$U^e_n(\cdot)$, $U^h_n(\cdot)$	Coefficients of the nth mode of the half-space Green's functions of TM and TE types, respectively.

CHAPTER I

INTRODUCTION

Telecommunication technology has reached the state of maturity which allows reliable contact between terrestrial points to be estabilished within seconds. As a prime contributor to this achievement, communication satellites have been used for a large number of diverse services. The early recognition of their potential use in world-wide communication prompted a rapid growth of international and military satellite communication systems, an industry which is barely ten years old.

One of the significant elements underlying this growth was the prospect of achieving band-widths exceeding those previously available for intercontinental communications. The exploitation of the wide band-widths now easily available in the use of satellites and the ever increasing demand for higher frequencies requires solution to a series of technical problems in the communication links. As an inherent part of these links, earth station and spacecraft antennas must also conform to the specific needs as they arise. This is why satellite antennas have developed from low-gain, omnidirectional antennas to multifrequency multi-function antenna systems now in use [1,2].

Still higher frequencies are under active consideration, not only because of spectrum crowding at the lower frequency bands, but because of the desire to accommodate higher data rates than are now being sent commercially. So far, there have been a number of different design approaches conforming to satellite stabilization considerations which have been tested for their performance in actual missions [1-9].

Generally speaking, the optimum goal in designing any satellite antenna is to attain a pre-specified high gain radiation pattern by using a low profile antenna with the least complex feed system, with low weight and volume occupied by the antenna assembly, ease of fabrication and, most important of all, lower manufacturing cost factor. The last two goals are becoming more important as the frequency spectrum is broadened constantly and satellite communication is exploited commercially.

The purpose of the present work is to study a new class of low profile radiating element for use in high frequency telecommunication systems. The structure may be used as the basic block in formation of high frequency filtering devices as well as low profile antenna systems for applications in aircrafts, spacecrafts and low cost earth stations. Due to the structural simplicity of the radiating element it looks quite promising for use at high frequencies and the production cost seems to be much lower than conventional types presently in use.

The basic element is essentially a slotted radial waveguide. It is formed by an array of co-centered electrically narrow annular slots etched on one side of a dielectric substrate which is sandwiched by two ground planes, figure 1. For applications as an antenna, depending on the excitation of the slots, the structure is capable of producing radiation patterns with the main lobe in the direction of the z-axis (end fire) or a doughnut type radiation field with a null in that direction (broad-side). Terminology is borrowed from conventional arrays by viewing the antenna as a compressed version of a stack of circular loop radiators.

An important consideration for antenna systems covering large angular regions lies in their polarization state over the coverage zone.

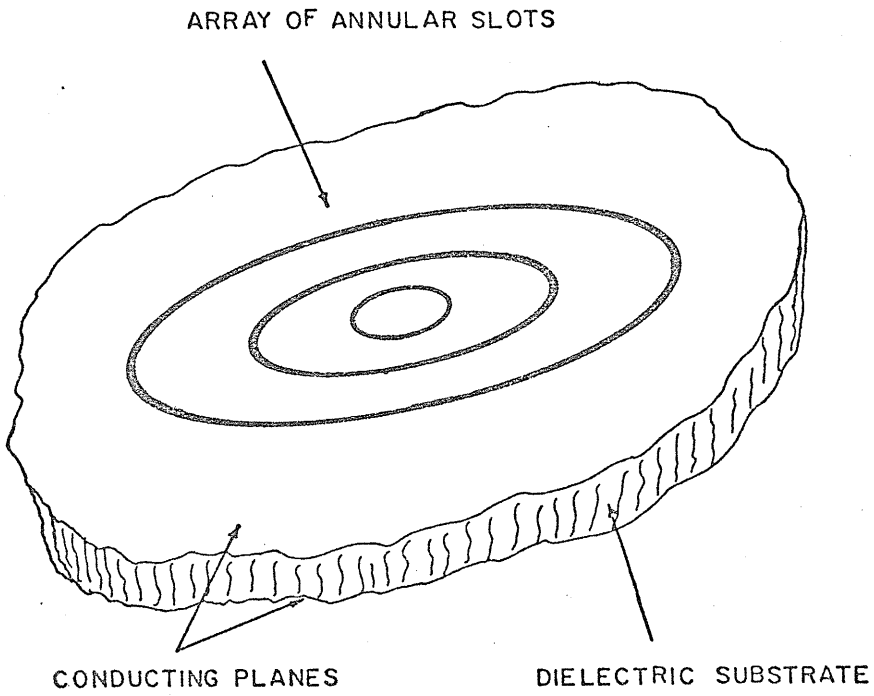

Figure 1.1: Basic radiating element.

For certain applications, namely, frequency reuse communication links, this parameter is of prime importance. The isolation degree between the orthogonal channels must stay below a certain level over the coverage zone in order to minimize interference problems. The polarization state of an annular slot antenna is basically determined by the exciting feed assembly located in the central region of the waveguide or cavity. A combination of vertical probes, which are merely the extended center conductors of a set of coaxial cables in different configurations, may be used for producing the required excitation mode or modes and the desired type of polarization within a certain angular region. However, as it will be shown later for single mode excitation the cross polarization component of this type of antenna may not meet the specific requirements for certain applications. For these cases multimode operation may prove successful.

The simplicity of the structure is promising for high the frequency range where small details of the element become an appreciable fraction of the wavelength and consequently any imperfection in the fabrication results in distortion of the electrical characteristics of the structure. In this regard, the designed pattern of annular slots can be tailored on a grounded dielectric substrate to a high degree of accuracy by microwave integrated circuit fabrication techniques. Furthermore, the low profile of the system makes it suitable for use as a printed-circuit stripline filtering device or as a flush-mounted antenna on high speed space vehicles. This will ensure meeting the requirements of re-entry vehicles, such as least disturbance to the flight dynamics and to the air frame structure. For satellite communications, depending on the method of stabilization, the annular slot antenna may be used in different modes of operation [10], that is, either as a despun antenna system or a high gain

directive radiator for use in body stabilized satellites. Since the antenna assembly is integrated onto satellite, it is less susceptible to accidental damage in the launch process. Furthermore, due to the fact that the slots are fed successively by a radial waveguide or a cylindrical cavity, one feed connection suffices. Therefore, space that is critically needed for other purposes is saved.

For applications such as filtering devices and couplers, two or more coupled radial waveguides may be used. The coupling is achieved by arrays of annular slots on the common boundary of the waveguides. By a proper arrangement of the apertures, the power injected by the source in a guiding region can be coupled out efficiently over a desired frequency band. The result is a band-pass, band-stop filtering characteristic which is controlled by the electrical dimensions of the structure and the constitutive parameters of the guiding regions. In the next chapter, in addition to a literature survey on the subject matter, an outline of the work to follow is given.

CHAPTER II

STATEMENT OF THE PROBLEM AND LITERATURE SURVEY

2.1 Introduction

From the design objectives stated in Chapter I, it is clear that the main concern is to find a solution to the problem of electromagnetic coupling between two radial waveguides through annular slots on the common boundary. The problem of the annular slot array antenna can be viewed as a special case in which the thickness of one guide approaches infinity.

Seeking an exact analytical solution to electromagnetic boundary value problems involving exterior and interior regions to boundaries of a discontinuous nature is a formidable task. Exact analytical techniques available are generally restricted to a small group of objects with simple geometrical shapes. The subject of electromagnetic penetration of a time harmonic plane incident wave through an aperture in an infinite plane, which is the simplest problem in this category, has been investigated extensively in the literature. Nevertheless, the problem remains a rather complicated subject with available analytical results for only a few aperture geometries. For this reason, attempts have been made to develop approximate techniques which could provide useful solutions to a variety of problems, subject to certain limiting conditions. A fairly extensive literature review of aperture theory can be found in a recent publication [11] with an emphasis on techniques.

The problem of electromagnetic diffraction by circular apertures has long been the focus of attention, primarily due to its amenability to analytical approaches. As is well known, the rigorous analytical approach

aims at a solution to a set of vector differential equations subject to some constraints. However, this approach has rarely proven to be fruitful. The Kirchoff approximation [12] is an attempt to gain some qualitative insight into the diffraction phenomenon. This approach was refined later by including charge distributions on the rim of the screen [13].

In contrast to Kirchoff's method which yields reasonable results at high frequencies, the Rayleigh approximation [14]-[16] is valid for low frequency operations for which the aperture field distribution can be obtained by treating the problem as a static case. A more refined and rigorous method was reported later by inclusion of an edge condition which is valid over a broader frequency range [17]-[18], yet the convergence of the solution in terms of spheroidal functions creates computational difficulties at high frequencies.

A more general approach for the formulation of the diffraction problem of an incident wave by an aperture in a perfectly conducting screen is found in [19]-[20]. Expressions for the field vectors in both regions are derived in terms of the tangential components of either electric or magnetic field on the common boundary using tensor (dyadic) Green's functions. The final formulation is then modified to obtain stationary formulas suitable for applying variational principles. As an example, the problem of scattering by an open-ended coaxial waveguide in an infinite conducting baffle is considered and only the principle mode of operation is treated (no azimuthal variation). However, the method like other variational formulations is dependent on trial functions.

An alternative approach to the solution of diffraction by a circular hole or slit and the complementary problem (disc or ribbon) is to utilize hypergeometric polynomials as the expansion functions [21]-[22].

However, the convergence of the infinite series obtained is slow for structures with large characteristic dimensions. Diffraction by small circular apertures has also been studied extensively. Among approximate techniques, the use of an integral equation approach suitable for numerical solutions are recently reported [23],[24]. For large aperture dimensions, the techniques based on the geometrical theory of diffraction [25] have successfully been applied to numerous geometries. Attempts to overcome the shortcomings of the theory related to the shadow boundaries and caustics are made and the results are presented in [26],[27].

The problem of an annular slot on an infinite ground plane backed by a cavity has also been studied by a number of authors. Examples are the study of radiation conductance of an annular slot backed by a hemispherical cavity of finite conductivity for applications at low frequencies [28] and the case of cylindrical cavity [29] which employs variational methods. The limiting assumptions are a highly idealized excitation by a uniform (no ϕ variations) radially directed current sheet in the slot plane and the solution breaks down for deep cavities.

As a possible flush-mounted antenna for use on the skin of missiles, the problem of a coaxial opening in a ground plane has been considered in the literature and typical examples to be cited here are [30]-[33]. In the first two, the principle of duality is employed to obtain the electromagnetic field components for the case of azimuthal symmetry. The basic assumption is to take the unperturbed coaxial TEM mode as the only existing mode which implies ignoring higher order modes created in the vicinity of the annular aperture. In the third reference, the slot field distribution is expressed in terms of TEM and the first five TM_{on} modes. The last work, however, accounts for the higher order modes for an

electrically thin slot.

Design procedure and performance of the annular planar array of linear slots in generating pencil beams and monopulse tracking rays is reported for a geometry consisting of a radial waveguide coupled to free space through groups of small linear slots [34]. The theory of linear arrays is employed and the slot field distribution is assumed to be the dominant TE mode of the unperturbed guide. The coupling between the slots is totally disregarded.

Among the earliest works in the area of radial waveguide fed antennas for possible use in communication satellites, are those presented in [36],[37]. The first reference is an extension to an earlier work [35], with the purpose of a qualitative analysis of the problem. The approach, however, is mostly experimental and a TEM excitation is assumed. The use of circular slots and rings as resonant structures in microstrip transmission lines has also been reported [38]-[40]. A rather qualitative approach is employed and the effects of the fringe field at the edge of the resonant element and the radiation from the rim are ignored.

For circular apertures in finite ground planes of circular and rectangular shapes, a method has been suggested which utilizes the geometrical theory of diffraction [38]. The expression for the field pattern is obtained by superposition of infinite ground plane solution, the first-order diffracted field solution and the axial caustic terms in their respective regions of validity. Again the slot field is assumed to be the unperturbed field of a TEM excited coaxial waveguide, hence, the fields are independent of the azimuth angle ϕ. Experimental results are also obtained and are compared against those computed. It is shown that over a wide angular region in the front direction, the result obtained assuming

an infinite ground plane closely matches the actual field, provided the slots are far from the rim. The difference between the experimental and computed results are attributed to higher order modes created by the slot discontinuity. However, the back scattered field, which the infinite plane solution fails to account for, can be computed with reasonable accuracy by this method.

2.2 Outline of the Subject under Investigation

The preceding literature review points out that in spite of numerous research works done in the area of electromagnetic coupling through annular apertures, the subject matter remains to be a challenging one. Most of the existing approaches to the problem are based on overly simplified and idealized models. Majority of the methods lie on the assumption that the aperture field distribution can be approximated by the unperturbed field of the feeding guide. In other words, the effect of all higher order modes that are excited in the vicinity of slot discontinuities and is proven to be significant [32] is disregarded. Furthermore, only the special cases of azimuthal symmetry (no ϕ variation) are considered in order to further simplify the formulation of the problem. One important consideration lies in the fact that an efficient radiator is generally formed by more than a single slot. That is, the number of slots and their relative locations are expected to be the key parameters for pattern shaping or optimization of the electrical characteristics. Therefore, any solution to the problem must take into account the mutual effects of the slots on one another.

So far, no attempt has been made to investigate the degree of coupling between the annular slots. The radiation and filtering characteristics of the radial waveguide fed or cavity backed annular slot arrays

have not been investigated and there is no information available for the geometries excited by a forcing function of a general nature. Therefore, the objective of the present work is to study the electrical characteristics of radial waveguide fed, or cavity backed annular slot structures. A boundary value treatment is employed to derive field expressions for a general case, that is, the electromagnetic field set up by the system is composed of both TE and TM modes (transverse to z-axis). With this formulation, the assumption of azimuthal symmetry is no longer necessary and the exciting field may be assumed to be quite general. This in turn allows for the use of dual feed systems to create orthogonal as well as circularly polarized fields.

Chapter III is intended to derive a field solution for radial waveguides in the presence of annular or cylindrical type discontinuities. The solution is obtained by first constructing the response of the system to a current ring of arbitrary excitation and location, Section 3.2. The final result is then expressed in terms of the appropriate Green's functions integrated over the source distribution. Both electric and magnetic current distributions are treated. The inclusion of the fictitious magnetic source distribution enables one to formulate the problem of coupling between two regions by circular slots. This is covered in Section 3.3 where the filtering characteristics of two coupled radial waveguides in conjunction with a study of slots admittances and the aperture field behaviour is investigated. The coupling is achieved by an array of concentric annular slots on the common boundary of the waveguide regions. The effects of higher order modes on both equivalent admittance of each slot and the aperture fields are pointed out. Alternately, the expressions for the total power injected by the source, the power coupled out of the

guide and the remaining power transmitted through the waveguide region are derived.

In Chapter IV, a field solution for annular slot array antennas fed by radial waveguides is developed. The appropriate Green's functions for the semi-infinite region is obtained for a magnetic current ring characterized by a general forcing function. Using the principle of duality, a similar result for an electric current ring is also obtained. The final formulation is achieved by integrating the spacial impulse response over the aperture field distribution, Section 4.4. Evaluation of the infinite integrals associated with the semi-infinite region is discussed in Section 4.5 and the expressions describing the radiation fields and the radiated power are presented in Section 4.6. The effects of the higher order modes of the feeding guide on the slots admittances and the aperture fields explained in Section 4.7. The field variation of slots as a function of their radii is also investigated and the applicability of the annular slot array antennas for use as a pencil beam launcher as well as uniform radiation fields in the azimuth plane (no ϕ variation) is shown, Sections 4.8 and 4.9.

Chapter V deals with a cavity backed-annular slot array, that is, the radial waveguide is terminated in a short circuit. A suitable set of Green's functions for the cavity region is obtained and a similar method as that of Chapters III and IV is employed to derive the final formulation. Source considerations for exciting particular mode or modes of radial waveguides is introduced in Section 5.5. Possible feed configurations using vertically directed thin probes for generating TM modes of the guide is discussed and a method for obtaining orthogonal and circular polarized radiation within a limited angular region is suggested. The

effects of a finite ground plane on the radiation pattern is qualitatively studied and a method toward a quantitative analysis is proposed, Section 5.6.

An experimental prototype model of a cavity-backed annular slot array is made and the measured radiation patterns in both principal planes are compared against the computed values, Section 5.7.

The present work is concluded in Chapter VI by a general discussion of the results and possible extensions of the subject studied in related problems.

CHAPTER III

FIELD SOLUTION FOR RADIAL WAVEGUIDES IN THE PRESENCE OF ANNULAR OR CYLINDRICAL TYPE GEOMETRICAL DISCONTINUITIES

3.1 Introduction

Two dimensional arrangements of slots or conducting plates to form resonant arrays are of practical interest for applications as band-pass or band-stop filters. Within a certain frequency band, the transmission coefficient of the array can vary from unity to zero and its resonant frequency and bandwidth may be controlled by varying the characteristic dimensions of the array [42]-[44].

For waveguide applications, similar geometrical discontinuities have been used in fabricating low-pass and high-pass printed-circuit strip-line filters [45]. They are usually formed by two sheets of low-loss dielectric material, with a photo-etched copper-foil sandwiched in between, and with metal plates on the outer surfaces of the dielectric pieces forming the waveguide structure. The great advantages of this type of filter are its extremely low cost, ease and accuracy of fabrication. The latter one is quite important at higher frequency bands of operation, where small details of the geometry become appreciable fractions of the operating wavelength.

So far, the subject matter has been investigated extensively for the cases where the basic array element is of rectangular, circular or cross-geometries. However, little information is available for the case where the electromagnetic scattering bodies are of either annular or cylindrical shape.

In this chapter, using a boundary value treatment, a method of solution is established which gives the interior field of a radial waveguide in the presence of annular and cylindrical discontinuities in the guide region. These geometrical interruptions are either on the surfaces of the conducting walls of the waveguide (for the case of slots) or inside the dielectric region (metallic plates). A solution for the case in which both types of discontinuity are present can simply be obtained by superposing the two sets of solutions. The common factors between these two sets, as it will be shown later, are a set of complex coefficients. The application of the last boundary condition over the apertures and the conducting bodies for determining these constant coefficients, then ensures the electromagnetic coupling between the two sets of solutions.

The exciting source which is placed in the central region of the radial waveguide is assumed to be of a general nature. The slots and plates are assumed to be electrically thin enough to suppress radially directed induced currents (magnetic in case of slots) over the surfaces of the scatterers. Thus, the induced surface currents of the array elements are in the azimuthal direction.

We develop the solution by first constructing the appropriate Green's functions describing the impulse response to the magnetic (or electric) current ring of strength I, located at a radius $\rho = \rho'$, figure 3.1. The final formulation of the problem is then obtained by integrating the impulse response over the induced source distributions. Depending on the electrical dimensions of the array elements, the induced current may be expressed in terms of a finite sum of a suitable set of basis functions with unknown complex coefficients. These constants are

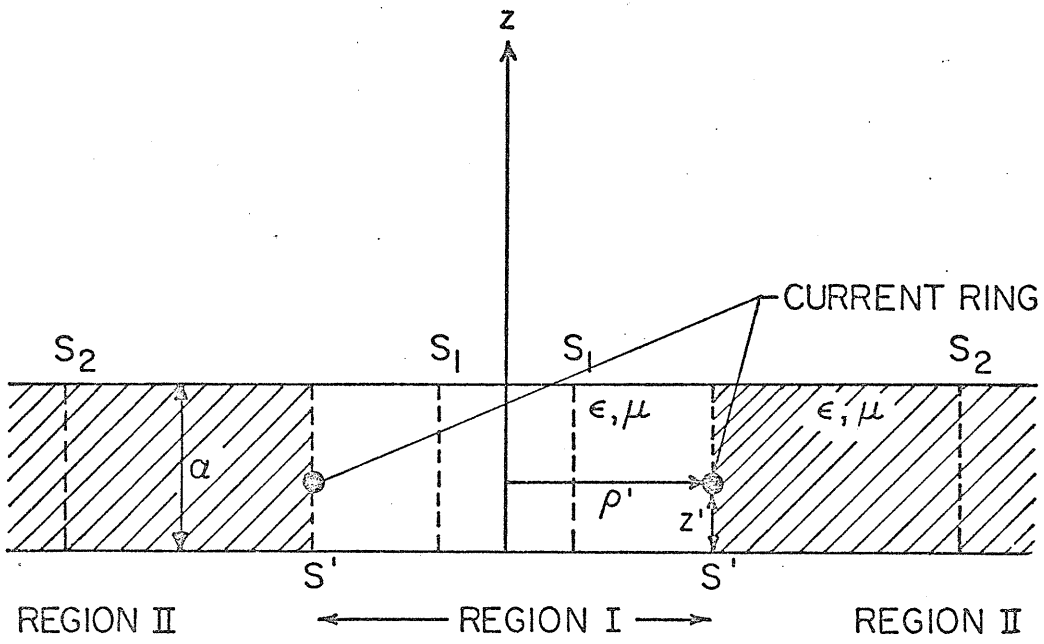

Figure 3.1: Current ring in a radial waveguide (impulse response)

then obtained by an application of the boundary condition over the surfaces of the scattering bodies. In fact, depending on the widths of the elements and the required degree of accuracy of the solution, suitable expressions describing the induced source distribution can be substituted into the formulation to obtain simplified versions of the solution with acceptable accuracies.

The most approximate, yet simplest set of basis functions is a series of pulses with equal widths but different strengths, characterizing the induced current distributions. The total number of pulses per element is directly related to its electrical width. For thin slots or plates, the current distribution may be assumed to be constant with respect to the radial variable ρ. Thus, using the constant field approximation, each element of the array is characterized by a single complex constant representing the strength of the element which is yet to be determined by an application of the last boundary condition. In fact, Wait and Hill [46],[47] by considering the problem of TEM coupling by a circumferential slot on a coated coaxial cable, have shown that differences between the results of the higher order approximations for the aperture field distribution and the constant field model are inconsequential.

For a waveguide fed slot array in which apertures are fed successively by a travelling wave, the effect of the mutual coupling between the slots cannot be generally ignored. In the methods based on the waveguide transmission line concept, the coupling between the array elements usually accounts for only the dominant propagating mode, that is, totally ignoring the effects of the higher order modes created in the vicinity of the slots discontinuities. Furthermore, the coupling due to the external field is generally overlooked. However, as it will

be shown later, depending on the arrangement of the slots and their electrical dimensions, the external coupling can become so strong as to recouple part of the radiated power by a number of the slots back into the waveguide containing the exciting source. An equivalent transmission line representation then gives a negative radiation conductance for the respective member (or members) of the array.

The contribution of the higher order modes can also become appreciable as to turn a resonant slot radiating by itself, into a reactive element when being used as an array member. The same argument also applies to the case when scattering bodies are in the form of metallic plates located inside a waveguide region. A distinct advantage of the present approach is the fact that all mutual coupling effects and the higher order modes are incorporated automatically into the solution. This is achieved by the simultaneous evaluation of the field unknown coefficients through the application of the boundary condition.

3.2 Problem-Formulation and Solution

3.2.1 Construction of the Appropriate Green's Functions, Magnetic Ring

In deriving the appropriate Green's functions for the problem depicted in figure 3.1, we essentially follow a similar approach to that taken by Collin [48] in which the field radiated by a current filament in a cylindrical waveguide is derived for the case when propagation is taking place in a cylindrical tube. The basic principle is to expand the radiated field in terms of a suitable set of waveguide modes with constant coefficients. These complex coefficients are then determined by an application of the Lorentz Reciprocity Theorem.

Consider the geometry shown in figure 3.1, formed by a radial waveguide of thickness a. The constitutive parameters of the medium between the perfectly conducting planes forming the waveguide walls are ε and μ. We assume the guide region is of infinite extent in the ρ direction, resulting in a zero reflection coefficient in region II. In practice, a matched load (absorber) may simulate this condition. The source is a magnetic filament of strength $I_m(\phi')$ characterized by

$$\vec{J}_m(\phi') = I_m(\phi')\,\delta(\rho - \rho')\,\delta(z - z')\hat{\phi}' \tag{3.1}$$

where $I_m(\phi')$ is a piece-wise continuous function of the azimuthal angle ϕ' and ρ', ϕ', z' are the source coordinates. $\hat{\phi}'$ is a unit vector tangent to the current source and representing the direction of the current flow. A time variation of $\exp(j\omega t)$ is assumed and suppressed throughout. The source function may be expanded in a Fourier series of the following form

$$I_m(\phi') = \sum_{n=0}^{\infty} (a_n \cos n\phi' + b_n \sin n\phi') \qquad 0 \leq \phi' < 2\pi \tag{3.2a}$$

where

$$a_n = \frac{\varepsilon_n}{2\pi} \int_0^{2\pi} I_m(\phi') \cos n\phi'\, d\phi'$$

$$b_n = \frac{\varepsilon_n}{2\pi} \int_0^{2\pi} I_m(\phi') \sin n\phi'\, d\phi' \tag{3.2b}$$

$$\varepsilon_n = \begin{cases} 1 & n = 0 \\ 2 & n \neq 0 \end{cases}$$

The source singularity at $\rho = \rho'$, $z = z'$ suggests dividing the medium between the conductors into two distinct regions separated by cylindrical surface S', namely, region I for $\rho < \rho'$ and region II for $\rho > \rho'$. An arbitrary electromagnetic field in a homogeneous cylindrical

region can be expressed as the sum of the TM (E waves) and TE (H waves) fields to the z-direction [49]. The total electric and magnetic fields can then be calculated from

$$\vec{E} = -\nabla \times (\hat{z}\psi^h) + \frac{1}{j\omega\varepsilon} \nabla \times \nabla \times (\hat{z}\psi^e)$$
$$\vec{H} = \nabla \times (\hat{z}\psi^e) + \frac{1}{j\omega\mu} \nabla \times \nabla \times (\hat{z}\psi^h) \qquad (3.3a)$$

where ψ^h and ψ^e are solutions of the wave equation. The set of equations (3.3a) in cylindrical coordinates are represented by

$$E_\rho = \frac{1}{j\omega\varepsilon} \frac{\partial^2\psi^e}{\partial\rho\partial z} - \frac{1}{\rho} \frac{\partial\psi^h}{\partial\phi} \qquad H\rho = \frac{1}{\rho} \frac{\partial\psi^e}{\partial\phi} + \frac{1}{j\omega\mu} \frac{\partial^2\psi^h}{\partial\rho\partial z}$$
$$E_\phi = \frac{1}{j\omega\varepsilon\rho} \frac{\partial^2\psi^e}{\partial\phi\partial z} + \frac{\partial\psi^h}{\partial\rho} \qquad H_\phi = -\frac{\partial\psi^e}{\partial\rho} + \frac{1}{j\omega\mu\rho} \frac{\partial^2\psi^h}{\partial\phi\partial z} \qquad (3.3b)$$
$$E_z = \frac{1}{j\omega\varepsilon} \left(\frac{\partial^2}{\partial z^2} + k^2\right)\psi^e \qquad H_z = \frac{1}{j\omega\mu} \left(\frac{\partial^2}{\partial z^2} + k^2\right)\psi^h$$

The next step is to expand the wave functions, ψ^e and ψ^h, in terms of the appropriate mode functions with unknown coefficients. Utilizing the boundary conditions at the source surface S' and also using the Lorentz Reciprocity Theorem,yields the desired constants. However, before proceeding further, a careful study of the set of equations (3.3b) and physical aspects of the problem provide us with useful priori information to reduce the mathematical labor involved in the formal determination of the coefficients. To satisfy the finiteness condition of the field due to the magnetic current ring in region I and the radiation condition in region II, Bessel and Hankel functions of second kind are chosen to represent the radial dependent parts of the mode functions, respectively. Since E_ϕ and H_ϕ components of the field must be continuous across the source surface S' and also as an anticipation for relating the field components to their source $I_m(\phi')$, we choose the functional form of the

ϕ dependence of the mode functions to be

$$\Phi_n^e(\phi) = a_n \cos n\phi + b_n \sin n\phi$$
$$\Phi_n^h(\phi) = \frac{d\Phi_n^e(\phi)}{d\phi} \tag{3.4}$$

where a_n and b_n are given by (3.2b).

The final results for the wave functions which also satisfy the boundary conditions on the conducting walls of the radial waveguide are

$$\psi^e = \sum_{n=o}^{\infty} \sum_{m=o}^{\infty} (a_n \cos n\phi + b_n \sin n\phi) \cos \frac{m\pi}{a} z \begin{cases} U_{mn}^e J_n(k_{\rho m}\rho) & \rho < \rho' \\ U_{mn}^e H_n^{(2)}(k_{\rho m}\rho) & \rho > \rho' \end{cases} \tag{3.5a}$$

$$\psi^h = \sum_{n=o}^{\infty} \sum_{m=o}^{\infty} n(b_n \cos n\phi - a_n \sin n\phi) \sin \frac{m\pi}{a} z \begin{cases} U_{mn}^h J_n(k_{\rho m}\rho) & \rho < \rho' \\ U_{mn}^h H_n^{(2)}(k_{\rho m}\rho) & \rho > \rho' \end{cases} \tag{3.5b}$$

where

$$k_{\rho m} = [k^2 - (\frac{m\pi}{a})^2]^{1/2}$$
$$k = \omega\sqrt{\varepsilon\mu} \tag{3.5c}$$

For a region V containing sources and bounded by a closed surface S, the formal statement of the Reciprocity Theorem is as follows

$$\oint_S (\vec{E}_a \times \vec{H} - \vec{E} \times \vec{H}_a) \cdot \hat{n} ds = \int_V (\vec{H} \cdot \vec{J}_{ma} - \vec{E} \cdot \vec{J}_a - \vec{H}_a \cdot J_m + \vec{E}_a \cdot \vec{J}) dv \tag{3.6a}$$

where the subscript a represents a set of auxiliary fields generated by the respective sources and $\hat{n}$ is the inward unit normal of the boundary S. We take the volume V to be the region enclosed by the conducting

walls and two arbitrarily located cylindrical surfaces S_1 and S_2 in regions I and II, respectively. As for the auxiliary fields, we are free to select their form in a manner to facilitate the derivation of the solution as long as they satisfy the Maxwell's equations. We, therefore, choose two separate sets of modes, where each set consists of two single modes of TE and TM types which are the solutions of the source free wave equations in volume V ($J_{ma} = J_a = 0$) and have the following forms

$$\begin{aligned} \psi_a^e &= (a_\ell \cos\ell\phi + b_\ell \sin\ell\phi) \cos \frac{p\pi}{a} z \cdot J_\ell(k_{\rho p}\rho) \\ \psi_a^h &= \ell(b_\ell \cos\ell\phi - a_\ell \sin\ell\phi) \sin \frac{p\pi}{a} z \cdot J_\ell(k_{\rho p}\rho) \end{aligned} \tag{3.7a}$$

$$\begin{aligned} \psi_a^e &= (a_\ell \cos\ell\phi + b_\ell \sin\ell\phi) \cos \frac{p\pi}{a} z \cdot H_\ell^{(2)}(k_{\rho p}\rho) \\ \psi_a^e &= \ell(b_\ell \cos\phi - a_\ell \sin\ell\phi) \sin \frac{p\pi}{a} z \cdot H_\ell^{(2)}(k_{\rho p}\rho) \end{aligned} \tag{3.7b}$$

Taking the auxiliary wave functions represented by (3.7a) and noting that there is no electric current source for the problem under consideration in volume V, one obtains [Appendix A]

$$\ell^2 \varepsilon U_{p\ell}^h - \mu U_{p\ell}^e = \frac{\pi\omega\varepsilon\mu\varepsilon_p}{2 k_{\rho p}^2 a} \cos \frac{p\pi}{a} z' [k_{\rho p}\rho' J_\ell'(k_{\rho p}\rho') - \ell^2 \frac{p\pi}{j\omega\mu a} J_\ell(k_{\rho p}\rho')] \tag{3.8a}$$

Similarly, substituting (3.7b) leads to

$$\ell^2 \varepsilon u_{p\ell}^h - \mu u_{p\ell}^e = -\frac{\pi\omega\varepsilon\mu\varepsilon_p}{2 k_{\rho p}^2 a} \cos \frac{p\pi}{a} z' [k_{\rho p}\rho' H_\ell^{(2)}(k_{\rho p}\rho') - \ell^2 \frac{p\pi}{j\omega\mu a} \cdot H_\ell^{(2)}(k_{\rho p}\rho')] \tag{3.8b}$$

Two other equations in terms of the four constant coefficients are needed to uniquely specify the field components inside the waveguide. To this

end, we utilize the boundary conditions imposed on the axial components of the electric and the magnetic fields (E_z, H_z) across the source surface S'. The continuity condition of the magnetic field is ensured by having

$$H_z^I - H_z^{II} = \frac{1}{j\omega\mu} \sum_{n=o}^{\infty} \sum_{m=o}^{\infty} n(b_n \cos n\phi - a_n \sin n\phi)\, k_{\rho m}^2 \sin \frac{m\pi}{a} z$$

$$\left| \begin{array}{l} \rho = \rho' \\ 0 \leq \phi < 2\pi \\ 0 \leq z \leq a \end{array} \right. \cdot [U_{mn}^h H_n^{(2)}(k_{\rho m}\rho') - u_{mn}^h J_n(k_{\rho m}\rho')] = 0 \qquad (3.9)$$

which upon using the orthogonality property of $\sin \frac{m\pi}{a} z$ over the range $0 \leq z \leq a$ and $\sin n\phi$ over the range $0 \leq \phi < 2\pi$ is reduced to

$$U_{p\ell}^h H_\ell^{(2)}(k_{\rho p}\rho') - U_{p\ell}^h J_\ell(k_{\rho p}\rho') = 0 \qquad (3.10)$$

The axial component of the electric field is discontinuous across the surface S' by an amount equal to the magnetic current density, that is

$$E_z^I - E_z^{II} = I_m(\phi')\, \delta(z - z')$$

$$\left| \begin{array}{l} \rho = \rho' \\ 0 \leq \phi \leq 2\pi \\ 0 \leq z \leq a \end{array} \right.$$

which upon using the property of the delta function and the orthogonality relations for sinusoidal functions yields

$$U_{p\ell}^e H_\ell^{(2)}(k_{\rho p}\rho') - U_{p\ell}^e J_\ell(k_{\rho p}\rho') = \frac{j\omega\varepsilon}{k_{\rho p}^2 a} \varepsilon_p \cos \frac{p\pi}{a} z' \qquad (3.11)$$

Equations (3.8), (3.10) and (3.11) can be solved for the constant coefficients. The final result after utilizing the Wronskian relationship

for the Bessel function are

$$
\begin{aligned}
U^{e}_{mn} &= \frac{\pi\omega\varepsilon\rho'}{2\, k_{\rho m} a}\, \varepsilon_m \cos\frac{m\pi}{a} z'\, J'_n (k_{\rho m}\rho') \\
U^{h}_{mn} &= -j\, \frac{\pi^2 m}{2(k_{\rho m} a)^2}\, \varepsilon_m \cos\frac{m\pi}{a} z'\, J_n (k_{\rho m}\rho') \\
u^{e}_{mn} &= \frac{\pi\omega\varepsilon\rho'}{2\, k_{\rho m} a}\, \varepsilon_m \cos\frac{m\pi}{a} z'\, H^{(2)\prime}_n (k_{\rho m}\rho') \\
u^{h}_{mn} &= -j\, \frac{\pi^2 m}{2(k_{\rho m} a)^2}\, \varepsilon_m \cos\frac{m\pi}{a} z'\, H^{(2)}_n (k_{\rho m}\rho')
\end{aligned}
\tag{3.12}
$$

The above coefficients in conjunction with (3.2), (3.3) and (3.5) uniquely define the electromagnetic field set up by a magnetic current filament of strength $I_m(\phi')$ located at a point, $\rho = \rho'$, $z = z'$.

3.2.2 Electric Ring

The mathematical routine for deriving the appropriate Green's functions for the case of an electric current radiating in a radial waveguide is similar to that of the magnetic case. For the sake of brevity only the main differences together with the final result will be presented here. Aside from subscript m, the defining equations for the current density and its Fourier expansion are the same as equations (3.1) and (3.2). Equations defined by (3.4) are replaced by

$$
\begin{aligned}
\Phi^{h}_n(\phi) &= a_n \cos n\phi + b_n \sin n\phi \\
\Phi^{e}_n(\phi) &= \frac{d\Phi^{h}_n(\phi)}{d\phi}
\end{aligned}
\tag{3.13}
$$

hence, the required wave functions are given by

$$\psi^e = \sum_{n=o}^{\infty} \sum_{m=o}^{\infty} n(b_n \cos n\phi - a_n \sin n\phi) \cos \frac{m\pi}{a} z \begin{cases} u^e_{mn} J_n (k_{\rho m}\rho) & \rho < \rho' \\ U^e_{mn} H^{(2)}_n (k_{\rho m}\rho) & \rho > \rho' \end{cases} \tag{3.14a}$$

$$\psi^h = \sum_{n=o}^{\infty} \sum_{m=o}^{\infty} (a_n \cos n\phi + b_n \sin n\phi) \sin \frac{m\pi}{a} z \begin{cases} u^h_{mn} J_n (k_{\rho m}\rho) & \rho < \rho' \\ U^h_{mn} H^{(2)}_n (k_{\rho m}\rho) & \rho > \rho' \end{cases} \tag{3.14b}$$

The Reciprocity relation for this case is stated as

$$\oint_S (\vec{E}_a \times \vec{H} - \vec{E} \times \vec{H}_a) \cdot \hat{n} ds = \int_V \vec{E}_a \cdot \vec{J} \, dv \tag{3.15}$$

The auxiliary wave functions are also changed accordingly, that is

$$\begin{aligned} \psi^e_a &= \ell(b_\ell \cos\ell\phi - a_\ell \sin\ell\phi) \cos \frac{p\pi}{a} z \, J_\ell (k_{\rho p}\rho) \\ \psi^h_a &= (a_\ell \cos\ell\phi + b_\ell \sin\ell\phi) \sin \frac{p\pi}{a} z \, J_\ell (k_{\rho p}\rho) \end{aligned} \tag{3.16a}$$

$$\begin{aligned} \psi^e_a &= \ell(b_\ell \cos\ell\phi - a_\ell \sin\ell\phi) \cos \frac{p\pi}{a} z \, H^{(2)}_\ell (k_{\rho p}\rho) \\ \psi^h_a &= (a_\ell \cos\ell\phi + b_\ell \sin\ell\phi) \sin \frac{p\pi}{a} z \, H^{(2)}_\ell (k_{\rho p}\rho) \end{aligned} \tag{3.16b}$$

Using these relations one finds:

$$\varepsilon U^h_{p\ell} - \ell^2 \mu U^e_{p\ell} = \frac{\pi\omega\varepsilon\mu\varepsilon_p}{2 k^2_{\rho p} a} \sin \frac{p\pi}{a} z' [k_{\rho p} J'_\ell (k_{\rho p}\rho') + \ell^2 \frac{p\pi}{j\omega\varepsilon\rho' a} J_\ell (k_{\rho p}\rho')] \tag{3.17a}$$

$$\begin{aligned} \varepsilon u^h_{p\ell} - \ell^2 \mu u^e_{p\ell} = \frac{\pi\omega\varepsilon\mu\varepsilon_p}{2 k^2_{\rho p} a} \sin \frac{p\pi}{a} z' [k_{\rho p} H^{(2)}_\ell (k_{\rho p}\rho') \\ + \ell^2 \frac{p\pi}{j\omega\varepsilon\rho' a} H^{(2)}_\ell (k_{\rho p}\rho')] \end{aligned} \tag{3.17b}$$

Now, in contrast to the magnetic case, the axial component of the electric

field E_z is continuous across the source surface S', but the magnetic field is discontinuous by an amount equal to

$$H_z^{I} - H_z^{II} = I(\phi')\ \delta(z - z') \Big|_{\substack{\rho = \rho' \\ 0 \leq \phi \leq 2\pi \\ 0 \leq z \leq a}} \tag{3.18}$$

An approach similar to that of the magnetic case yields the following results for the constant coefficients

$$\begin{aligned} U_{mn}^{e} &= j \frac{\pi^2 m}{2(k_{\rho m}a)^2} \varepsilon_m \sin \frac{m\pi}{a} z'\ J_n\ (k_{\rho m}\rho') \\ U_{mn}^{h} &= -\frac{\pi\omega\mu\rho'}{k_{\rho m}a} \varepsilon_m \sin \frac{m\pi}{a} z'\ J_n'\ (k_{\rho m}\rho') \\ u_{mn}^{e} &= j \frac{\pi^2 m}{2(k_{\rho m}a)^2} \varepsilon_m \sin \frac{m\pi}{a} z'\ H_n^{(2)}\ (k_{\rho m}\rho') \\ u_{mn}^{h} &= -\frac{\pi\omega\mu\rho'}{k_{\rho m}a} \varepsilon_m \sin \frac{m\pi}{a} z'\ H_n^{(2)'}\ (k_{\rho m}\rho') \end{aligned} \tag{3.19}$$

Equations (3.19) together with (3.1), (3.2), (3.3) and (3.14) uniquely define the electromagnetic field set up by an electric current filament of strength $I(\phi')$ located at a point, $\rho = \rho'$, $z = z'$.

It is interesting to note that as z' approaches zero or a (the conducting boundaries), the field due to an electric current filament vanishes. It can be shown by reciprocity that an electric current just in front of an electric current conductor and parallel to its surface produces a null field [49]. This can be explained by thinking of the conductor as shorting out the current. In contrast to this case, the field produced by a magnetic current filament does not vanish as it approaches the conducting planes. This is expected, since a fictitious

magnetic current filament is equivalent to an infinitely thin slot (slit) and as will be shown later it can effectively couple appreciable amount of electromagnetic energy into the waveguide region.

3.3 Application to the Problem of Two-Coupled Radial Waveguides

The field set up by a combination of sources of electric and magnetic types may be looked upon as a superposition problem. Based on the theory presented earlier, this section is devoted to demonstrate the application of the previous results to problems involving annular slots of finite width as geometrical discontinuities in radial waveguides. To show the general feature of the theory, the problem of coupling between two radial waveguides by concentric annular apertures on the common boundary is considered, figure 3.2. The exciting source is placed in the central region of the lower waveguide.

Solution to the problems involving annular or cylindrical conducting plates as the scatterers of electromagnetic field inside a radial waveguide can be obtained in a similar manner. That is, using the appropriate Green's functions of electric type developed earlier, the solution can be found by integrating the impulse response of the system over the induced current distributed over the surfaces of the conducting plates. The unknown coefficients representing the induced source strength are then determined by an application of the condition of vanishing tangential electric field over the plates.

These geometries may have applications as band-pass printed-circuit strip-line filters. They can also be used for the design of feed systems suitable for launching a particular mode or modes for use in

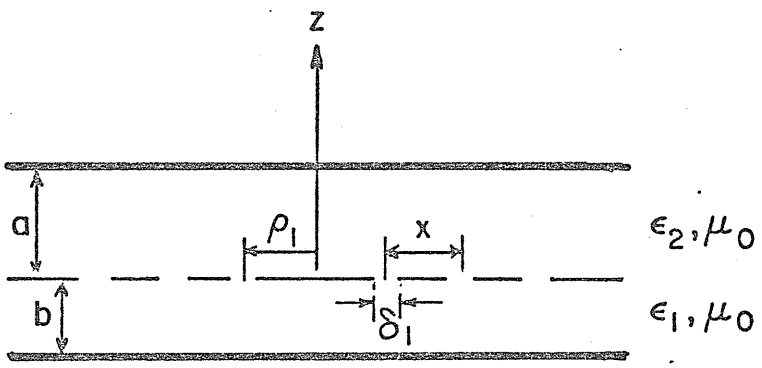

Figure 3.2: Typical two coupled radial waveguides of infinite extent

radial waveguides.

3.3.1 Formulation of the Problem of Two Coupled Radial Waveguides

An annular slot on the conducting wall of a radial waveguide, as far as the internal field is concerned, may be viewed as an annular distribution of magnetic surface current with a density given by

$$\vec{J}_m = \vec{E} \times \hat{n}\Big|_{\text{aperture}} \tag{3.20}$$

where $\hat{n}$ is the inward unit normal to the aperture plane. Noting the fact that E_ϕ component of the electric field must vanish at the edges of the slot, it is expected that for electrically narrow slots, the contribution from E_ϕ to the total scattered field is negligible. Hence, we may assume the aperture electric field to be mainly in the radial direction. That is,

$$\vec{J}_m \simeq E_\rho \, (\hat{\rho} \times \hat{n}) \tag{3.21}$$

where $\hat{\rho}$ is the radial unit vector. Expanding the radial component of the aperture electric field into a Fourier series of the azimuthal variable ϕ leads to

$$E_\rho \, (\rho', \phi') = \sum_{n=o}^{\infty} R_n(\rho')(a_n \cos n\phi + b_n \sin n\phi) \tag{3.22}$$

where $R_n(\rho')$ is the nth mode's radial dependent part of the aperture electric field and a_n, b_n are the Fourier coefficients. Now, the contribution from the slot to the total field can be obtained by integrating the product of $R(\rho')$ and the Green's functions (3.5) over the aperture radial coordinate ρ'.

The above steps are essentially an application of the equivalent principle to the slot problem, which replaces slots by an equivalent

magnetic current sheet over a perfectly conducting surface expressed by (3.20). According to Uniqueness Theorem [49], a field in a region is uniquely specified by the sources within the region plus the tangential component of the electric field (or magnetic field) over the boundary enclosing the region. Therefore, as far as the field inside the waveguide is concerned, the total field in the waveguide region is the sum of the contribution from the magnetic surface current and the sources inside the dielectric region. Both types of sources are radiating in the presence of an uninterrupted radial waveguide. In the case of the geometry shown in figure 3.2, the incident field launched by the exciting source in the lower guide must be added to the field set up by the magnetic surface current (contribution from the external region). However, the total field in the upper guide is entirely determined by the aperture field.

To be more specific, let us assume a general TM_{pq} mode of the radial waveguide [49] to be incident in the lower waveguide. This mode is characterized by

$$\psi^{e}_{inc}_{pql} = \cos \frac{p\pi}{b} z \cos q\phi \; H_q^{(2)} (k_{\rho pl}\rho)$$
$$k_{\rho pl} = [k_1^2 - (\frac{p\pi}{b})^2]^{1/2} \qquad k_1 = \sqrt{\varepsilon_1 \mu_0} \tag{3.23}$$

The wave functions due to the magnetic surface current over the coupling aperture in the two waveguides are specified by

$$\psi_2^e = -\frac{\pi\omega\varepsilon_2}{2a} \sum_{\ell=1}^{L} \sum_{m=0}^{\infty} \sum_{n=0}^{\infty} \frac{\varepsilon_m}{k_{\rho m2}} (a_n \cos n\phi + b_n \sin n\phi) \cos \frac{m\pi}{a} z$$
$$\cdot \frac{H_n^{(2)} (k_{\rho m2}\rho)}{J_n (k_{\rho m2}\rho)} \int_{\bar{\rho}_\ell}^{\bar{\rho}_\ell} \rho' R_{\ell n}(\rho') \frac{J_n' (k_{\rho m2}\rho')}{H_n^{(2)'} (k_{\rho m2}\rho')} d\rho' \tag{3.24a}$$

$$\psi_2^h = j\frac{\pi^2}{2a^2}\sum_{\ell=1}^{L}\sum_{m=0}^{\infty}\sum_{n=0}^{\infty}\frac{\varepsilon_m \cdot n}{k_{\rho m2}^2}(b_n \cos n\phi - a_n \sin n\phi)\sin\frac{m\pi}{a}z$$

$$\cdot \begin{matrix} H_n^{(2)}(k_{\rho m2}\rho) \\ J_n(k_{\rho m2}\rho) \end{matrix} \int_{\bar{\rho}_\ell}^{\rho_\ell^+} R_{\ell n}(\rho') \begin{matrix} J_n(k_{\rho m2}\rho') \\ H_n^{(2)}(k_{\rho m2}\rho') \end{matrix} d\rho' \qquad (3.24b)$$

$$\psi_1^e = \frac{\pi\omega\varepsilon_1}{2b}\sum_{\ell=1}^{L}\sum_{m=0}^{\infty}\sum_{n=0}^{\infty}\frac{\varepsilon_m}{k_{\rho m1}}(a_n \cos n\phi + b_n \sin n\phi)\cos\frac{m\pi}{b}z$$

$$\cdot \begin{matrix} H_n^{(2)}(k_{\rho m1}\rho) \\ J_n(k_{\rho m1}\rho) \end{matrix} \int_{\bar{\rho}_\ell}^{\rho_\ell^+} \rho' R_{\ell n}(\rho') \begin{matrix} J_n'(k_{\rho m1}\rho') \\ H_n^{(2)}(k_{\rho m1}\rho') \end{matrix} d\rho' \qquad (3.25a)$$

$$\psi_1^h = -j\frac{\pi^2}{2b^2}\sum_{\ell=1}^{L}\sum_{m=0}^{\infty}\sum_{n=0}^{\infty}\frac{\varepsilon_m \cdot n}{k_{\rho m1}^2}(b_n \cos n\phi - a_n \sin n\phi)\sin\frac{m\pi}{b}z$$

$$\cdot \begin{matrix} H_n^{(2)}(k_{\rho m1}\rho) \\ J_n(k_{\rho m1}\rho) \end{matrix} \int_{\bar{\rho}_\ell}^{\rho_\ell^+} R_{\ell n}(\rho') \begin{matrix} J_n(k_{\rho m1}\rho') \\ H_n^{(2)}{}'(k_{\rho m1}\rho') \end{matrix} d\rho' \qquad (3.25b)$$

where L is the total number of slots, and $R_{\ell n}(\rho')$ is the nth mode's radial dependent part of the tangential electric field over the ℓth aperture. Furthermore, depending on the relative position of the observation and the source points ($\rho > \rho'$ or $\rho < \rho'$) the top or the bottom row of the Bessel functions must be selected. The symbols ρ_ℓ^+ and $\bar{\rho}_\ell$ stand for

$$\begin{aligned} \rho_\ell^+ &= (\rho_\ell + \frac{\delta_\ell}{2}) \\ \bar{\rho}_\ell &= (\rho_\ell - \frac{\delta_\ell}{2}) \end{aligned} \qquad (3.26)$$

It should be noted that the change of the sign in the two sets of wave functions (3.24), (3.25) is due to opposite directions for the respective inward normals of the two radial waveguides. As it is evident, (3.24) and (3.25) are merely obtained by integrating the Green's functions developed earlier on the aperture source distribution. Note also that the continuity condition for the tangential component of the electric field over the apertures is already implemented in the formulation by insertion of equal aperture field distributions into the wave functions sets.

The coefficients a_n and b_n entirely depend on the functional form of the azimuthal dependent part of the incident field. An examination of the total tangential magnetic field over the coupling apertures and utilizing the orthogonality property of the sinusoidal functions over the range of $0 \leq \phi \leq 2\pi$ reveal that for our particular choice of the incident mode (3.23), we must have

$$b_n = 0 \qquad \text{for all } n$$

$$a_n = \begin{cases} 0 & n \neq q \\ 1 & n = q \end{cases} \tag{3.27}$$

This eliminates the infinite summation over n in equations (3.24) and (3.25). For most practical cases, the feed system and the guide dimension are selected in such a manner as to support either a single mode or a finite combination of the first few modes of the radial waveguide. Therefore, the summation on n, generally, is a finite one.

The radial dependent part $R_{\ell n}(\rho')$ of the tangential aperture electric field is generally not a known function. However, depending on the electrical widths of the slots, the aperture field distribution may be expressed in terms of a finite sum of a particular set of basis functions with unknown coefficients. These coefficients are then obtained by

an application of the boundary condition on the tangential magnetic field over the apertures. The choice of the set of basis functions and the total number of the elements of the set for each slot depends on the electrical dimensions of the slots and the required degree of accuracy of the solution thus obtained. In fact, depending on the widths of the apertures, suitable expressions describing the aperture source distribution can be substituted into the formulation to obtain simplified versions of the solution with acceptable accuracies.

The simplest, but the crudest set of basis functions, is a series of pulses of equal width but different strength, located side by side, characterizing the aperture field distribution. Since over each pulse we assume the field is constant with respect to ρ variations, the width of each pulse should be selected electrically small enough to physically substantiate such an assumption. Therefore, the number of pulses (unit cells) per - slot and hence, the total number of field strength coefficients is directly related to the aperture size. Evaluation of these complex constants can be performed using the continuity condition of either H_ϕ or H_ρ. The extra boundary condition appearing here, is the result of our previous assumption made on the tangential electric field. E_ϕ component of this field was assumed to be negligible compared to E_ρ for slots of electrically narrow widths. In fact, it seems quite possible to construct an extra set of wave functions describing the contribution from a ρ directed magnetic current distribution over the apertures. Then, following the same routine as that of the ϕ directed magnetic current, we can expand E_ϕ over the slots in terms of a finite sum of the basis functions with a new set of complex constant coefficients. The two continuity conditions can then be employed to determine the two

sets of coefficients simultaneously. However, since the primary objective for the present study is to investigate scattering bodies of small widths, we assume the geometrical discontinuities are electrically thin enough to produce mainly, ϕ directed surface currents over the scattering bodies. Hence, we may take H_ϕ component of the total magnetic field in each region to be matched on the aperture openings. This is done by equating the values of H_ϕ over each slot or each cell (in case the slot width is divided into more than one unit cell) for the two regions in an average sense. If the cells are thin enough, this is a good approximation to the true value of H_ϕ over the cells. That is, since ϕ component of the magnetic field is tangent to the edges, it has a finite value over the entire surface of each individual slot. To this end, we start by expressing the aperture function $R_n(\rho')$ in terms of a finite number of pulses with different amplitudes E_{in}. At this point, we make the following convention for numbering the cells forming the entire coupling aperture. The cells are characterized by their central radii and the numbering starts from the cell with smallest radius of the smallest slot and ends by the cell with largest radius of the last slot. Therefore, the aperture function is represented by

$$R_n(\rho') = \sum_{i}^{IC} E_{in} P_i (\rho' - \rho'_i) \tag{3.28a}$$

where, P_i is the ith pulse and has the following property

$$P_i (|\rho' - \rho'_i|) = \begin{cases} 1 & -\frac{\delta_i}{2} \leq \rho' - \rho'_i < \frac{\delta_i}{2} \\ 0 & \text{elsewhere} \end{cases} \tag{3.28b}$$

and IC is the total number of cells of the entire aperture.

Substituting (3.28) in (3.25) and noting (3.27) one obtains the following expressions for the azimuthal component of the magnetic field in the respective regions

$$H_{\phi 2} = \frac{\pi\omega\varepsilon_2}{2a} \sum_{i=1}^{IC} \sum_{m=0}^{\infty} E_{in}\varepsilon_m \cos q\phi \cos \frac{m\pi}{a} z \int_{\bar{\rho}_i}^{\rho_i^+} \frac{J_q'(k_{\rho m2}\rho')}{\rho' \; H_q^{(2)\prime}(k_{\rho m2}\rho')} d\rho'$$

$$\cdot H_q^{(2)\prime}(k_{\rho m2}\rho) - \frac{\pi^3 q^2}{2\rho\mu_o a^3} \sum_{i=1}^{IC} \sum_{m=0}^{\infty} \frac{E_{in} m^2 \varepsilon_m}{k_{\rho m2}^2} \cos q\phi \cos \frac{m\pi}{a} z$$

$$\cdot J_q'(k_{\rho m2}\rho) \int_{\bar{\rho}_i}^{\rho_i^+} \frac{J_q(k_{\rho m2}\rho')}{H_q^{(2)}(k_{\rho m2}\rho')} d\rho' \cdot H_q^{(2)}(k_{\rho m2}\rho) \cdot J_q(k_{\rho m2}\rho) \qquad (3.29a)$$

$$H_{\phi 1} = -\frac{\pi\omega\varepsilon_1}{2b} \sum_{i=1}^{IC} \sum_{m=0}^{\infty} E_{in}\varepsilon_m \cos q\phi \cos \frac{m\pi}{b} z \int_{\bar{\rho}_i}^{\rho_i^+} \frac{J_q'(k_{\rho m1}\rho')}{\rho' \; H_q^{(2)\prime}(k_{\rho m1}\rho')} d\rho'$$

$$\cdot H_q^{(2)\prime}(k_{\rho m1}\rho) + \frac{\pi^3 q^2}{2\rho\mu_o b^3} \sum_{i=1}^{IC} \sum_{m=0}^{\infty} \frac{E_{in} m^2 \varepsilon_m}{k_{\rho m2}^2} \cos \frac{m\pi}{b} z$$

$$\cdot J_q'(k_{\rho m1}\rho) \int_{\bar{\rho}_i}^{\rho_i^+} \frac{J_q(k_{\rho m1}\rho')}{H_q^{(2)}(k_{\rho m2}\rho)} d\rho' \cdot H_q^{(2)}(k_{\rho m1}\rho) \cdot J_q(k_{\rho m1}\rho)$$

$$- k_{\rho p1} \cos q\phi \cos \frac{p}{b} z \, H_q^{(2)}(k_{\rho p}\rho) \qquad (3.29b)$$

Now, we equate $H_{\phi 1}$ and $H_{\phi 2}$ over the cells forming the slots in an average sense. That is,

$$\bar{H}_{\phi ij} = \bar{H}_{\phi 2j} \quad \Big| \; z = 0, \; |\rho - \rho_j| \leq \frac{\delta_j}{2}, \; 0 \leq \phi < 2\pi \qquad j = 1, 2, \ldots . \text{IC} \qquad (3.30)$$

where the bar stands for the average value of the field components. In view of equations (3.29), we define the average value of the magnetic field for the jth slot to be

$$\bar{H}_{\phi j} = \sum_{i=1}^{I} \bar{h}_{ji} \qquad (3.31a)$$

where

$$\bar{h}_{ji} = \frac{1}{\delta_j} \int_{\bar{\rho}_j}^{\rho_j^+} H_{i\phi} \, d\rho \qquad i \neq j \qquad (3.31b)$$

where $H_{i\phi}$ is the contribution of the ith slot to the magnetic field at the jth slot. For $i = j$ term that can be viewed as the contribution of the jth cell to the average value of H_ϕ associated with the jth slot, such a definition as (3.31b) creates some unnecessary mathematical complications in evaluating integrals involving products of Bessel functions of both different argument and order. However, due to the electrically thin dimension of each cell, these problems can be avoided by taking the average value as the mean of three sampled points over each cell, namely the two edges and the center of the cell. Note that H_ϕ is tangent to the edges of the slots and, therefore, according to the edge condition [56], is bounded even on the edges of the aperture. Hence, choosing the sampling points on the edges should not create any numerical complication.

We, therefore, have

$$\bar{h}_{ii} = \frac{1}{3}\left[H_\phi(\bar{\rho}_i) + H_\phi(\rho_i) + H_\phi(\overset{+}{\rho}_i)\right] \tag{3.31c}$$

It should be mentioned that even though the integrals as defined by (3.31b) can be evaluated exactly, simpler results with no significant loss of accuracy can be obtained by neglecting the variations of terms like ρ and $\frac{1}{\rho}$ in the integrands and replacing them by their mean value over each cell. Note that the same approximation may not be effected for the Bessel functions due to the existence of $k_{\rho m}$ in the arguments which becomes large for higher order modes.

In the light of the above arguments, one obtains a set of simultaneous linear equations in terms of the aperture field coefficients in the form

$$\left[y_{ji}\right]\left[E_{jq}\right] = \left[y_j^{inc}\right] \tag{3.32a}$$

with

$$y_j = -\frac{1}{\delta_j}\left[H_q^{(2)}(k_{\rho p1}\overset{+}{\rho}_j) - H_q^{(2)}(k_{\rho p1}\bar{\rho}_j)\right] \tag{3.32b}$$

and

$$y_{\substack{ji \\ i\neq j}} = \frac{\pi\omega\varepsilon_2}{2a}\cdot\sum_{m=0}^{\infty}\frac{\rho_i}{k_{\rho m2}^2\delta_j}\varepsilon_m\cdot\begin{bmatrix} J_q(k_{\rho m2}\rho_i) \\ \\ H_q^{(2)}(k_{\rho m2}\rho_i)\end{bmatrix}_+\cdot\begin{bmatrix} H_q^{(2)}(k_{\rho m2}\rho_j) \\ \\ J_q(k_{\rho m2}\rho_j)\end{bmatrix}_+$$

$$-\frac{\pi^3 q^2}{2\rho_j\mu a^3}\sum_{m=0}^{\infty}\frac{m^2}{k_{\rho m2}^2\delta_j}\varepsilon_m\begin{bmatrix} C_{qm2}^{J,H}(\rho_i)\end{bmatrix}_+\cdot\begin{bmatrix} C_{qm2}^{H,J}(\rho_j)\end{bmatrix}_+$$

$$-\frac{\pi\omega\varepsilon_1}{2b}\cdot\sum_{m=0}^{\infty}\frac{\rho_i}{k_{\rho m1}^2\delta_j}\varepsilon_m\cdot\begin{bmatrix} J_q(k_{\rho m1}\rho_i) \\ \\ H_2^{(2)}(k_{\rho m1}\rho_i)\end{bmatrix}_+\cdot\begin{bmatrix} H_q^{(2)}(k_{\rho m1}\rho_j) \\ \\ J_q(k_{\rho m1}\rho_j)\end{bmatrix}_+$$

$$+ \frac{\pi^3 q^2}{2\rho_j \mu_0 b^3} \sum_{m=0}^{\infty} \frac{m^2}{k_{\rho m1}^2 \delta_j} \varepsilon_m \left[C_{qm1}^{J,H}(\rho_i) \right]_-^+ \cdot \left[C_{qm1}^{H,J}(\rho_j) \right]_-^+ \qquad (3.32c)$$

where the top rows are for $j > i$ and the first superscripts represent the appropriate Bessel function in the definition of $C_{qm}(\rho)$, which is presented later. The diagonal elements are of different form and are given by

$$\begin{aligned}
Y_{ii} = {} & \frac{\pi\omega\varepsilon_2}{6a} \cdot \sum_{m=0}^{\infty} \frac{\rho_i}{k_{\rho m2}} \varepsilon_m \cdot J_q'(k_{\rho m2} \bar{\rho}_i) \cdot \left[H_q^{(2)}(k_{\rho m2}\rho_i) \right]_-^+ \\
& + H_q^{(2)\prime}(k_{\rho m2} \overset{+}{\rho}_i) \cdot \left[J_q(k_{\rho m2} \rho_i) \right]_-^+ + J_q'(k_{\rho m2}\rho_i) \cdot \left[H_q^{(2)}(k_{\rho m2}\rho_i) \right]_{\rho_i}^+ \\
& + H_q^{(2)\prime}(k_{\rho m2}\rho_i) \cdot \left[J_q(k_{\rho m2}\rho_i) \right]_-^{\rho_i} - \frac{\pi^3 q^2}{6\rho_i \mu_0 a^3} \sum_{m=0}^{\infty} \frac{m^2}{k_{\rho m2}} \varepsilon_m \\
& J_q(k_{\rho m2} \bar{\rho}_i) \cdot \left[C_{qm2}^{H}(\rho_i) \right]_-^+ + H_q^{(2)}(k_{\rho m2} \overset{+}{\rho}_i) \cdot \left[C_{qm2}^{J}(\rho_i) \right]_-^+ \\
& + J_q(k_{\rho m2}\rho_i) \cdot \left[C_{qm2}^{H}(\rho_i) \right]_{\rho_i}^+ + H_q^{(2)}(k_{\rho m2}\rho_i) \cdot \left[C_{qm2}^{J}(\rho_i) \right]_-^{\rho_i} \\
& - \frac{\pi\omega\varepsilon_1}{6b} \cdot \sum_{m=0}^{\infty} \frac{\rho_i}{k_{\rho m1}} \varepsilon_m \; J_q'(k_{\rho m1} \bar{\rho}_i) \cdot \left[H_q^{(2)}(k_{\rho m1}\rho_i) \right]_-^+ \\
& + H_q^{(2)\prime}(k_{\rho m1} \overset{+}{\rho}_i) \cdot \left[H_q^{(2)}(k_{\rho m1}\rho_i) \right]_-^+ + J_q'(k_{\rho m1}\rho_i) \cdot \left[H_q^{(2)}(k_{\rho m1}\rho_i) \right]_{\rho_i}^+ \\
& + H_q^{(2)\prime}(k_{\rho m1}\rho_i) \cdot \left[J_q(k_{\rho m1}\rho_i) \right]_-^{\rho_i} + \frac{\pi^3 q^2}{6\rho_i \mu_0 b^3} \sum_{m=0}^{\infty} \frac{m^2}{k_{\rho m1}} \varepsilon_m \\
& J_q(k_{\rho m1} \bar{\rho}_i) \cdot \left[C_{qm1}^{H}(\rho_i) \right]_-^+ + H_q^{(2)}(k_{\rho m1} \overset{+}{\rho}_i) \cdot \left[C_{qm1}^{J}(\rho_i) \right]_-^+ \\
& + J_q(k_{\rho m1}\rho_i) \cdot \left[C_{qm1}^{H}(\rho_i) \right]_{\rho_i}^+ + H_q^{(2)}(k_{\rho m1}\rho_i) \cdot \left[C_{qm1}^{J}(\rho_i) \right]_-^{\rho_i}
\end{aligned} \qquad (3.32d)$$

where [50]

$$C_{qm}(\rho) = \int_{\rho > 0}^{\rho} B_q(k_{\rho m}\rho')\, d\rho' = \begin{cases} -\sum_{n=0}^{N} \varepsilon_n B_{2n}(k_{\rho m}\rho)/k_{\rho m} & 0 < q = 2N+1 \\ 2\left[\sum_{n=0}^{\infty} B_{2(N+M)+1}(k_{\rho m}\rho)\right]/k_{\rho m} & 0 < q = 2N \end{cases} \tag{3.32e}$$

Note that for the case $q = 0$ (ϕ symmetry), the field is TM to z and is solely determined from ψ^e.

Superscripts J and H denote to Bessel and Hankel functions, respectively, and $B_q(z)$ represents any cylindrical function. The infinite series in (3.32e) which appear for the cases when the incident field is an even mode of the radial waveguide is a fast converging series and can be truncated after the first few terms.

Once the aperture field coefficients E_{iq} are determined from the matrix equation (3.32a), the field components in the two regions away from the slots can be obtained from the following relations and (3.3b).

$$\psi_2^e = -\frac{\pi\omega\varepsilon_2}{2a} \sum_{i=1}^{IC} \sum_{m=0}^{\infty} \frac{\rho_i}{k_{\rho m2}^2} E_{iq}\, \varepsilon_m \cos q\phi \cos \frac{m\pi}{a} z \cdot \begin{bmatrix} J_q(k_{\rho m2}\rho_i) \\ H_q^{(2)}(k_{\rho m2}\rho_i) \end{bmatrix} + \begin{bmatrix} H_q^{(2)}(k_{\rho m2}\rho) \\ J_q(k_{\rho m2}\rho) \end{bmatrix} -$$

$$\psi_2^h = -j\frac{\pi^2}{2a^2}\sum_{i=1}^{IC}\sum_{m=0}^{\infty}\frac{m^{\bullet}q}{k_{\rho m2}^2}E_{iq}\,\varepsilon_m \sin q\phi \quad \sin\frac{m\pi}{a}z \cdot \left[C_{mq2}^{J,H}(\rho_i)\right]_{-}^{+}$$

$$H_q^{(2)}(k_{\rho m2}\rho)$$

$$\cdot$$

$$J_q(k_{\rho m2}\rho)$$

$$\psi_1^e = \frac{\pi\omega\varepsilon_1}{2b}\sum_{i=1}^{IC}\sum_{m=0}^{\infty}\frac{\rho_i}{k_{\rho m1}^2}E_{iq}\,\varepsilon_m \cos q\phi \quad \cos\frac{m\pi}{b}z \cdot \begin{bmatrix} J_q(k_{\rho m1}\rho_i) \\ \\ H_q^{(2)}(k_{\rho m1}\rho_i) \end{bmatrix}_{-}^{+}$$

$$H_q^{(2)}(k_{\rho m1}\rho)$$

$$\cdot$$

$$J_q(k_{\rho m1}\rho)$$

$$\psi_{pq1}^{e_{inc}} = \cos\frac{p\pi}{b}z \cos q\phi\, H_q^{(2)}(k_{\rho p1}\rho)$$

$$\psi_1^h = j\frac{\pi^2}{2b^2}\sum_{i=1}^{IC}\sum_{m=0}^{\infty}\frac{m^{\bullet}q}{k_{\rho m1}^2}E_{iq}\,\varepsilon_m \sin q\phi \sin\frac{m\pi}{b}z \cdot \left[C_{mq1}^{J,H}(\rho_i)\right]_{-}^{+}$$

$$H_q^{(2)}(k_{\rho m1}\rho)$$

$$\cdot \qquad (3.33)$$

$$J_q(k_{\rho m1}\rho)$$

3.3.2 Expressions for the Total, Transmitted and the Coupled Power

The power-transfer characteristic is generally the most important parameter for structures used as filtering devices. The band-width efficiency and frequency sensitivity of the filters are mainly determined by a study of their power transfer functions. For the problem under investigation, there is another feature to the power flow characteristic. Since the conservation of energy is not utilized explicitely in deriving the aperture field coefficients, this principle can be used as a check on the accuracy of the numerical results. That is, the difference between the total power injected by the source and the sum of the powers coupled to the upper waveguide and transmitted through the lower guide is an indication of the accuracy of the solution thus obtained. Throughout all the numerical examples presented in the thesis, this property is utilized and difference values smaller than 0.01 per-cent of the total power are obtained.

The power transfer across a surface S is defined as,

$$P = \mathrm{Re} \int_S (\vec{E} \times \vec{H}^*) \cdot \hat{n} \, ds \tag{3.34}$$

where Re stands for the real part of a complex quantity, $\hat{n}$ is the unit normal to S in the direction of power flow and asterisk is due to complex conjugate operation. To calculate the total power we take the surface S to be formed by an arbitrarily located cylindrical surface, with a radius ρ_x smaller than the first slot, and the conducting walls. Since S encloses the feed system in the lower waveguide, an application of (3.34) to the volume bounded by S yields the power leaving this region and hence equal to the total power injected by the source system located

at the central region of the lower waveguide. For practical considerations, the guides thicknesses are generally selected to be smaller than one-half of the intrinsic wavelength λ. Therefore, all the higher order modes with $m > 0$ have a complex $k_{\rho ml}$, equation (3.5c), and do not contribute to power-transfer. In this regard, expressions for the power components are only derived for the propagating mode.

The coupled power can be obtained by taking S to be the surface of an arbitrarily located cylinder in the upper waveguide with a radius greater than the last slot. By a similar approach, one can obtain the transmitted power through the lower waveguide by selecting the cylindrical surface in this region. In fact, power coupled by individual slots to the upper guide can also be calculated by taking the respective slot's aperture as the surface S and an application of equation (3.34) to the slot's field components.

Using the theory presented in this section and the expressions derived for the wave functions in the earlier sections, (3.33), the total, coupled and transmitted power for two coupled radial waveguides, figure 3.2, are formulated [Appendix B] and the final results are as follows

$$P_{Total} = \sum_{q=0}^{\infty} \frac{(a_q^2 + b_q^2)}{\varepsilon_q} \{480\,\pi\, k_o b + 2\pi\, \varepsilon_{r1} \cdot \sum_{i=1}^{IC} k_o \rho_i \, Re[k_o E_{iq} H_q^{(2)}(k_1 \rho_i)]_-^+\} \tag{3.35a}$$

$$P_{Coupled} = \sum_{q=0}^{\infty} \frac{(a_q^2 + b_q^2)\pi(\varepsilon_{r2})^{3/2}}{120 \varepsilon_q k_o a} \sum_{i=1}^{IC} \sum_{m=1}^{IC} k_o \rho_i \cdot k_o \rho_m \cdot Re(k_o E_{iq} E_{mq}^*)[J_q(k_2 \rho_i)]_-^+ \tag{3.35b}$$

$$P_{Transmitted} = \sum_{q=0}^{\infty} \frac{(a_q^2 + b_q^2)}{\varepsilon_q} \{480\,\pi\, k_o b + \frac{(\varepsilon_{r1})^{3/2}}{120 \cdot k_o b} \sum_{i=1}^{IC} \sum_{m=1}^{IC} k_o \rho_i \cdot k_o \rho_m \cdot Re(k_o E_{iq} \cdot E_{mq}^*)[J_q(k_1 \rho_i)]_-^+ + 4\pi \sqrt{\varepsilon_{r1}} \sum_{i=1}^{IC} k_o \rho_i \, Re(k_o E_{iq}) \cdot [J_q(k_1 \rho_i)]_-^+\} \tag{3.35c}$$

Note that for single mode operation the infinite summation on q is eliminated.

4.3 Equivalent Admittance of an Annular Slot

As an equivalent, principal-mode circuit representation, it is often desired to associate an admittance with each slot on the conducting boundaries. For this reason, we must define two quantities representing the slot current and voltage I_i, V_i. As a measure of the slot current, we define

$$I_i = 2\pi\rho_i H_\phi(\phi_o, \rho_i) \tag{3.36a}$$

where ρ_i is the average radius of the slot and ϕ_o is a reference value which for single mode operations can be taken as the angle for which H_ϕ is maximum. For voltage V_i we take

$$V_i = \int_{\rho_i^-}^{\rho_i^+} \vec{E}(\rho', \phi_o) \cdot \hat{\rho} d\rho' \tag{3.36b}$$

The admittance characterizing the ith slot is then defined by

$$Y_i = \frac{I_i}{V_i} \tag{3.36c}$$

In the next section, the equivalent admittance of a single slot as a function of its radius is computed with the aid of the above definitions. The effects of the higher order modes on the admittance value and the field distribution of the slot are also investigated.

3.4.1 Effects of the Higher Order Modes on the Admittance and Field of the Slot

Based on the theory presented in the earlier sections, the admittance of an annular slot, coupling two radial waveguides, is computed as a function of the radius of its leading edge. The thicknesses of the

waveguides are smaller than half the intrinsic wavelength, therefore, only the dominant mode propagates. The conductance and the susceptance terms are depicted in figures 3.3a, 3.3b, respectively. The ratio of the radii of the slot edges is kept constant and equal to 2.36 (a TM_{00} excitation is assumed). In order to study the effects of the higher order modes excited by the slot discontinuity on the equivalent admittance, the results obtained by taking only the propagating mode are also shown, the dotted lines. Whereas, the solid lines are due to the inclusion of the first ten modes which was observed to be sufficient to yield a convergent solution for all the examples presented in this thesis. These results indicate that for most applications, the dominant mode representation, such as that in the transmission line theory, adequately describes the slot admittance. However, the accuracy of the results, particularly for central slots where $k\rho$ is small, is not satisfactory. As a further check on the dominant mode approximation, the field distribution over the slot is also calculated and is shown in figures 3.4a, 3.4b. The slot is located at a radial distance $k\bar{\rho} = 2.00$ which corresponds to the last plotted point of figure 3.3. For this calculation, due to the large electrical width of the slot, the aperture is divided into 13 cells (annular rings) of equal width. The tangential electrical field over each cell, which for the TM_{00} excitation is equal to E_ρ, is then computed by applying the continuity of the tangential magnetic field in an average sense. Comparing the results, one notes that the dominant mode theory yields reasonable results for the field magnitude, except in the vicinity of the slot's leading edge. On the other hand, it fails to describe the phase of the field accurately. The actual phase of the slot field which is calculated by including higher order modes excited by the slot discontinuity is virtually constant across the aperture.

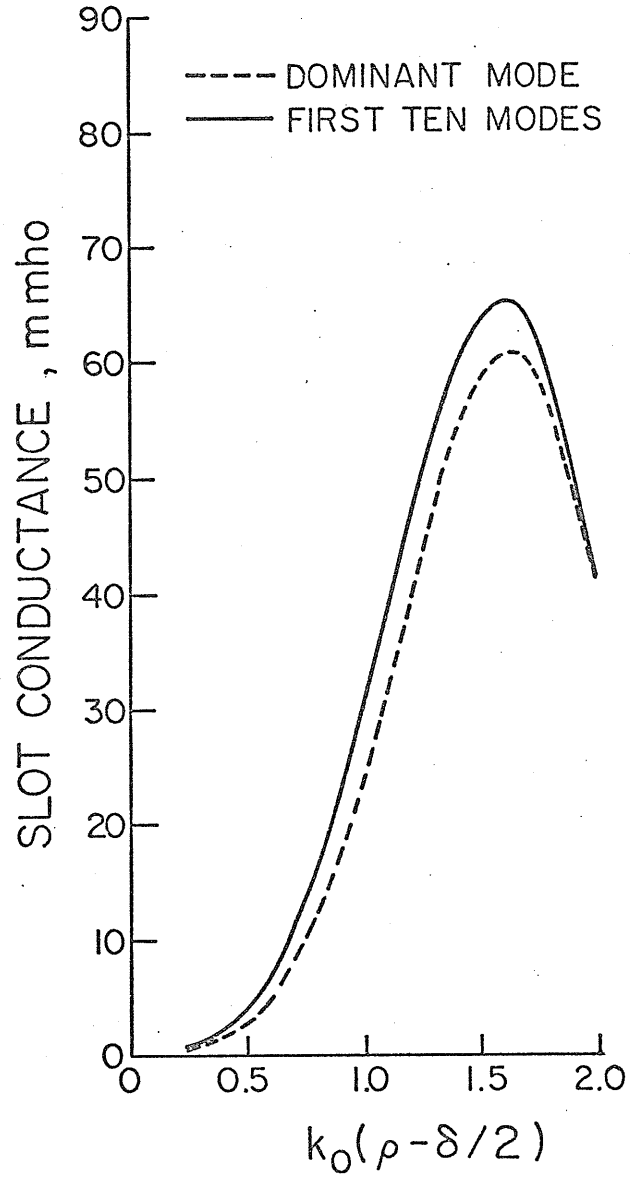

Figure 3.3a: Effect of higher order modes on the equivalent conductance of the slot. Ratio of the edges = 2.36, $k_o a = k_o b = 0.49$, $\varepsilon_{r1} = \varepsilon_{r2} = 1.00$, k_o is free space propagation constant. TM_{00} exciting mode.

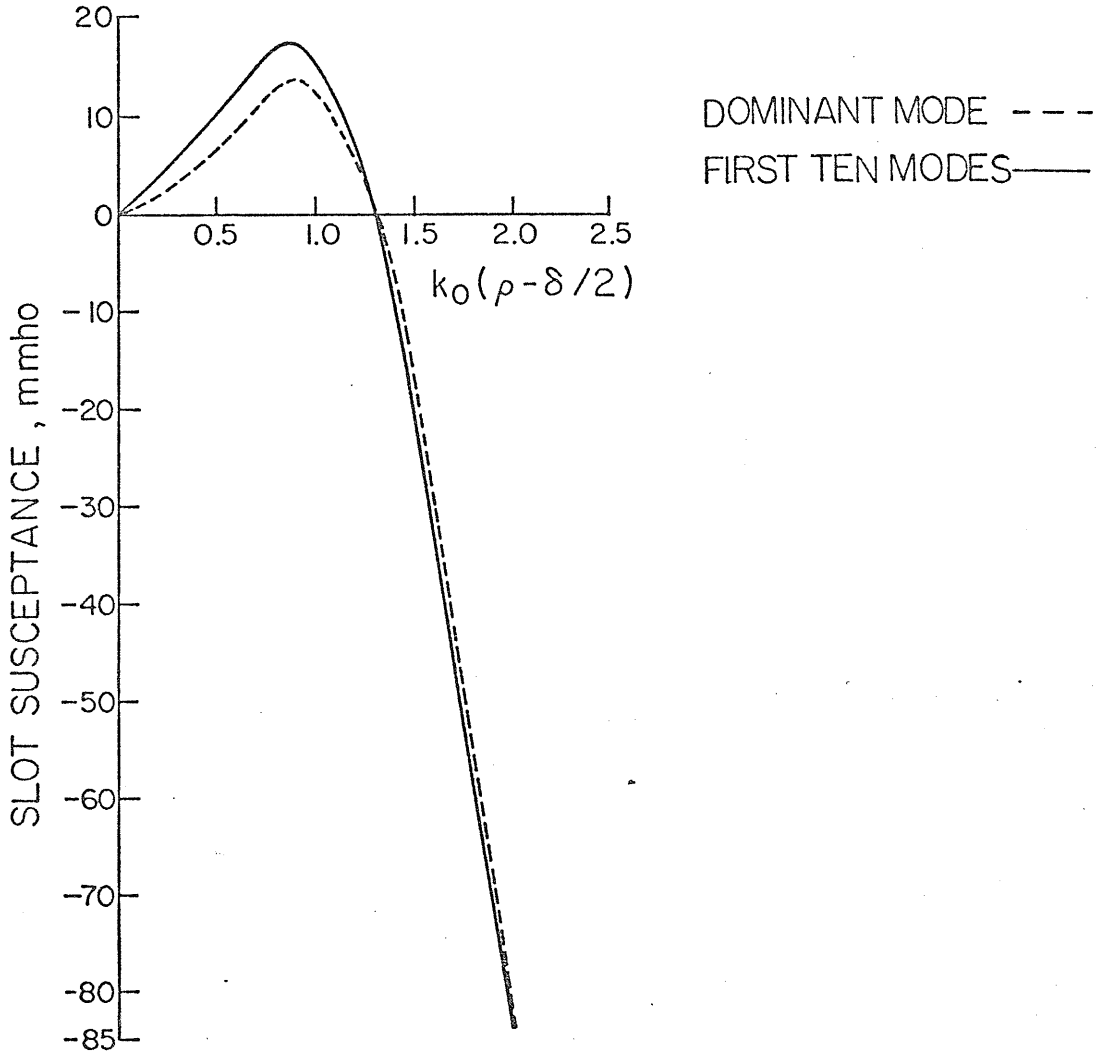

Figure 3.3b: Effect of higher order modes on the equivalent susceptance of the slot

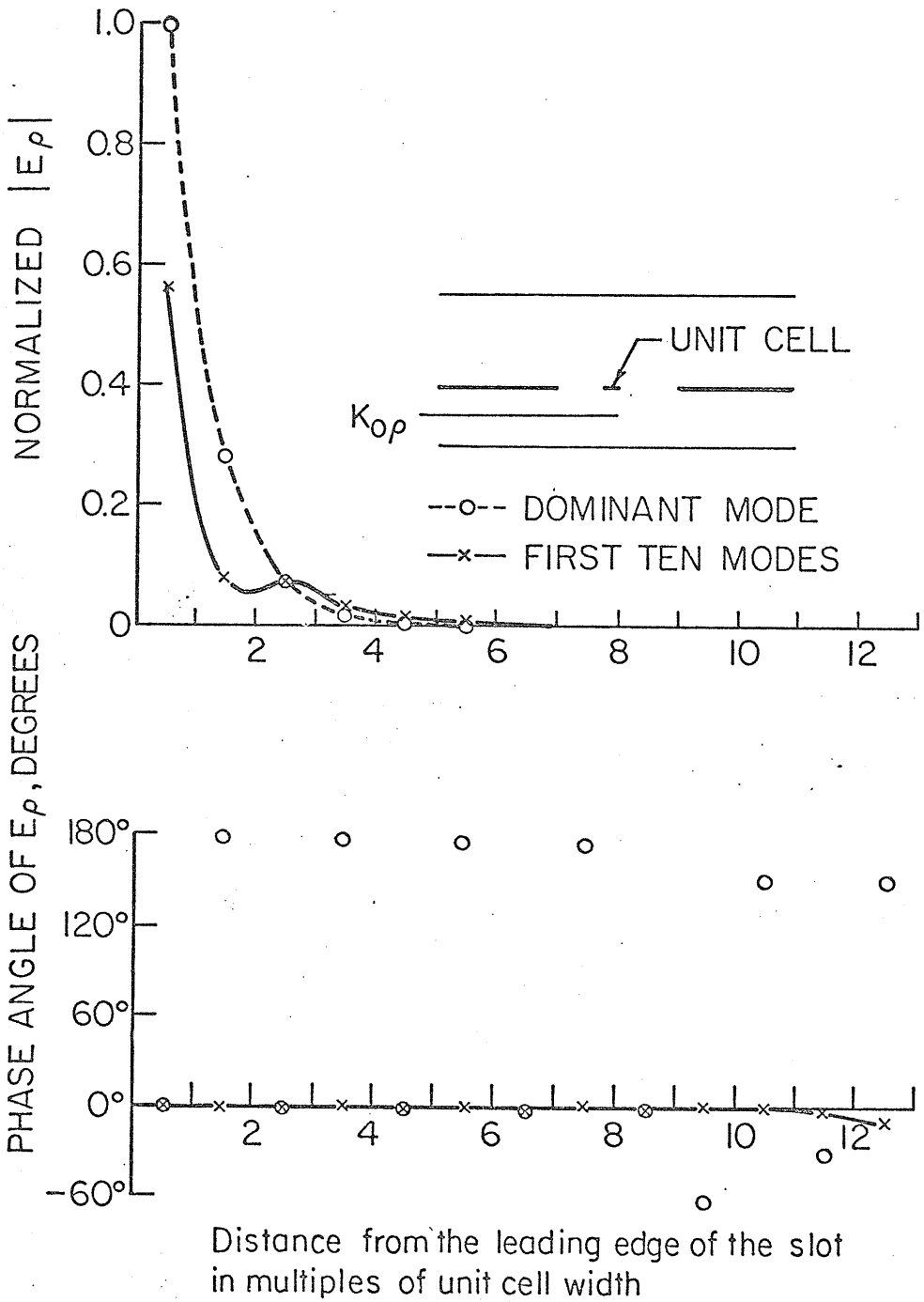

Figure 3.4: Amplitude and phase distributions over the slot, $k_o\delta = 2.72$, $k_o\rho = 3.36$, $k_o a = k_o b = 0.49$, $\varepsilon_{r1} = \varepsilon_{r2} = 1.00$, TM_{00} exciting mode.

Whereas, the result due to the dominant mode alone oscillates between 0 and 180 degrees for adjacent matching points. These calculations also show that the field distribution of an annular slot is similar to the current distribution on a conducting strip illuminated by a plane wave [51]. It should also be noted that even though the dominant mode approximation gives inaccurate phase distribution, it yields a reasonably accurate result for the equivalent slot voltage defined by equation (3.3b). This is due to the fact that the voltage depends on the integral of the slot field and the phase oscillation compensates for inaccuracies in the slot field amplitude. As a result, the slot admittance calculated by the dominant mode alone has a reasonable accuracy.

3.5 Filtering Characteristics of Two Coupled Radial Waveguides

Two dimensional arrangement of annular slots to form resonant arrays are of practical interest for applications as band-pass or band-stop filters. The filtering characteristic can be controlled by varying the dimensions of the slots, their relative locations, the waveguide thickness and the constitutive parameters of the two coupled regions. In the methods based on the waveguide transmission line concept, the coupling due to the external field (upper waveguide region) is generally overlooked. However, as it is shown in table 3.1, depending on the arrangement of the slots and their electrical dimensions, the external coupling can become so strong as to cause part of the radiated power to be recoupled back into the waveguide containing the exciting source. The geometry is formed by five annular slots of widths $k_o\delta = 0.20$, separated by a distance $k_o x = 2.00$ located on the common boundary. Since the slots are electrically thin, the calculations are carried out by representing each slot by

Slot No.	Power Coupled by Each Slot (Percentage of Total Power)
1	+ 8.49
2	+ 2.11
3	-23.32
4	- 2.77
5	+52.00
Total Coupled Power	+36.51

Table 3.1: Contribution of each slot to the total power coupled into the waveguide number two, TM_{00} exciting mode.

$N = 5$

$\varepsilon_{r1} = 2.55$

$\varepsilon_{r2} = 1.00$

$k_o\delta = 0.20$

$k_o\rho_1 = 4.00$

$k_o x = 2.00$

$k_o a = 0.25$

$k_o b = 0.49$

a single cell. That is, each slot is characterized by a constant complex field E_i which is found by matching the average of the magnetic field over its surface. The results for the coupled power by individual slots show that the external coupling is quite strong and causes a portion of the already coupled power to be returned back into the exciting waveguide through the slots 3 and 4. An equivalent transmission line representation is then a negative slot conductance (a source) associated with the respective elements.

Figures 3.5 - 3.7 are intended to show the application of annular arrays as band-pass filters. The filtering characteristics of a single slot excited by a TM_{00} radial mode is shown in figure 3.5. It is interesting to note that by a proper selection of the geometry, a single narrow slot can effectively couple a major part of the total power to the upper waveguide over a wide frequency band with a sharp cut-off characteristic.

More selective filtering response can be obtained by increasing the number of slots. Figure 3.6 illustrates the transfer function of a filter having four slots as its coupling elements for the TM_{00} excitation mode. All the dimensions given are at the frequency f_o and k_o is the free space propagation constant. The response of the same geometry to the TM_{01} exciting mode is depicted in figure 3.7. The resonance peak is slightly shifted toward the higher frequencies and the bandwidth is decreased compared to the TM_{00} mode of operation. To demonstrate the sensitivity of the filtering characteristic to the slot spacing, $k_o x$ is increased by an amount equal to four per-cent of its value for the solid line and the result is indicated by the dotted curve.

In conclusion, the work of this chapter establishes a method of solution for the electromagnetic field inside a radial waveguide in the

presence of annular and cylindrical type discontinuities in the waveguide region. The forcing function may be of a general nature, however, the geometrical interruptions are assumed to be electrically thin enough as to only support azimuthal directed current distributions (electric or magnetic) on the surface of the scattering bodies. The inclusion of the fictitious magnetic current distribution in the general formulation proves to be useful for treating problems involving coupled waveguides by annular shaped apertures on the common boundary. One possible application of the method is in the design and fabrication of microwave printed-circuit strip-line filters with band-pass characteristics.

Another possible application is in the design of annular slot array antennas for producing pencil beam radiation patterns. However, treating these types of geometries requires solution to the field excited by an annular slot of a finite width on a conducting plane radiating into a semi-infinite region. The next chapter is devoted to the development and formulation of problems of this nature.

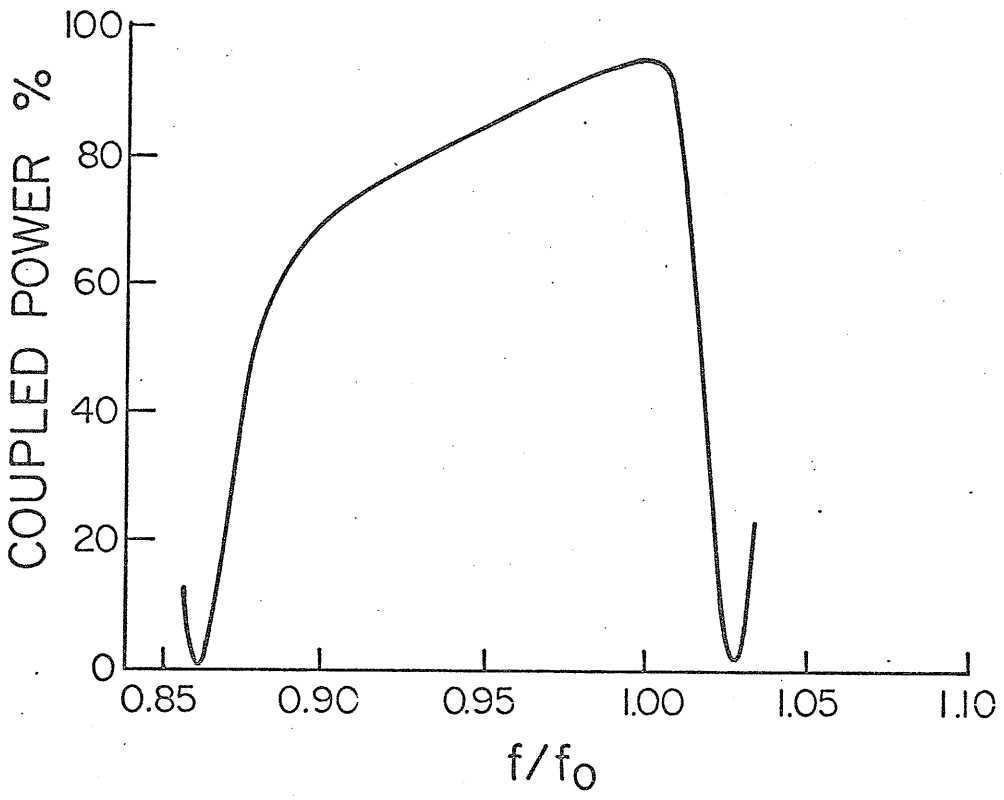

Figure 3.5: Filter characteristic of a single slot, TM_{00} exciting mode. $\varepsilon_{r1} = 2.60$, $\varepsilon_{r2} = 5.20$, $k_o a = 0.34$, $k_o b = 0.04$, $k_o \delta = 0.05$, $k_o \rho = 8.39$. All dimensions are at f_o.

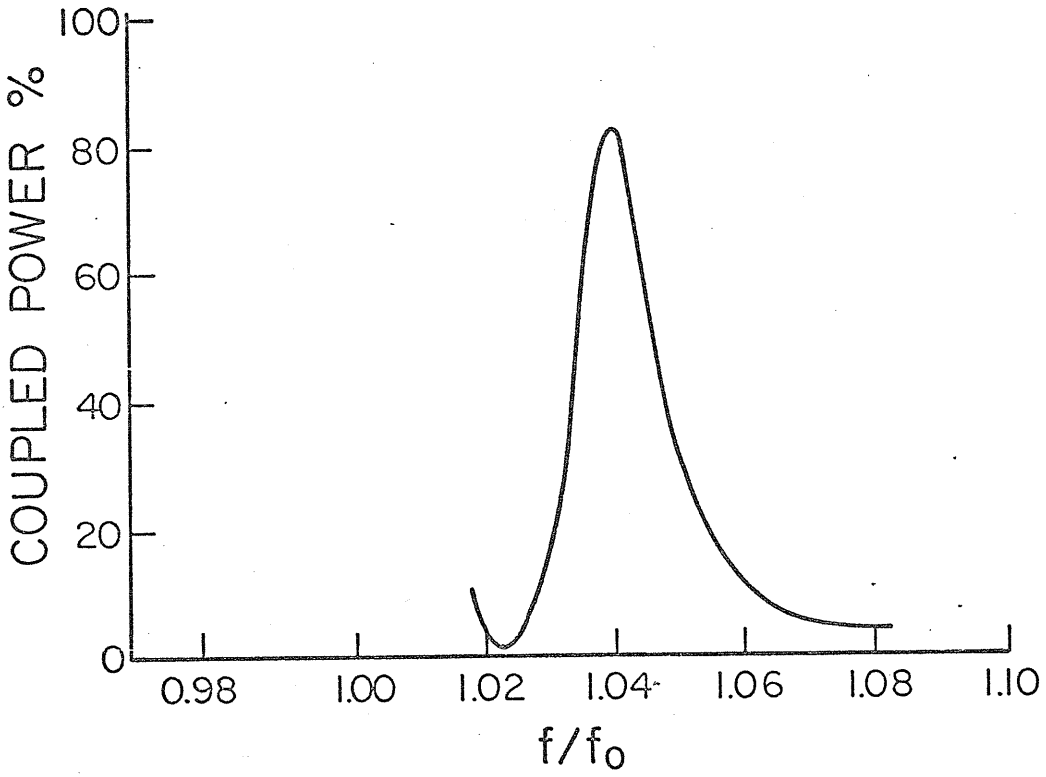

Figure 3.6: Filter characteristics of four slots, TM_{00} exciting mode. $\varepsilon_{r1} = 2.60$, $\varepsilon_{r2} = 5.20$, $k_o a = k_o b = 0.34$, $k_o \delta = 0.08$, $k_o \rho = 10.08$, $k_o x = 4.05$.

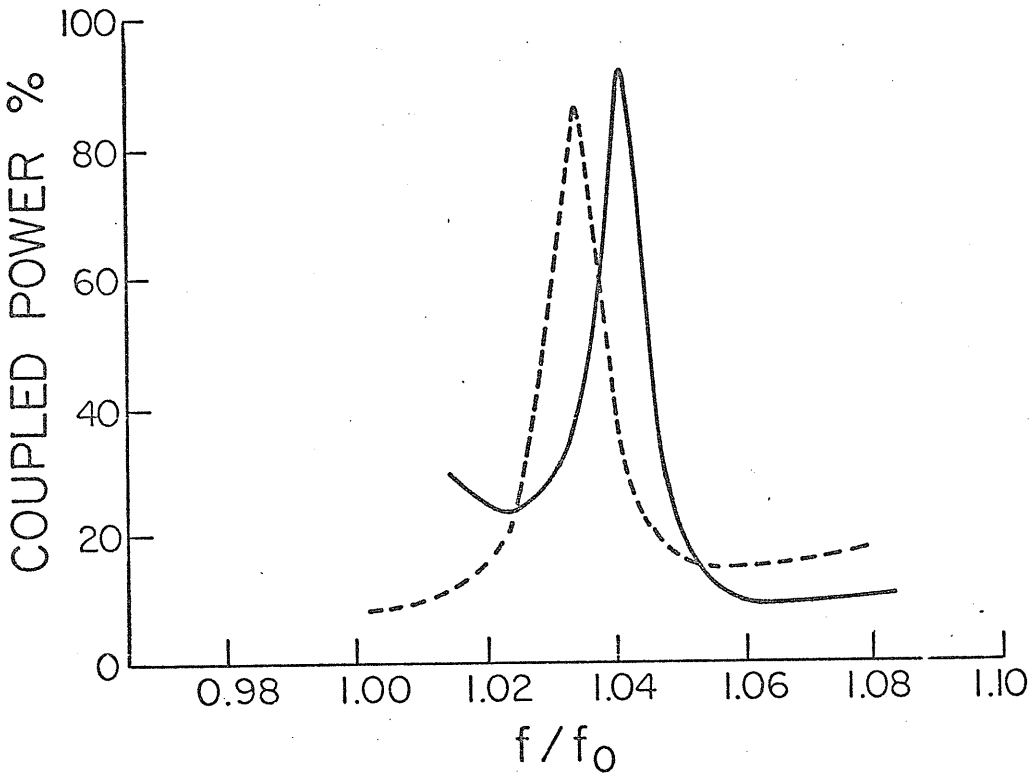

Figure 3.7: Filtering response of the same geometry as in Figure 3.6, TM_{01} mode of operation. The dotted curve is due to a 4% increase in slot spacing $k_o x$.

CHAPTER IV

FIELD SOLUTION FOR ANNULAR SLOT ARRAYS FED BY RADIAL WAVEGUIDES

4.1 Introduction

Slot arrays in conducting surfaces have drawn considerable interest for applications as flush-mounted antennas for use in aircrafts and spacecrafts. With the exception of structures using isolated feed assembly for individual slots [52], such antennas are formed by cutting slots on one side of a waveguide which is also used as the feeding system for the slot array. The array elements are successively fed by a travelling wave inside the waveguide. This form of excitation eliminates the aperture blockage problems usually faced in the design process of reflecting type aperture antennas.

Among slotted structures, annular type apertures have also been of interest for applications as low profile antennas. However, due to mathematical complexity generally associated with problems involving aperture coupling, existing design techniques are mostly based on overly simplified models. This in turn imposes a number of restricting conditions which limit the range of applicability of these techniques in providing acceptable results.

Earlier investigations of the problems of annular type apertures were generally based on assuming a field distribution over the aperture and then solving for the radiated field in the external region [53]. However, for waveguide fed arrays where the strong coupling between the array members is the determining factor for aperture field distribution, this approach does not yield the required information for design purposes. The

mutual coupling in these cases can become so strong as to turn a resonant slot, when isolated, into a predominantly reactive one when placed in an array of slots.

As it was mentioned earlier, a procedure commonly used for treating waveguide fed slot arrays is an extension of transmission line theory to waveguide structures. However, this method is unable to account for higher order modes excited by the slot discontinuities. Furthermore, the coupling effects of the external region are totally disregarded in this manner.

Earlier works dealing with cavity or waveguide fed annular type aperture antennas in which attention is paid to higher order modes excited by the geometrical interruptions are based on assuming a uniform forcing function (no ϕ variation) giving rise to a TM field in the two regions. Furthermore, the problems of mutual coupling are avoided by considering single slot structures.

In the present work, a new type of slot antenna is considered, figure 4.1. Concentric annular slots are arrayed on one side of a radial waveguide. The conducting walls of the guide may be supported by a dielectric substrate (with or without loss). The slots are of finite widths δ_m located at radii $\rho = \rho_m$. The exciting source is placed at the central region of the guide and its field may be of a general nature. Again, the slots are assumed to be electrically thin enough as to suppress radially directed induced currents (magnetic) over their surfaces.

We develop the formulation for the field in the semi-infinite region by first constructing the appropriate Green's functions. These functions describe the impulse response to a magnetic current ring (annular slit) on the common boundary of the interior and the exterior regions.

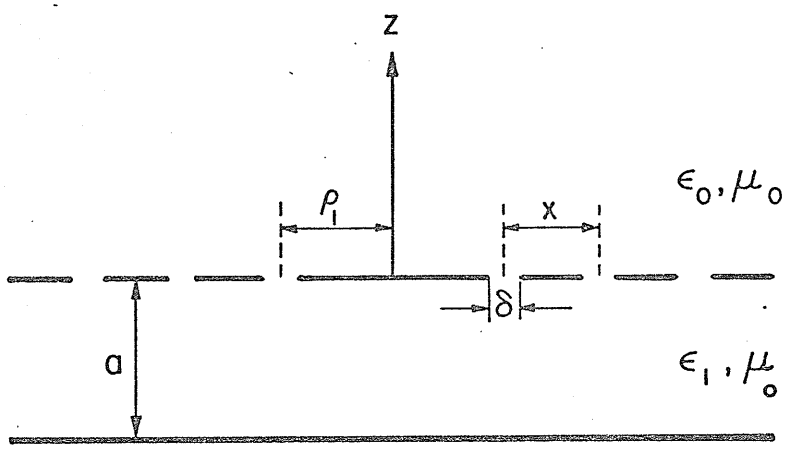

Figure 4.1: Typical radial waveguide fed annular slot array antenna of infinite extent.

Then, the final formulation is achieved by integrating the impulse response over the aperture field distribution in a similar manner as was described in the previous chapter.

In the next section, the appropriate Green's functions for the exterior region (semi-infinite space) is constructed and the external field will be formulated in terms of these functions. The expressions for the field components in the feeding guide are obtained in Chapter III and are used for the problem under consideration.

Even though the present study is mainly oriented toward a solution to annular slot array antennas, for the sake of completeness the appropriate Green's functions of electric type are also derived by a simple application of the concept of duality [49]. This would enable one to formulate problems dealing with annular or cylindrical type sources or scattering bodies in free space.

4.2 Problem Formulation and Solution

4.2.1 Construction of the Appropriate Green's Functions, Magnetic Ring

In deriving the appropriate Green's functions for the problem depicted in figure 4.2, we utilize the properties of a set of Hankel Transforms of order n [55]. The basic principle is to transform the wave equation into its spacial frequency domain counterpart. The Green's functions are then constructed by imposing the constraints on the field components. The result is then transformed to the spacial domain, using the Hankel Transform. Evaluation of the infinite integrals is discussed in the subsequent sections.

Consider the geometry shown in figure 4.2a. An annular slot on a conducting plane of infinite extent may be viewed as an annular distribution

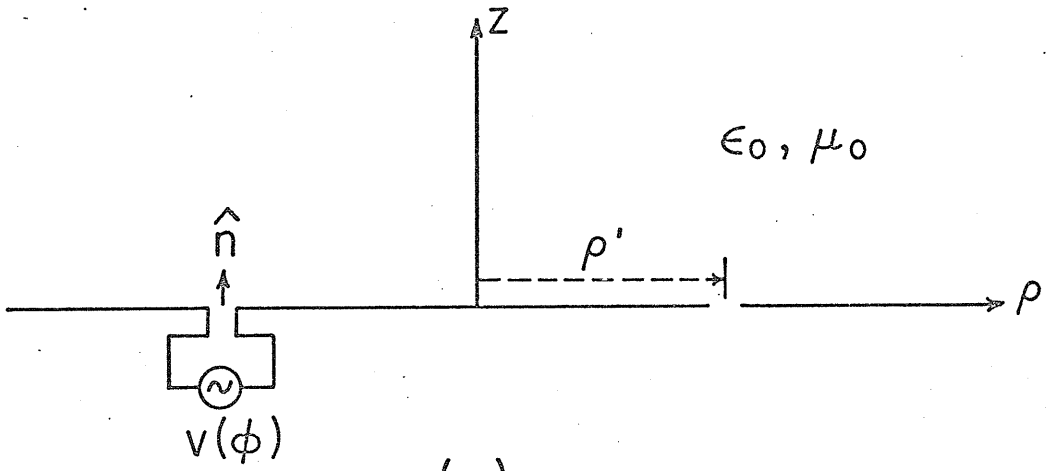

(a)

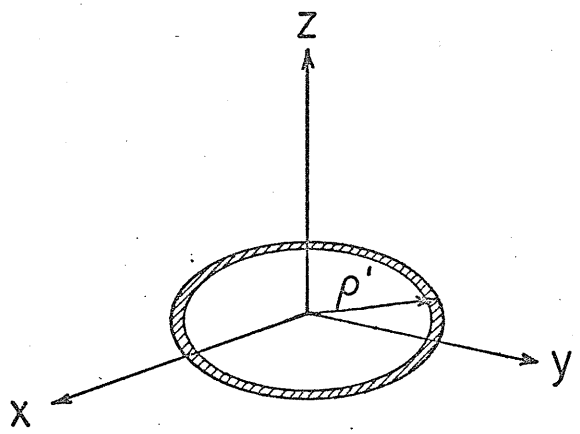

$$\vec{J}_m = -2\,v(\phi)\,\delta(\rho-\rho')\,\delta(z)\,\hat{\phi}$$

(b)

Figure 4.2: A delta-function generated annular slit on an infinite ground plane and the equivalent problem.

of magnetic surface current given by

$$\vec{J}_{ms} = \vec{E}_{aperture} \times \hat{n} \tag{4.1}$$

where $\hat{n}$ is the unit normal of the aperture. For an infinitely thin slot (slit), the magnetic current filament can be characterized by

$$\vec{J}_{ms} = - V(\phi') \, \delta(\rho - \rho') \hat{\phi}' \tag{4.2}$$

where $V(\phi)$ is a piece-wise continuous function of the azimuthal angle ϕ', representing the equivalent voltage across the infinitesimal gap and ρ', ϕ' are the source coordinates. $\hat{\phi}'$ is a unit vector tangent to the current ring and represents the direction of the current flow. We expand the source strength $V(\phi')$ in terms of Fourier series as

$$V(\phi') = \sum_{m=0}^{\infty} (a_n \cos n\phi' + b_n \sin n\phi') \quad 0 \leq \phi' \leq 2\pi \tag{4.3a}$$

where

$$a_n = \frac{\varepsilon_n}{2\pi} \int_0^{2\pi} V(\phi') \cos n\phi' \, d\phi'$$

$$b_n = \frac{\varepsilon_n}{2\pi} \int_0^{2\pi} V(\phi') \sin n\phi' \, d\phi' \tag{4.3b}$$

$$\varepsilon_n = \begin{cases} 1 & n = 0 \\ 2 & n \neq 0 \end{cases}$$

Now, an arbitrary electromagnetic field in a homogeneous cylindrical region can be expressed as the sum of the TM (E waves) and the TE (H waves) fields to the z-direction, equations (3.3). The proper forms for the wave functions ψ^e and ψ^h can be determined by an application of the Hankel Transforms. The transform pairs of order n of a function $\psi(\rho, \phi, z)$ are defined as

$$\bar{\psi}(\alpha, \phi, z) = \int_0^{\infty} \psi(\rho, \phi, z) \, J_n(\alpha\rho) \rho \, d\rho \tag{4.4a}$$

$$\psi(\rho, \phi, z) = \int_0^\infty \bar{\psi}(\alpha, \phi, z)\, J_n(\alpha\rho)\alpha d\alpha \tag{4.4b}$$

In view of the periodic nature of the geometry in the azimuthal direction, the wave equation in cylindrical coordinates is expressed as [49]

$$\frac{\partial^2\psi}{\partial\rho^2} + \frac{1}{\rho}\frac{\partial\psi}{\partial\rho} - \frac{n^2}{\rho^2}\psi + \frac{\partial^2\psi}{\partial z^2} + k_o^2\psi = 0 \tag{4.5a}$$

where

$$k_o = \omega\sqrt{\varepsilon_o\mu_o} \tag{4.5b}$$

Taking the Hankel transform of (4.5a) by using (4.4b) and expressions available for the derivatives of a function as [55]

$$\int_0^\infty \rho\left(\frac{d^2f}{d\rho^2} + \frac{1}{\rho}\frac{df}{d\rho} - \frac{n^2}{\rho^2} f\right) J_n(\alpha\rho)d\rho = -\alpha^2\bar{f} \tag{4.6a}$$

one obtains

$$\left(\frac{\partial^2}{\partial z^2} - \gamma^2\right)\bar{\psi}\,(\alpha, \phi, z) = 0 \tag{4.6b}$$

where

$$\gamma = (\alpha^2 - k_o^2)^{1/2} \tag{4.6c}$$

γ so defined is a double valued function, therefore, a unique value requires defining a specific branch by invoking the physical constraints of the problem. This will be done in a later section; however, at this point, it is assumed that the appropriate branch has been selected and it suffices to say that γ may have a complex value of the following form

$$\gamma = \gamma' + j\gamma'' \qquad \gamma', \gamma'' > 0 \quad \text{for all} \quad \alpha \tag{4.6d}$$

Hence, we proceed to express the wave functions of e and h types in terms of suitable sets of mode functions with unknown coefficients. To this end, as an anticipation for relating the field components to their source $V(\phi)$ and in view of equation (4.6b) we take

$$\bar{\psi}^e(\alpha, \phi, z) = \sum_{n=0}^{\infty} (a_n \cos n\phi + b_n \sin n\phi) [U_n^e(\alpha) e^{-\gamma z} + u_n^e(\alpha) e^{\gamma z}] \quad (4.7a)$$

$$\bar{\psi}^h(\alpha, \phi, z) = \sum_{n=0}^{\infty} (b_n \cos n\phi - a_n \sin n\phi) [U_n^h(\alpha) e^{-\gamma z} + u_n^h(\alpha) e^{\gamma z}] \quad (4.7b)$$

Since $\psi(\rho, \phi, z)$ must behave according to the radiation condition at large distances, considering (4.6d), the appropriate forms for $\bar{\psi}^e$ and $\bar{\psi}^h$ in the semi-infinite region are obtained by setting u_n^e and u_n^h in equation (4.7) equal to zero which leads to

$$\bar{\psi}^e(\alpha, \phi, z) = \sum_{n=0}^{\infty} (a_n \cos n\phi + b_n \sin n\phi) U_n^e(\alpha) e^{-\gamma z} \quad (4.8a)$$

$$\bar{\psi}^h(\alpha, \phi, z) = \sum_{n=0}^{\infty} n(b_n \cos n\phi - a_n \sin n\phi) U_n^h(\alpha) e^{-\gamma z} \quad (4.8b)$$

From the boundary conditions, E_ϕ component of the field must vanish over the conducting plane, including the edges of the slit (edge condition) [56], that is

$$E_\phi = 0 \qquad \begin{matrix} 0 \leq \phi \leq 2\pi \\ 0 \leq \rho < \infty \\ z = 0 \end{matrix} \quad (4.9a)$$

However, E_ρ component of the field is singular at the edges, hence, we may represent it by

$$E_\rho = V(\phi)\, \delta(\rho - \rho') \qquad \begin{matrix} 0 \leq \phi \leq 2\pi \\ 0 \leq \rho < \infty \\ z = 0 \end{matrix} \quad (4.9b)$$

Therefore, using (4.9), (4.8), (4.4b) and recalling the relations for E_ϕ and E_ρ in terms of the e and h type wave functions, equations (3.3b), one finds

$$- \frac{1}{j\omega\varepsilon_o} \sum_{n=0}^{\infty} (a_n \cos n\phi + b_n \sin n\phi) \int_o^{\infty} \gamma\alpha^2 J_n'(\alpha\rho)\ U_n^e(\alpha)\, d\alpha$$

$$+ \frac{1}{\rho} \sum_{n=0}^{\infty} n^2 (a_n \cos n\phi + b_n \sin n\phi) \cdot \int_o^{\infty} \alpha J_n(\alpha\rho)\ U_n^h(\alpha)\, d\alpha = V(\phi)\ \delta(\rho - \rho') \tag{4.10a}$$

$$- \frac{1}{j\omega\varepsilon_o\rho} \sum_{n=0}^{\infty} n(b_n \cos n\phi - a_n \sin n\phi) \int_o^{\infty} \gamma\alpha J_n(\alpha\rho)\ U_n^e(\alpha)\, d\alpha$$

$$+ \sum_{n=0}^{\infty} n(b_n \cos n\phi - a_n \sin n\phi) \cdot \int_o^{\infty} \alpha^2 J_n'(\alpha\rho)\ U_n^h(\alpha)\, d\alpha = 0 \tag{4.10b}$$

where $V(\phi)$ is given by equation (4.3a). Using the orthogonality relations for sinusoidal functions over the range $0 \leq \phi \leq 2\pi$, the above set of equations can be reduced to

$$- \frac{1}{j\omega\varepsilon_o} \int_o^{\infty} \gamma\alpha^2 J_n'(\alpha\rho)\ U_n^e(\alpha)\, d\alpha + \frac{n^2}{\rho} \int_o^{\infty} \alpha J_n(\alpha\rho)\ U_n^h(\alpha)\, d\alpha = \delta(\rho - \rho') \tag{4.11a}$$

$$- \frac{n}{j\omega\varepsilon_o\rho} \int_o^{\infty} \gamma\alpha J_n(\alpha\rho)\ U_n^e(\alpha)\, d\alpha + n \int_o^{\infty} \alpha^2 J_n'(\alpha\rho)\ U_n^h(\alpha)\, d\alpha = 0 \tag{4.11b}$$

An addition of the above two equations leads to

$$- \frac{1}{j\omega\varepsilon_o} \int_o^{\infty} \gamma\alpha^2 J_{n-1}(\alpha\rho)\ U_n^e(\alpha)\, d\alpha + n \int_o^{\infty} \alpha^2 J_{n-1}(\alpha\rho)\ U_n^h(\alpha)\, d\alpha = \delta(\rho - \rho') \tag{4.12a}$$

and their subtraction yields

$$\frac{1}{j\omega\varepsilon_o} \int_o^{\infty} \gamma\alpha^2 J_{n+1}(\alpha\rho)\ U_n^e(\alpha)\, d\alpha + n \int_o^{\infty} \alpha^2 J_{n+1}(\alpha\rho)\ U_n^h(\alpha)\, d\alpha = \delta(\rho - \rho') \tag{4.12b}$$

where a use has been made of the available relations for the derivatives of Bessel functions in the form [50]

$$J_n'(z) = J_{n-1}(z) - \frac{n}{z} J_n(z)$$

$$J_n'(z) = \frac{n}{z} J_n(z) - J_{n+1}(z) \tag{4.12c}$$

Now, taking the Hankel Transform of order $(n - 1)$ and $(n + 1)$ of equations (4.12a) and (4.12b) respectively, and utilizing the properties of delta functions, one obtains a set of equations which after solving for the coefficients result in

$$U_n^e(\alpha) = -j\omega\varepsilon_o\rho' \frac{J_n'(\alpha\rho')}{\gamma\alpha} \tag{4.13a}$$

$$U_n^h(\alpha) = \frac{J_n(\alpha\rho')}{\alpha^2} \tag{4.13b}$$

The above coefficients in conjunction with equations (3,3), (4,3), (4.4b) and (4.7) uniquely define the electromagnetic field set up by an annular slit of strength $V(\phi)$ over an infinite conducting plane. The evaluation of the generated infinite integrals for obtaining the field components in the space domain is described later.

Note that by substituting (4.13) and (4.11), one obtains identities in the form

$$\rho' \int_o^\infty J_n(\alpha\rho)\, J_n'(\alpha\rho')d\alpha + \rho \int_o^\infty J_n'(\alpha\rho)\, J_n(\alpha\rho')d\alpha = 0 \tag{4.14a}$$

$$\rho' \int_o^\infty J_n'(\alpha\rho)\, J_n'(\alpha\rho')\alpha d\alpha + \frac{n^2}{\rho} \int_o^\infty \frac{1}{\alpha} J_n(\alpha\rho)\, J_n(\alpha\rho')d\alpha = \delta(\rho - \rho') \tag{4.14b}$$

Proof of the above identities which ensures satisfaction of the boundary condition over the surface of the conducting plane is given in Appencix C.

4.2.2 Electric Ring

The field generated by an annular slit cut on a conducting plane of infinite extent was derived in the previous section. According to equivalence principle [49], as far as the field in the semi-infinite region

defined by $z \geq 0$ is concerned, the problem is equivalent to a magnetic current ring placed in front of an infinite ground plane and characterized by

$$\vec{J}_m = I_m(\phi')\ \delta(\rho - \rho')\ \delta(z)\hat{\phi}' \tag{4.15}$$

where, $I_m(\phi') = -V(\phi')$ and the source is radiating in presence of the infinite ground plane. Using the Image Theory [49], the result is also valid for a geometry as illustrated in figure 4.2b, where, the strength of the source is now given by $-2V(\phi')$ and is radiating in free space. The field components for this source can be derived from equations (3.3) by substituting the following results developed in the earlier section for ψ^e and ψ^h

$$\psi^e = -j\omega\varepsilon_o\rho' \sum_{n=0}^{\infty} (a_n \cos n\phi + b_n \sin n\phi) \int_o^{\infty} \frac{1}{\gamma} J_n'(\alpha\rho')\ J_n(\alpha\rho)\ e^{-\gamma z}\ d\alpha \tag{4.16a}$$

$$\psi^h = \sum_{n=0}^{\infty} n(b_n \cos n\phi - a_n \sin n\phi) \int_o^{\infty} \frac{1}{\alpha} J_n(\alpha\rho')\ J_n(\alpha\rho)\ e^{-\gamma z}\ d\alpha \tag{4.16b}$$

Using the concept of duality for electromagnetic fields [49], it is straight forward to derive the field set up by an electric current filament characterized by

$$\vec{J} = I(\phi')\ \delta(\rho - \rho')\ \delta(z)\hat{\phi} \tag{4.17}$$

This can be done by replacing $E \rightarrow -H$, $H \rightarrow E$ and $\varepsilon \rightleftarrows \mu$ in equations 3.3a. These transformations modify the set of vectorial equations to

$$\begin{aligned} \vec{E} &= -\nabla \times (-\hat{z}\ \psi^e) + \frac{1}{j\omega\varepsilon} \nabla \times \nabla \times (\hat{z}\ \psi^h) \\ \vec{H} &= \nabla \times (\hat{z}\ \psi^h) + \frac{1}{j\omega\mu} \nabla \times \nabla \times (-\hat{z}\ \psi^e) \end{aligned} \tag{4.18}$$

Comparing (4.18) against (3.3a), one concludes that the solution for the electric current filament can simply be obtained by replacing ψ^h by

$-\psi^e$, ψ^e by ψ^h and exchanging ε_o and μ_o in the respective relations derived for the magnetic ring. The final result is of the following form

$$\psi^e = \frac{1}{2} \sum_{n=0}^{\infty} n(b_n \cos n\phi - a_n \sin n\phi) \int_o^{\infty} \frac{1}{\alpha} J_n(\alpha\rho') J_n(\alpha\rho) e^{-\gamma z} d\alpha \quad (4.19a)$$

$$\psi^h = \frac{1}{2} j\omega\mu_o\rho' \sum_{n=0}^{\infty} (a_n \cos n\phi + b_n \sin n\phi) \int_o^{\infty} \frac{1}{\alpha} J_n'(\alpha\rho) J_n(\alpha\rho) e^{-\gamma z} d\alpha \quad (4.19b)$$

where a_n and b_n are the Fourier coefficients obtained by expanding $I(\phi')$ over the range $0 \leq \phi' \leq 2\pi$. The appearance of the factor $\frac{1}{2}$ in equations (4.19) is related to the way that a_n and b_n are defined in the two cases.

Equations (4.19) together with (3.3b) and (4.17) uniquely define the field set up by an electric current ring of strength $I(\phi')$ located at a point $\rho = \rho'$, $z = 0$. The coefficients a_n and b_n are defined by similar relations as equations (3.2b).

4.3 A Note on the Branch Cuts of the Function $\gamma = (\alpha^2 - k_o^2)^{1/2}$

As it was discussed earlier, γ so defined is a double-valued function in the complex α-plane. Therefore, it is necessary to specify the branch of γ function in order to uniquely define the representation given in (4.6c). This is done by invoking the radiation condition, which specifies, either an outgoing or evanescent wave for large $r = \sqrt{\rho^2 + z^2}$. The details of the principle involved can be found in [56], [57] (with $e^{-j\omega t}$ time convention), and is briefly discussed here.

The Green's functions for half space are proportional to integrals of the types

$$I_1 = \int_0^\infty \frac{1}{\alpha} J_n(\alpha\rho') J_n(\alpha\rho) e^{-\gamma z} d\alpha \tag{4.20a}$$

$$I_2 = \int_0^\infty \frac{1}{\gamma} J_n'(\alpha\rho') J_n(\alpha\rho) e^{-\gamma z} d\alpha \tag{4.20b}$$

Using the relation expressing the Bessel function is terms of the Hankel functions of the first and second kind [50]

$$J_n(\alpha\rho) = \frac{1}{2} [H_n^{(2)}(\alpha\rho) + H_n^{(1)}(\alpha\rho)] \tag{4.21}$$

and noting the fact that both integrands are odd functions of α, the above infinite integrals can be transformed to

$$I_1 = \frac{1}{2} \int_{-\infty}^{\infty} J_n(\alpha\rho') H_n^{(2)}(\alpha\rho) e^{-\gamma z} d\alpha \tag{4.22a}$$

$$I_2 = \frac{1}{2} \int_{-\infty}^{\infty} \frac{1}{\gamma} J_n'(\alpha\rho') H_n^{(2)}(\alpha\rho) e^{-\gamma z} d\alpha \tag{4.22b}$$

where a use has been made of a change of variable, $\alpha \to \alpha e^{j\pi}$, in the integrand involving $H_n^{(1)}(\alpha\rho)$ and the expressions available for analytic continuation of Bessel functions are utilized [50]. The term $H_n^{(2)}(\alpha\rho)\, e^{-\gamma z}$ is recognized as that of a two-dimensional plane wave. Therefore, the rest of the integrand may be interpreted as the amplitude of a spectral plane wave with wave numbers α and $-j\gamma$. The radiation condition will be satisfied if I_1 and I_2 vanish for $r \to \infty$. This will be satisfied if the integrands in (4.22) vanish for either $\rho \to \infty$ or $z \to \infty$. For $H_n^{(2)}(\alpha\rho)$, the convergence of the integrands is assured by taking the integration path in regions for which the imaginary part of α is smaller or equal to zero. In order to ensure the convergence as $z \to \infty$, we must require,

$$\begin{aligned} \mathrm{Re}(\gamma) &\geq 0 \\ I_m(\gamma) &\geq 0 \end{aligned} \tag{4.23}$$

To avoid unnecessary mathematical complications, it is generally assumed that the medium under consideration is lossy, that is,

$$k_o = k_o' - jk_o'' \qquad \begin{matrix} k' \geq 0 \\ k'' > 0 \end{matrix} \tag{4.24}$$

The lossless case, then, can be viewed as the limiting case when k_o'' approaches zero. The conditions specified by (4,23) uniquely determine the location of the branch cut shown in figure 4.3. These lines correspond to the intersection of the two sheeted α plane. In each sheet γ is a single-valued analytic function of α. For the limiting case (lossless medium) as far as our analysis is concerned, the transition of γ from a purely imaginary value $(\alpha < k_o)$ to a positive real value $(\alpha > k_o)$ is then uniquely defined as,

$$\begin{aligned} \gamma &= j(k_o^2 - \alpha^2)^{1/2} && \alpha < k_o \\ \gamma &= (\alpha^2 - k_o^2)^{1/2} && \alpha > k_o \end{aligned} \tag{4.25}$$

Based on the theory presented earlier, the next section is devoted to demonstrate the application of the previous results to the problem of annular slot arrays of finite widths fed by radial waveguides.

4.4 Formulation of the Problem of a Waveguide-Fed Annular Slot Array Antenna

Employing a similar approach as Section 3.3.1, an annular slot on a conducting plane can be viewed as an annular distribution of magnetic surface current. The aperture field can be expanded into a Fourier series, equation (3.22), and the wave functions for the semi-infinite space can be obtained by integrating the product of $R(\rho')$ and the Green's functions, equations (4.19), over the aperture radial coordinate ρ'. To be more

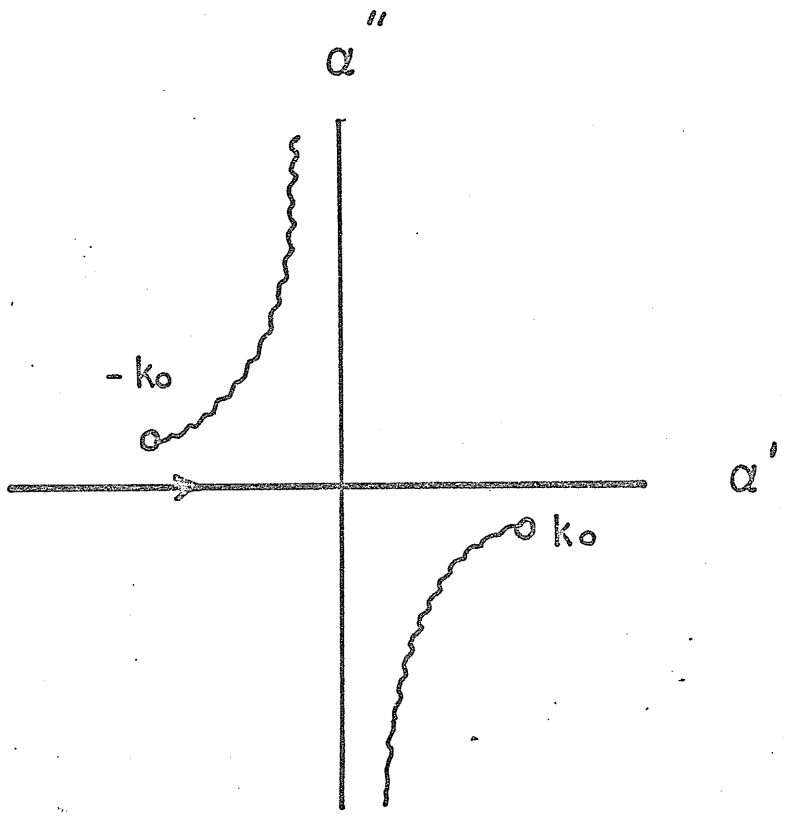

Figure 4.3: Branch cuts for $\gamma = (\alpha^2 - k_o^2)^{1/2}$

specific, TM_{pq} mode of the radial waveguide can be assumed to be incident, figure 4.1. This mode is characterized by

$$\psi^{e}_{inc_{pq}} = \cos\frac{p\pi}{a} z \cos q\phi \; H^{(2)}_{q}(k_{\rho p}\rho) \tag{4.26}$$

$$k_{\rho p} = [k^2 - (\frac{p\pi}{a})^2]^{1/2} \qquad k = \sqrt{\varepsilon\mu_o}$$

The wave functions due to the magnetic surface current over the coupling aperture for the semi-infinite region are specified by

$$\psi^{e}_{2} = -j\omega\varepsilon_o \sum_{\ell=1}^{L} \sum_{n=o}^{\infty} (a_n \cos n\phi + b_n \sin n\phi) \int_{+\rho_\ell}^{\bar{\rho}_\ell} \int_{o}^{\infty} \rho' \, J'_n(\alpha\rho') \, J_n(\alpha\rho) \, \frac{e^{-\gamma z}}{\gamma}$$

$$R_{\ell n}(\rho')d\rho'd\alpha \tag{4.27a}$$

$$\psi^{h}_{2} = \sum_{\ell=1}^{L} \sum_{m=0}^{\infty} n(b_n \cos n\phi - a_n \sin n\phi) \int_{-\rho_\ell}^{+\rho_\ell} \int_{o}^{\infty} J_n(\alpha\rho') \, J_n(\alpha\rho) \, \frac{e^{-\gamma z}}{\alpha}$$

$$R_{\ell n}(\rho')d\rho'd\alpha \tag{4.27b}$$

where L represents the total number of slots and $R_{\ell n}(\rho')$ is the nth mode's radial dependent part of the electric field over the ℓth aperture. The wave functions due to the slot for the waveguide region are similar to those derived earlier (Section 3.3.1) and for the present geometry can be expressed as

$$\psi^{e}_{1} = \frac{\pi\omega\varepsilon}{2a} \sum_{\ell=1}^{L} \sum_{m=0}^{\infty} \sum_{n=0}^{\infty} \frac{\varepsilon_m}{k_{\rho m}} (a_n \cos n\phi + b_n \sin n\phi) \cos\frac{m\pi}{a} z$$

$$\begin{matrix} H^{(2)}_n(k_{\rho m}\rho) \\ J_n(k_{\rho m}\rho) \end{matrix} \int_{-\rho_\ell}^{+\rho_\ell} \rho' R_{\ell n}(\rho') \begin{matrix} J'_n(k_{\rho m}\rho') \\ H^{(2)\prime}_n(k_{\rho m}\rho') \end{matrix} d\rho' \tag{4.28a}$$

$$\psi_1^h = -j \frac{\pi^2}{2a^2} \sum_{\ell=1}^{L} \sum_{m=0}^{\infty} \sum_{n=0}^{\infty} \frac{\varepsilon_m \, m \, n}{k_{\rho m}^2} (b_n \cos n\phi - a_n \sin n\phi) \sin \frac{m\pi}{a} z$$

$$\cdot \begin{matrix} H_n^{(2)}(k_{\rho m}\rho) \\ J_n(k_{\rho m}\rho) \end{matrix} \int_{\bar{\rho}_\ell}^{\rho_\ell^+} R_{\ell n}(\rho') \begin{matrix} J_n(k_{\rho m}\rho') \\ H_n^{(2)}(k_{\rho m}\rho') \end{matrix} d\rho' \qquad (4.28b)$$

where depending on the observation point ($\rho > \rho'$ or $\rho < \rho'$) the top or the bottom row of the Bessel functions must be selected. Again, the continuity condition for the tangential electric field over the apertures is implemented in the formulation by insertion of equal aperture field distributions in the two sets of wave functions.

As before, the coefficients a_n and b_n entirely depend on the functional form of the azimuthal dependent part of the incident field. For the particular choice of incident mode, equation (4.26), these coefficients are given by (3.27) which eliminates the infinite summation over n in equations (4.27) and (4.28).

Using a similar method as in Section 3,3.1 for determining the aperture electric field, $R_{\ell n}(\rho')$ can be expressed by equations (3.28). The field strength E'_{in}s associated with the cells are obtained by matching the average values of the azimuthal component of the total magnetic fields of the two regions over each cell. Using equations (3.3b) in conjunction with (4.27) and (4.28), one obtains

$$H_{\phi 2} = j\omega\varepsilon_o \sum_{i=1}^{IC} E_{iq} \cos q\phi \int_{\bar{\rho}_i}^{\rho_i^+} \int_o^\infty \rho' J_q'(\alpha\rho') J_q'(\alpha\rho) \frac{e^{-\gamma z}}{\gamma} \alpha d\rho' d\alpha$$

$$+ \frac{q^2}{j\omega\mu_o\rho} \sum_{i=1}^{IC} E_{iq} \cos\phi \int_{\bar{\rho}_i}^{\rho_i^+} \int_o J_q(\alpha\rho') J_q(\alpha\rho) \frac{\gamma}{\alpha} e^{-\gamma z} d\rho' d\alpha$$

(4.29a)

$$H_{\phi 1} = -\frac{\pi\omega\varepsilon}{2a} \sum_{i=1}^{IC} \sum_{m=1}^{\infty} E_{iq}\, \varepsilon_m \cos q\phi \cos \frac{m\pi}{a} z \int_{\rho_i^-}^{\rho_i^+} \frac{J_q'(k_{\rho m}\rho')}{H_q^{(2)\prime}(k_{\rho m}\rho')} \rho'\, d\rho'$$

$$\cdot \frac{H_q^{(2)\prime}(k_{\rho m}\rho)}{J_q'(k_{\rho m}\rho)} + \frac{\pi^3 q^2}{2\rho\mu_o a^3} \sum_{i=1}^{IC} \sum_{m=0}^{\infty} \frac{E_{iq}\, m^2 \varepsilon_m}{k_{\rho m}^2} \cos q\phi \cos \frac{m\pi}{a} z$$

$$\int_{\rho_i^-}^{\rho_i^+} \frac{J_q(k_{\rho m}\rho')}{H_q^{(2)}(k_{\rho m}\rho')} d\rho' \cdot \frac{H_q^{(2)}(k_{\rho m}\rho)}{J_q(k_{\rho m}\rho)} - k_{\rho p} \cos q\phi \cos \frac{p\pi}{a} z\, H_q^{(2)\prime}(k_{\rho p}\rho) \tag{4.29b}$$

In order to equate $H_{\phi 1}$ and $H_{\phi 2}$ over the cells in an average sense, we use a similar approach as Section 3.3.1, that is, for region 2 we define

$$\bar{H}_{\phi 2j} = \sum_{i=1}^{IC} \bar{h}_{2ji} \tag{4.30a}$$

where for $z = 0$, $|\rho - \rho_j| \leq \frac{\delta_j}{2}$, $0 \leq \phi \leq 2\pi$

$$\bar{h}_{2ji} = \frac{1}{\delta_j} \int_{\rho_j^-}^{\rho_j^+} H_{i\phi 2}\, d\rho \qquad \begin{matrix} i = 1,\ldots IC \\ j = 1,\ldots IC \end{matrix} \tag{4.31b}$$

and $H_{i\phi}$ is the contribution of the ith slot to the magnetic field of the jth slot. Note that for this region, a separate definition for terms $i = j$ is not needed, however, for the radial waveguide region, we use the respective equations given in Section 3.3.1. Evaluation of the integrals defined by (4.31b) is simplified by ignoring the variation of the terms ρ and $\frac{1}{\rho}$ in the integrands over the electrically thin cells. Note that due

to the presence of α in the arguments of the Bessel functions, the same approximation cannot be effected for these functions.

The final result of the above argument is a set of simultaneous linear equations in terms of the aperture field coefficients. The elements of the equivalent matrix equation, (3.32a) and (3.32b), are given by

$$
\begin{aligned}
Y_{\substack{ji \\ i\neq j}} = {} & (j\omega\varepsilon_o) \cdot \frac{\rho_i}{\delta_j} \int_o^\infty [J_q(\alpha\rho_i)]_-^+ \cdot [J_q(\alpha\rho_j)]_-^+ \frac{d\alpha}{\alpha\gamma} \\
& + \frac{q^2}{(j\omega\mu_o)\rho_j\delta_j} \int_o^\infty [C_q(\alpha\rho_i)]_-^+ \cdot [C_q(\alpha\rho_j)]_-^+ \cdot \frac{\gamma}{\alpha}\, d\alpha \\
& - \frac{\pi\omega\varepsilon}{2a} \frac{\rho_i}{\delta_i} \cdot \sum_{m=0}^{\infty} \frac{\varepsilon_m}{k_{\rho m}^2} \cdot \begin{bmatrix} J_q(k_{\rho m}\rho_i) \\ H_q^{(2)}(k_{\rho m}\rho_i) \end{bmatrix}_-^+ \cdot \begin{bmatrix} H_q^{(2)}(k_{\rho m}\rho_j) \\ J_q(k_{\rho m}\rho_j) \end{bmatrix}_-^+ \\
& + \frac{\pi^3 q^2}{2\rho_j\mu_o a^3\delta_j} \sum_{m=0}^{\infty} \frac{m^2}{k_{\rho m}^2} \varepsilon_m [C_{qm}^{J,H}(\rho_i)]_-^+ \cdot [C_{qm}^{H,J}(\rho_i)]_-^+
\end{aligned}
\tag{4.32a}
$$

$$
\begin{aligned}
Y_{ii} = {} & (j\omega\varepsilon_o) \cdot \frac{\rho_i}{\delta_j} \int_o^\infty [J_q(\alpha\rho_i)]_-^+ \cdot [J_q(\alpha\rho_i)]_-^+ \frac{d\alpha}{\alpha\gamma} \\
& + \frac{q^2}{(j\omega\mu_o)\rho_i\delta_i} \int_o^\infty [C_q(\alpha\rho_i)]_-^+ \cdot [C_q(\alpha\rho_i)]_-^+ \cdot \frac{\gamma}{\alpha}\, d\alpha \\
& - \frac{\pi\omega\varepsilon}{6a} \frac{\rho_i}{\sum_{m=0}^{\infty}} \frac{\varepsilon_m}{k_{\rho m}} \{J_q'(k_{\rho m}\bar{\rho}_i) \cdot [H_q^{(2)}(k_{\rho m}\rho_i)]_-^+ + H_q^{(2)\prime}(k_{\rho m}\overset{+}{\rho}_i) \\
& \cdot [H_q^{(2)}(k_{\rho m}\rho_i)]_-^+ + J_q'(k_{\rho m}\rho_i) \cdot [H_q^{(2)}(k_{\rho m}\rho_i)]_i^+ + H_q^{(2)\prime}(k_{\rho m}\rho_i) \\
& \cdot [J_q(k_{\rho m}\rho_i)]_-^{\rho_i}\} + \frac{\pi^3 q^2}{6\rho_j\mu_o a^3} \sum_{m=0}^{\infty} \frac{m^2}{k_{\rho m}} \varepsilon_m \{J_q(k_{\rho m}\bar{\rho}_i) \cdot [C_{qm}^H(\rho_i)]_-^+ \\
& + H_q^{(2)}(k_{\rho m}\overset{+}{\rho}_i)\ [C_{qm}^J(\rho_i)]_-^+ + J_q(k_{\rho m}\rho_i) \cdot [C_{qm}^H(\rho_i)]_{\rho_i}^+ + H_q^{(2)}(k_{\rho m}\rho_i) \\
& \cdot [C_{qm}^J(\rho_i)]_-^{\rho_i}\}
\end{aligned}
\tag{4.32b}
$$

where [50]

$$C_q(\alpha\rho) = \int_0^{\rho} B_q(\alpha\rho')d\rho' = \begin{cases} -\sum_{n=0}^{N} \varepsilon_n B_{2n}(\alpha\rho)/\alpha & 0 < q = 2N+1 \\ 2\left[\sum_{n=0}^{\infty} B_{2(N+n)+1}(\alpha\rho)\right]/\alpha & 0 < q = 2N \end{cases} \tag{4.32c}$$

and $C_{qm}^{J,H}(\rho)$ is given by (3.32e). Note that for the case $q = 0$ (ϕ symmetry), the field is TM to z and is solely determined from ψ^e. Evaluation of the infinite integrals is described in the next section.

Once the aperture field coefficients E_{iq} are determined from the matrix equation (3.32a), the field components in region 1, for points away from the slots, can be obtained from equations (3.3b) and the following relations for the respective wave functions

$$\psi_1^e = \frac{\pi\omega\varepsilon}{2a} \sum_{i=1}^{IC} \sum_{m=0}^{\infty} \frac{\rho_i}{k_{\rho m}^2} E_{iq}\varepsilon_m \cos q\phi \cos\frac{m\pi}{a} z \cdot \begin{bmatrix} J_q(k_{\rho m}\rho_i) \\ H_q^{(2)}(k_{\rho m}\rho_i) \end{bmatrix}_{-}^{+} \cdot \begin{bmatrix} H_q^{(2)}(k_{\rho m}\rho) \\ J_q(k_{\rho m}\rho) \end{bmatrix}$$

$$\psi_{pq}^{e\,inc} = \cos\frac{p\pi}{a} z \cos q\phi\, H_q^{(2)}(k_{\rho p}\rho) \tag{4.33}$$

The radiation field which is the quantity of most interest in the open-region problems is dealt with in a later section.

4.5 Evaluation of the Infinite Integrals

As was seen in the earlier section, the field coefficients are determined by matching the average values of the azimuthal component of

the total magnetic field across the coupling apertures. This, in turn, generates two types of infinite integrals which are yet to be evaluated, namely

$$I^e = \int_o^\infty J_m(\alpha x)\, J_m(\alpha y)\, \frac{d\alpha}{\alpha(\alpha^2 - k_o^2)^{1/2}} \tag{4.34}$$

$$I^h = \int_o^\infty J_m(\alpha x)\, J_n(\alpha y)\, \frac{(\alpha^2 - k_o^2)^{1/2}}{\alpha^3}\, d\alpha \tag{4.35}$$

We assume the smallest of x, y is large enough to allow for replacing the Bessel functions by their asymptotic forms over the range $\alpha \geq k_o$. This is a practical assumption, since, as a measure for minimizing the interaction between the slots and the feed assembly, generally the first slot is placed far enough from the central region of the feeding guide. In fact, Irzinski [33], when considering the problem of TEM excitation of an annular slot by a coaxial waveguide, has shown that satisfactory results can be obtained even for radii as small as one radian. Therefore, using the above mentioned scheme and separating the integrals into their real and imaginary parts, one obtains

$$\mathrm{Re}(I^e) \sim \frac{1}{k_o \pi}\,(k_o x k_o y)^{-1/2} \int_1^\infty \cos\left(k_o x\beta - \frac{2m+1}{4}\pi\right) \cos\left(k_o y\beta - \frac{2m+1}{4}\pi\right) \frac{d\beta}{\beta^2(\beta^2 - 1)^{1/2}} \tag{4.36a}$$

$$\mathrm{Im}(I^e) = -\frac{j}{k_o} \int_o^\infty J_m(k_o x\beta)\, J_m(k_o y\beta)\, \frac{d\beta}{\beta(1 - \beta^2)^{1/2}} \tag{4.36b}$$

$$\mathrm{Re}(I^h) \sim \frac{1}{k_o\pi}(k_o x\, k_o y)^{-1/2} \int_o^\infty \cos(k_o x\beta - \frac{2m+1}{4}\pi)\cos(k_o y\beta - \frac{2n+1}{4}\pi) \cdot \frac{(\beta^2-1)^{1/2}}{\beta^4}\, d\beta \tag{4.37a}$$

$$I_m(I^h) = -\frac{j}{k_o}\int_o^1 J_m(k_o x\beta)\, J_n(k_o y\beta)\, \frac{(1-\beta^2)^{1/2}}{\beta^3}\, d\beta \tag{4.37b}$$

where the following change of variable is affected

$$\beta = \frac{\alpha}{k_o} \tag{4.38a}$$

and Bessel function is replaced by its principal asymptotic form [50]

$$J_\nu(z) \underset{z\ \text{large}}{\sim} \sqrt{\frac{2}{\pi z}}\cos(z - \frac{2\nu+1}{4}\pi) \tag{4.38b}$$

The imaginary parts which are over a finite range of β are carried out numerically. However, the real parts of I^e and I^h, using the formula for products of cosines and also noting that $(m \pm n)$ is an even integer, can be transformed to

$$\mathrm{Re}(I^e) \sim \frac{1}{k_o\pi}(k_o x\, k_o y)^{-1/2}\{\int_1^\infty (\cos[k_o(x-y)\beta]\, \frac{d\beta}{\beta^2(\beta^2-1)^{1/2}} - \int_1^\infty \sin[k_o(x+y)\beta]\, \frac{d\beta}{\beta^2(\beta^2-1)^{1/2}}\} \tag{4.39}$$

$$\mathrm{Re}(I^h) \sim \frac{1}{k_o\pi}(k_o x\, k_o y)^{-1/2}\{(-1)^{\frac{m-n}{2}}\int_1^\infty \cos[k_o(x-y)\beta]\, \frac{(\beta^2-1)^{1/2}}{\beta^4}\, d\beta + (-1)^{m+n+1}\int_1^\infty \sin[k_o(x+y)\beta]\, \frac{(\beta^2-1)^{1/2}}{\beta^4}\, d\beta\} \tag{4.40}$$

Equation (4.39) can be shown (Appendix D) to be given by

$$\mathrm{Re}(I^e) \sim \frac{1}{2k_o}(k_o x\, k_o y)^{-1/2}\{k_o|x-y|\,[\int_o^{k_o|x-y|} N_0(z)dz - N_1(k_o|x-y|)]$$

$$- k_o(x+y)\,[1 - \int_o^{k_o(x+y)} \frac{J_1(z)}{z}\,dz]\} \qquad (4.41)$$

where the integrals in the above equation are known and given by [58]

$$\int_o^z \frac{J_1(t)}{t}\,dt = \frac{4}{z}\sum_{p=0}^{\infty}(p+1)\,J_{2(p+1)}(z) \qquad (4.42a)$$

$$\int_o^z N_0(t)dt = zN_0(z) + \frac{\pi z}{2}\,[|H|_0(z)\,N_1(z) - |H|_1(z)\,N_0(z)] \qquad (4.42b)$$

$$|H|_0(z) = \frac{4}{\pi}\sum_{p=0}^{\infty}\frac{J_{2p+1}(z)}{2p+1} \qquad |H|_1(z) = \frac{2}{\pi}[1 - J_0(z) + 2\sum_{p=1}^{\infty}\frac{J_{2p}(z)}{4p^2-1}] \qquad (4.42c)$$

Evaluation of the real part of I^h, however, is done by expanding $(\beta^2-1)^{1/2}$ into a Binomial series and retaining the first two terms. The infinite integrals in (4.40) are then approximated by

$$\int_1^{\infty}\cos[k_o(x-y)\beta]\,\frac{(\beta^2-1)^{1/2}}{\beta^4}\,d\beta \sim \int_1^{\infty}\cos[k_o(x-y)\beta]\,(\frac{1}{\beta^3} - \frac{1}{2\beta^5})\,d\beta \qquad (4.43a)$$

$$\int_1^{\infty}\sin[k_o(x-y)\beta]\,\frac{(\beta^2-1)^{1/2}}{\beta^4}\,d\beta \sim \int_1^{\infty}\sin[k_o(x+y)\beta]\,(\frac{1}{\beta^3} - \frac{1}{2\beta^5})\,d\beta \qquad (4.43b)$$

The right hand side of equations (4.43) are known integrals [50] and can be shown (Appendix E) to have a final result of the following form

$$\mathrm{Re}(I^h) = \frac{1}{48\pi k_o}(k_o x\, k_o y)^{-1/2}\left\{(-1)^{\frac{m-n}{2}}\left[(z_1^2 + 18)\cos z_1 - z_1(z_1^2 + 22)\sin z_1 + z_1^2(z_1^2 + 24)\,\mathrm{Ci}(z_1)\right] + (-1)^{m+n+1}\left[z_2(z_2^2 + 22)\cos z_2 + (z_2^2 + 18)\sin z_2 + z_2^2(z_2^2 + 24)\,\mathrm{Si}(z_2)\right]\right\} \tag{4.44a}$$

where

$$z_1 = k_o\,|x - y|$$
$$z_2 = k_o\,|x + y| \tag{4.44b}$$

and $\mathrm{Si}(z)$, $\mathrm{Ci}(z)$ are the Sine and Cosine integrals and can be expressed in terms of a fast converging series [50]. In the next section, the radiation field of a waveguide fed annular slot antenna is derived.

4.6 Radiation Field

The far field which is the quantity of most interest in the open-region problems is generally obtained by asymptotic integration techniques. However, for the present problem an equivalent approach which does not require contour integration is employed. That is, instead of evaluating asymptotic behaviour of the field expressions obtained earlier, the equivalence principle and the image theory are utilized. In order to obtain the solution, the apertures in the ground plane are replaced by an equivalent array of magnetic current distribution radiating in free space. Therefore, the electric field is expressed as [59]

$$\vec{E}(\vec{r}) = -\frac{1}{4\pi}\nabla \times \int_{\text{aperture}} 2\,\vec{J}_{ms}(\vec{r}')\,\frac{e^{-jk_o R}}{R}\,ds' \tag{4.45}$$

where, $\vec{J}_{ms} = \vec{E}_a \times \hat{n}$ and $R = |\vec{r} - \vec{r}'|$. Following the standard procedure for approximating the free space Green's function at large distances from

the source, that is

$$\nabla \frac{e^{-jk_o R}}{R} \sim -\frac{jk_o}{r} e^{-jk_o r} \exp(jk_o \hat{r}\cdot\vec{r}')\hat{r} \tag{4.46}$$

one obtains

$$\vec{E}(\vec{r}) \underset{k_o r\to\infty}{\sim} -\frac{jk_o}{2\pi r} e^{-jk_o r} \int_{\text{aperture}} \vec{J}_{ms}(\vec{r}') \times \hat{r} \exp(jk_o \hat{r}\cdot\vec{r}')ds' \tag{4.47}$$

Assuming constant electric field over the unit cells of the strength E_{in} and expressing the vectors in terms of their spherical components, it follows

$$\vec{E}_{k_o r\to\infty} \sim \frac{jk_o e^{-jk_o r}}{2\pi r} \sum_{i=1}^{IC} \sum_{n=0}^{\infty} E_{in} \int_{\phi'} \int_{-\rho_i}^{+\rho_i} (a_n \cos n\phi' + b_n \sin n\phi')$$

$$[\sin(\phi - \phi')\cos\theta\hat{\phi} + \cos(\phi - \phi')\hat{\theta}] \cdot \exp[jk_o\rho' \sin\theta \cos[\phi - \phi')]$$

$$\cdot \rho' d\rho' d\phi' \tag{4.48}$$

Since the integration on ϕ' represents the contribution from all points over an angular range equal to 2π, we are free to select the starting point in the integration on ϕ' to be $\phi - \pi$. This and a change of variable in the form $\phi' - \phi = u$ leads to

$$\vec{E}_{k_o r\to\infty} \sim \frac{jk_o e^{-jk_o r}}{2\pi r} \sum_{i=1}^{IC} \sum_{n=0}^{\infty} E_{in} \int_{-\rho_i}^{+\rho_i} \rho' d\rho' \int_{-\pi}^{\pi} [a_n \cos n(\phi+u) + b_n \sin n(\phi+u)]$$

$$\cdot [\cos u\hat{\theta} - \cos\theta \sin u\hat{\phi}] \exp(jk_o\rho' \sin\theta \cos u)du \tag{4.49}$$

Using the addition formulas for sinusoidal functions, the integral part of (4.49) on u can be shown (Appendix F) to be given by

$$U = (a_n \cos n\phi + b_n \sin n\phi)\hat{\theta} \{ \int_o^{\pi} [\cos(n-1)u + \cos(n+1)u] \exp(jk_o\rho' \sin\theta$$

$$\cos u)du\} + \cos\theta \cdot (b_n \cos n\phi - a_n \sin n\phi)\hat{\phi} \{ \int_o^{\pi} [\cos(n-1)u + \cos(n+1)u]$$

$$\cdot \exp(jk_o\rho' \sin\theta \cos u)du\} \tag{4.50}$$

The integrals of (4.50) are of the type [50]

$$\int_0^{\pi} e^{j\beta\cos t} \cos nt\, dt = j^n \pi J_n(\beta) \tag{4.51}$$

This reduces (4.49) to

$$\vec{E}_{k_o r\to\infty} \sim \frac{jk_o e^{-jk_o r}}{\pi r} \sum_{i=1}^{IC} \sum_{n=0}^{\infty} E_{in}\, \rho_i \int_{-\rho_i}^{+\rho_i} [a_n \cos n\phi + b_n \sin n\phi)\, J_n'(k_o\rho' \sin\theta)\hat{\theta} + (b_n \cos n\phi - a_n \sin n\phi) \cdot \frac{n\cos\theta}{k_o\rho_i\sin\theta} J_n(k_o\rho' \sin\theta)\hat{\phi}]d\rho' \tag{4.52}$$

where a use has been made of recurrence relations for the Bessel functions and the variation of ρ' over each cell is ignored.

Next, noting equations (4.32c), the integration on ρ' is carried out with the final result

$$\vec{E}_{k_o r\to\infty} \sim \frac{jk_o e^{-jk_o r}}{\pi r} \sum_{i=1}^{IC} \sum_{n=0}^{\infty} \frac{E_{in}\, \rho_i}{k_o \sin\theta} \{(a_n \cos n\phi + b_n \sin n\phi)[J_n(k_o\rho\sin\theta)]_{-\rho_i}^{+\rho_i}\hat{\theta} + (b_n \cos n\phi - a_n \sin n\phi) \cdot \frac{n\cos\theta}{\rho_i}[C_n^J(k_o\rho\sin\theta)]_{-\rho_i}^{+\rho_i}\hat{\phi}\} \tag{4.53}$$

For single mode operation, the infinite summation on n is eliminated. For instance, the radiation fields for a TM_{01} and TM_{00} modes of operation, which are the only modes considered in the examples given in this thesis, are

$$\vec{E}_{TM_{01}} \sim \frac{jk_o e^{-jk_o r}}{\pi r} \sum_{i=1}^{IC} \frac{E_{in}\, \rho_i}{k_o \sin\theta} [J_1(k_o \sin\theta) \cos\phi\hat{\theta} + \cos\theta \frac{J_o(k_o\rho\sin\theta)}{k_o\rho_i \sin\theta} \sin\phi\hat{\phi}]_{-\rho_i}^{+\rho_i} \tag{4.54}$$

$$\vec{E}_{TM_{00}} \sim \frac{jk_o e^{-jk_o r}}{\pi r} \sum_{i=1}^{IC} \frac{E_{in}\rho_i}{k_o \sin\theta} [J_o(k_o \rho \sin\theta)]_{\bar{\rho}_i}^{\rho_i^+} \hat{\theta} \tag{4.55}$$

It should be noted that the electric field in $\theta = 0$ direction for TM_{01} case is x polarized and can be evaluated by letting $\theta \to 0$ before performing the integration on ρ'. The corresponding relations are

$$\vec{E}_{TM_{01}}(\theta=0) \sim \frac{jk_o e^{-jk_o r}}{2k_o r} \sum_{i=1}^{IC} k_o \delta_i k_o \rho_i E_i \hat{x}$$

$$E_{TM_{00}}(\theta=0) = 0 \tag{4.56}$$

In the next section an expression for the radiated power by an annular slot array will be obtained.

4.6.1 Expression for the Radiated Power

An application of equation (3.39) to a semi-spherical surface of a large radius $(k_o r \to \infty)$ on top of the slotted structure yields the desired relation for the radiated power. To this end, we express (3.34) in terms of the field components in spherical coordinates, that is

$$P = \mathrm{Re} \int_o^{\pi/2} \int_o^{2\pi} (E_\theta \cdot H_\phi^* - E_\phi \cdot H_\theta^*) r^2 \sin\theta d\theta d\phi \tag{4.57}$$

The magnetic field components H_ϕ and H_θ are easily obtainable from E_θ and E_ϕ by noting that at large distances from the source system, the fields are locally TEM. The electric and the magnetic fields are related by

$$\vec{H} = \frac{1}{\eta_o} \hat{r} \times \vec{E} \tag{4.58a}$$

where

$$\eta_o = \left(\frac{\mu_o}{\varepsilon_o}\right)^{1/2} = 120\pi \tag{4.58b}$$

An application of (4.58) to (4.53) yields

$$\vec{H} = \frac{j\omega\varepsilon_o e^{-jk_o r}}{\pi r} \sum_{i=1}^{IC} \sum_{n=0}^{\infty} \frac{E_{in}\rho_i}{k_o \sin\theta} \{(a_n \cos n\phi + b_n \sin n\phi)[J_n(k_o\rho\sin\theta)]_{\rho_i}^{+} \hat{\phi}$$

$$-(b_n \cos n\phi - a_n \sin n\phi) \cdot \frac{n\cos\theta}{\rho_i}[C_n(k_o\rho\sin\theta)]_{\rho_i}^{+} \hat{\theta}\} \qquad (4.59)$$

By substituting (4.53) and (4.59) in (4.57), it can readily be shown that the radiated power has the following form

$$P = \frac{\pi}{\eta_o} \sum_{i=1}^{IC} \sum_{j=1}^{IC} \sum_{n=0}^{\infty} \frac{(a_n^2 + b_n^2)}{\varepsilon_n} \mathrm{Re}(E_{in} \cdot E_{jn}^*) \{\rho_i\rho_j \int_o^1 [J_n(k_o\rho_i\beta)]_-^+$$

$$\cdot [J_n(k_o\rho_j\beta)]_-^+ \frac{d\beta}{\beta(1-\beta^2)^{1/2}} + \int_o^1 [C_n(k_o\rho_i\beta)]_-^+$$

$$\cdot [C_n(k_o\rho_j\beta)]_-^+ \frac{(1-\beta^2)}{\beta} d\beta\} \qquad (4.60)$$

where $C_n(\rho\alpha)$ is given by (4.32c) and (4.60) is obtained by affecting a change of variable in the form

$$\beta = \sin\theta \qquad (4.61)$$

Note that the integrals in (4.60) have the same form as the finite integrals computed for determining the field strength coefficients E_{in}.

4.7 Effects of the Higher Order Modes on the Admittance and the Field of a Waveguide Fed Annular Slot Antenna

Based on the theory presented in the earlier sections, the associated admittance of a radial waveguide fed annular slot antenna is computed as a function of the radius of its leading edge. The thickness of the feeding guide is smaller than half the intrinsic wavelength of the region, therefore, only the dominant mode propagates in the radial waveguide. The admittance is defined as before, Section 3,4, and the conductance and the

susceptance terms are depicted in figures 4.4a and 4.4b. The ratio of the radii of the slot edges is kept constant for each curve and expressed by

$$\tau = (\rho + \frac{\delta}{2})/(\rho - \frac{\delta}{2}) \tag{4.62}$$

A TM_{00} excitation is assumed and the results are compared against the theoretical results as well as the experimental ones obtained earlier [20]. The latter results are due to a TM_{00} excited annular slot fed by a coaxial waveguide of the same cross-section. The admittance values are normalized by the characteristic admittance of a coaxial waveguide given by [20]

$$Y_o = \frac{2\pi}{\eta_o^2 \ell_n \tau} \tag{4.63}$$

and η_o is defined by (4.58b). Figures 4.4a and 4.4b indicate that for electrically narrow slots, the admittance of the slot approaches that of an infinitely thin antenna driven by a delta function generator [32]. That is, the admittance is chiefly determined by the external region and the interior medium has a small effect on the admittance. Since for both geometries (radial and coaxial waveguide fed slots), the exterior region is the same, the corresponding admittances are expected to approach a common value for thin slots. However, as is clear from figures 4.4, the conductance and the susceptance terms of the radial waveguide fed antenna, for wider slots and with the exception of the peak values of the conductance, are generally smaller than those of the coaxial one. It might be of interest to mention that the result obtained for $\tau = 2.36$, at $k_o(\rho - \frac{\delta}{2}) = 2.00$, which shows a resonance case also corresponds to the maximum radiated power. This power was observed to be about 90 percent of the total power injected by the source.

Figures 4.5a and 4.5b illustrate the effects of the higher order modes of the feeding guide on the admittance of the same geometry. The

dotted lines represent the results obtained by taking only the propagating mode, whereas the solid lines are due to the inclusion of the first ten modes which was observed to be sufficient to yield a convergent solution for all examples presented in this work. These results suggest a similar conclusion as for the case of two coupled radial waveguides, that is, for most applications, the dominant mode representation adequately describes the equivalent admittance of the slot. However, the accuracy of the results, particularly the susceptance part for this case, can be substantially improved by including the higher order modes excited by the slot discontinuities. The field distribution over the slot is also calculated for the geometry corresponding to the last plotted point in figures 4.5. The results presented in figures 4.6a and 4.6b show that the dominant mode approximation yields reasonable results for both amplitude and phase of the electric field over the aperture. This is in contrast to the results obtained for two coupled waveguides, figures 3.4. However, it should be pointed out that since the field representation of the external region is in terms of infinite integrals over the entire range of the continuous spectrum $(o \leq \alpha < \infty)$, they include both the visible and invisible ranges of the spectral representation. Hence, omission of the beyond cut-off modes of the feeding guide alone does not affect the accuracy of the solution to the degree that was observed in the case of two coupled waveguides. It should be mentioned that due to large electrical width of the slot, the aperture for the geometry of figures 4.6 is divided into 13 cells (annular rings) of equal widths. Then the tangential electric field over each cell, which for TM_{00} excitation assumed is equal to E_ρ, is computed by applying the continuity of H_ϕ across the coupling aperture.

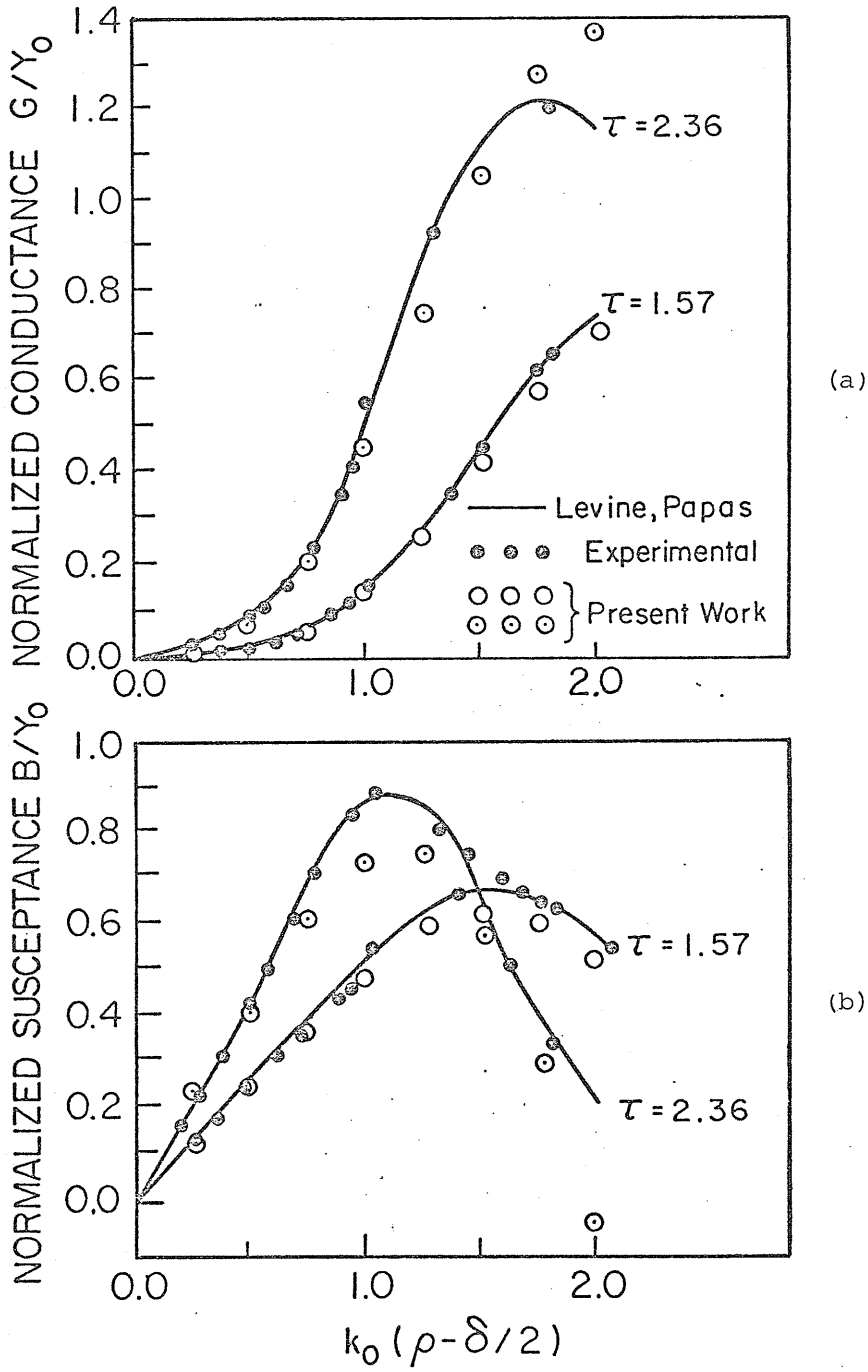

Figure 4.4: Comparison of the admittance of a radial waveguide fed annular slot against that of a coaxial fed slot of the same aperture size. τ is the ratio of the edges of the slot, $k_o a = 0.49$, $\varepsilon_r = 1.00$, k_o is the free space propagation constant and Y_o is the characteristic admittance of a coaxial waveguide. TM_{00} excitation

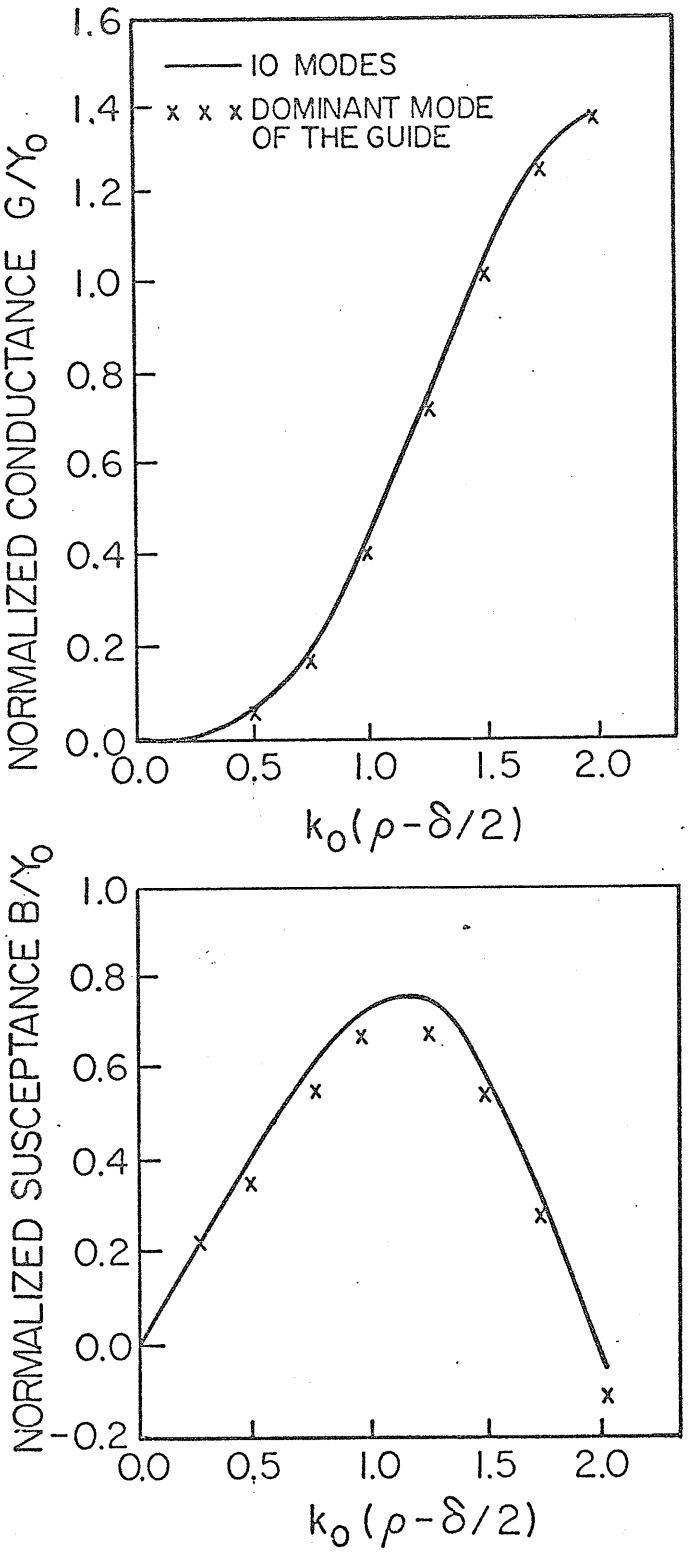

Figure 4.5: Effect of higher order modes of the feeding guide on the equivalent admittance of the slot. $\tau = 2.36$, $k_o a = 0.49$, $\varepsilon_{r1} = 1.00$, TM_{00} excitation

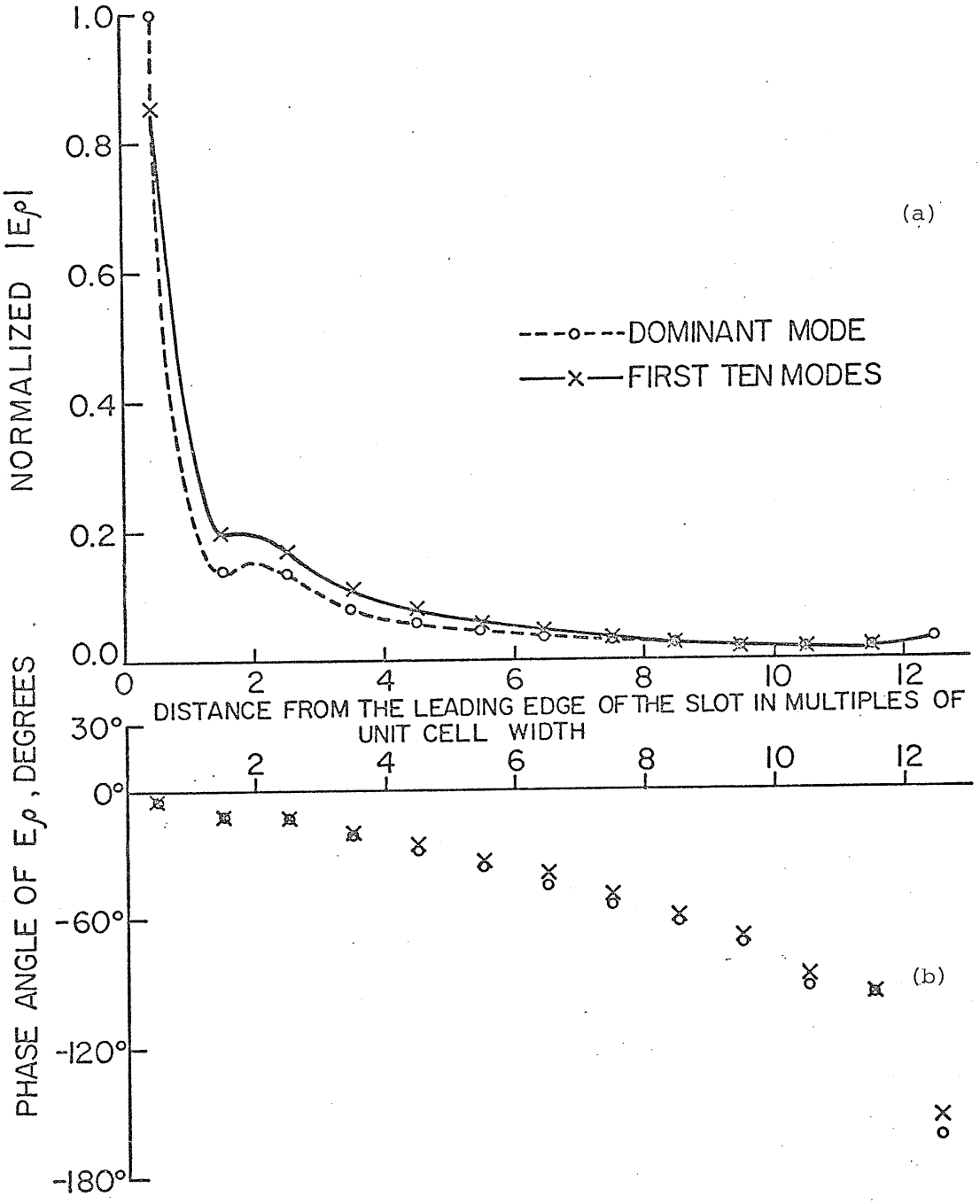

Figure 4.6: Aperture field distribution over the slot, $k_o\delta = 2.72$, $k_o\rho = 3.36$, $k_oa = 0.49$, $\varepsilon_r = 1.00$, TM_{00} excitation

4.8 Amplitude and Phase Variation of an Isolated Annular Slot as a Function of its Average Radius

For a waveguide fed slot array, the field strength of individual slots, and their relative phases are of prime importance in the antenna design problems. Generally, the information available for an isolated slot is not sufficient for representing the same slot when placed in an array structure. The mutual coupling effects among the members may change the characteristics of the slot appreciably. To study the amplitude and phase variation of both single elements as well as the array groups, a number of cases are considered. Electrically narrow slots are selected, therefore, each slot is characterized by a single cell of the field strength E_i. Figure 4.7 depicts the phase variation of the slot field as a function of its average radius (TM_{01} excitation). The two sets of curves are due to two different dielectric constants of the waveguide region. These results indicate that the nonlinear phase variation has a periodicity of one λ (the intrinsic wavelength of the guide). It is also interesting to note that the phases of 0 and $180°$ correspond to radii, which have electrical dimensions $(k\rho)$ approximately equal to zeros of $J_1'(z)$. In view of the assumed incident field, the incident magnetic field is proportional to $-H_1^{(2)'}(k\rho)$. Therefore, the slot phase lags the incident magnetic field at the respective points by 90 degrees.

The amplitude variation of the slot field as a function of its average radius is studied in figure 4.8. The total power delivered by the source is kept constant for all the slot locations. This is accomplished by introducing a constant factor for the incident field, which is adjusted for each slot location to yield the same value for the total power as the slot radius is increased. The results of figure 4.7

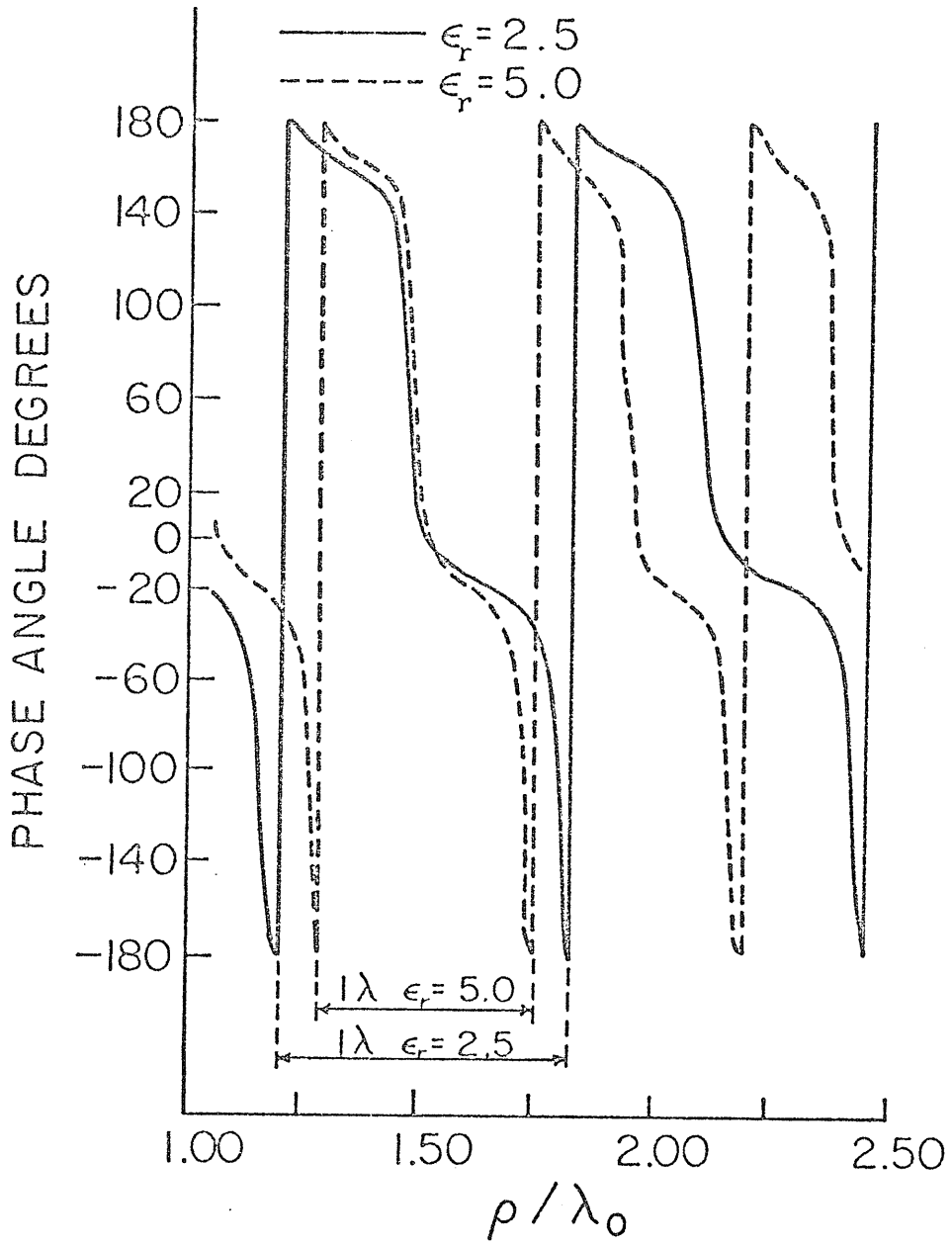

Figure 4.7: Phase variation of the slot field as a function of it average radius. $k_o\delta = 0.05$, $k_o a = 0.21$, TM_{01} exciting mode.

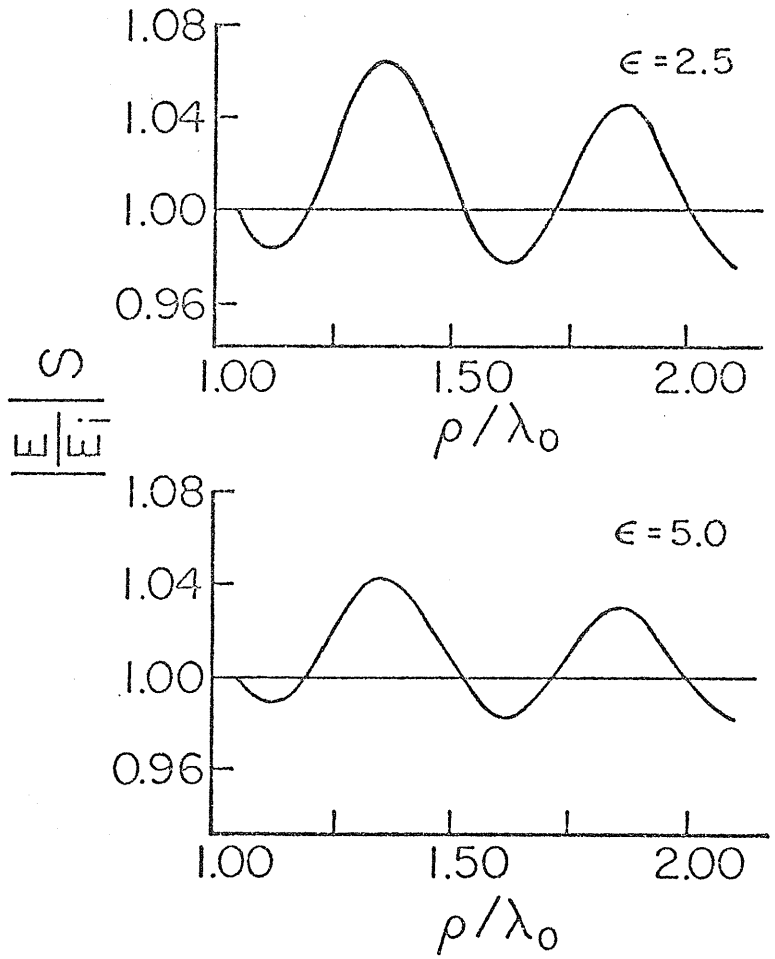

Figure 4.8: Weighted amplitude variation of the slot field as a function of its average radius.

are first normalized by the field strength E_I of the slot at the first computed location $(\rho = \rho_I)$ and then are weighted by the ratio $S = (\rho/\rho_I)^{1/2}$. The radii are measured from the center of the slot at the respective radius. These results show that the so normalized slot field has an asymptotic value of unity and the actual result oscillates about this level with a maximum deviation of six per-cent. It is also found that the power radiated by the slot has a similar trend as this factor. Assuming that the radiation conductance of the slot at each location is proportional to its area, the similarity can be explained by noting that the factor so defined is proportional to the square root of the power ratio. An increase in the dielectric constant of the guide region yields similar results but has a more damped oscillatory behaviour.

The above observation suggests that knowing an initial value for the field strength of a single slot located at ρ_I, the respective field amplitudes of slots of different radii can be anticipated, within few per-cent error, by using the factor $S\left|\frac{E}{E_I}\right|$.

4.8.1 Amplitude and Phase Variations of Two Coupled Slots

To study the effects of mutual coupling between two slots, the phase and amplitude variation of two slots separated by a fixed distance equal to $x = 0.25\lambda_o$ (free space wavelength) are obtained as a function of their radial locations, figures 4.9 and 4.10. It is interesting to note that the phase variation for the leading slot is quite similar to the result obtained for the isolated case, figure 4.8 (solid line), and the points corresponding to 0 and 180° occur at similar radii. However, the results for the second slot are affected by a somewhat constant phase lag. This may be attributed to a complex equivalent transmission coefficient at the leading slot which changes the phase of the exciting field

for the second slot. The phase variation still shows a periodicity of one wavelength, however, the nonlinear phase variation is tapering to its asymptote (linear phase variation for the propagating mode) as a result of mutual coupling.

The weighted field variation $S\left|\frac{E}{E_I}\right|$ for both slots are shown in figure 4.10. The initial field strength and radius are taken to be those of the leading slot at a radius $\rho_I = 1.05\lambda_o$. The small oscillations still occur about two constant levels for the two slots. The result for the second slot, however, is relatively lower than that of the leading slot and its level (67%) may be considered as an indication of the magnitude of the total equivalent transmission coefficient at the location of the leading slot. The maximum deviation of the normalized field is again within six per-cent of the constant levels.

It is also found that the relative position of the constant levels is more sensitive to the feeding waveguide thickness. That is, depending on the other parameters of the geometry under consideration, a critical depth may be found such that it will create a small transmission coefficient after the first few members of an annular slot array. This results in a sharp drop in the field strengths of the other slots relative to the first few members. In other words, the system experiences a large input impedance after the first few resonant slots which consequently radiate most of the power into the external region. However, for slot arrays with a large number of elements, it is often desired to distribute the power among the elements of the array more evenly as to produce more directive radiation patterns. For these cases, the dimensions which produce large differences between the constant levels must be avoided when considering arrays with a large number of elements. It is observed that a useful and effective way of pre-selecting an initial value for the thickness is to

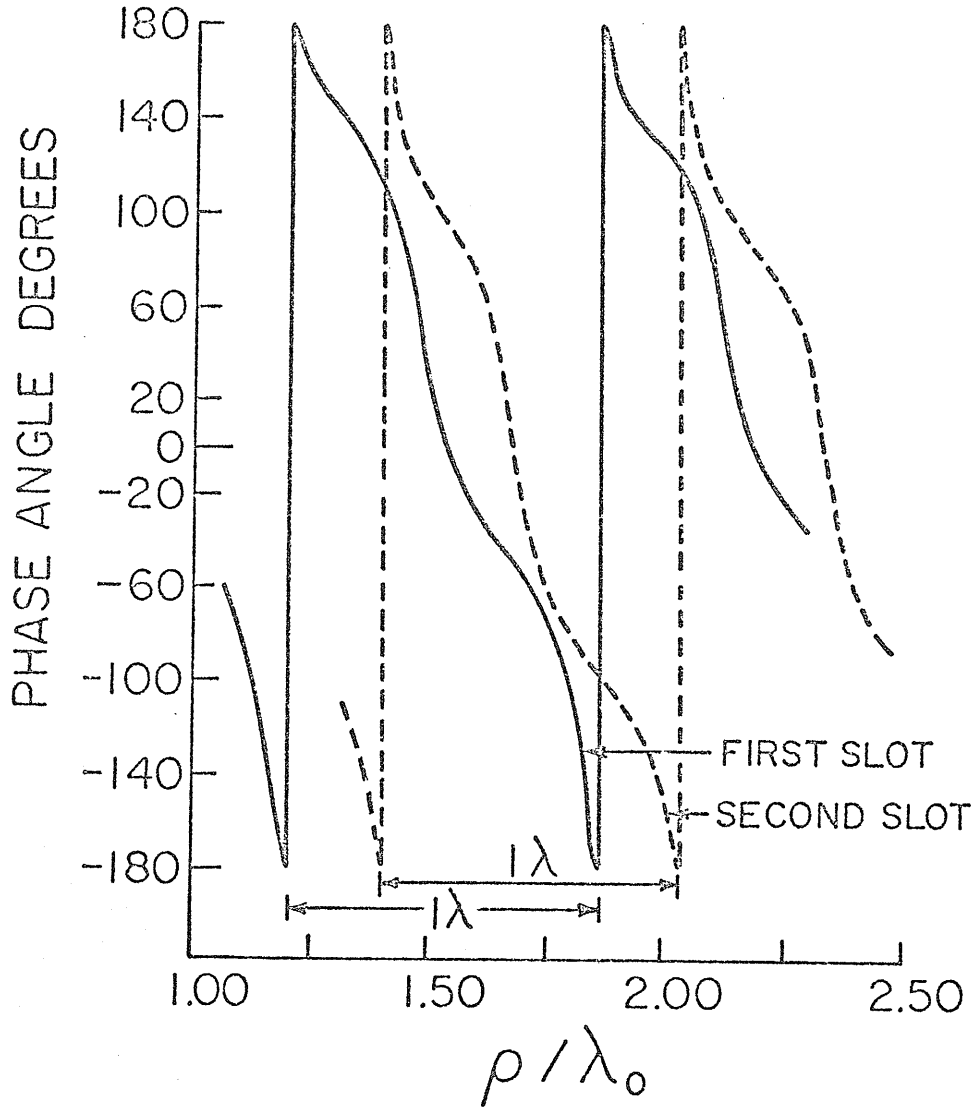

Figure 4.9: Phase variation of the slot field of two coupled annular slots as a function of their average radii. $k_o\delta = 0.05$, $k_oa = 0.21$, $k_ox = 1.57$, $\varepsilon_r = 2.50$, TM_{01} exciting mode.

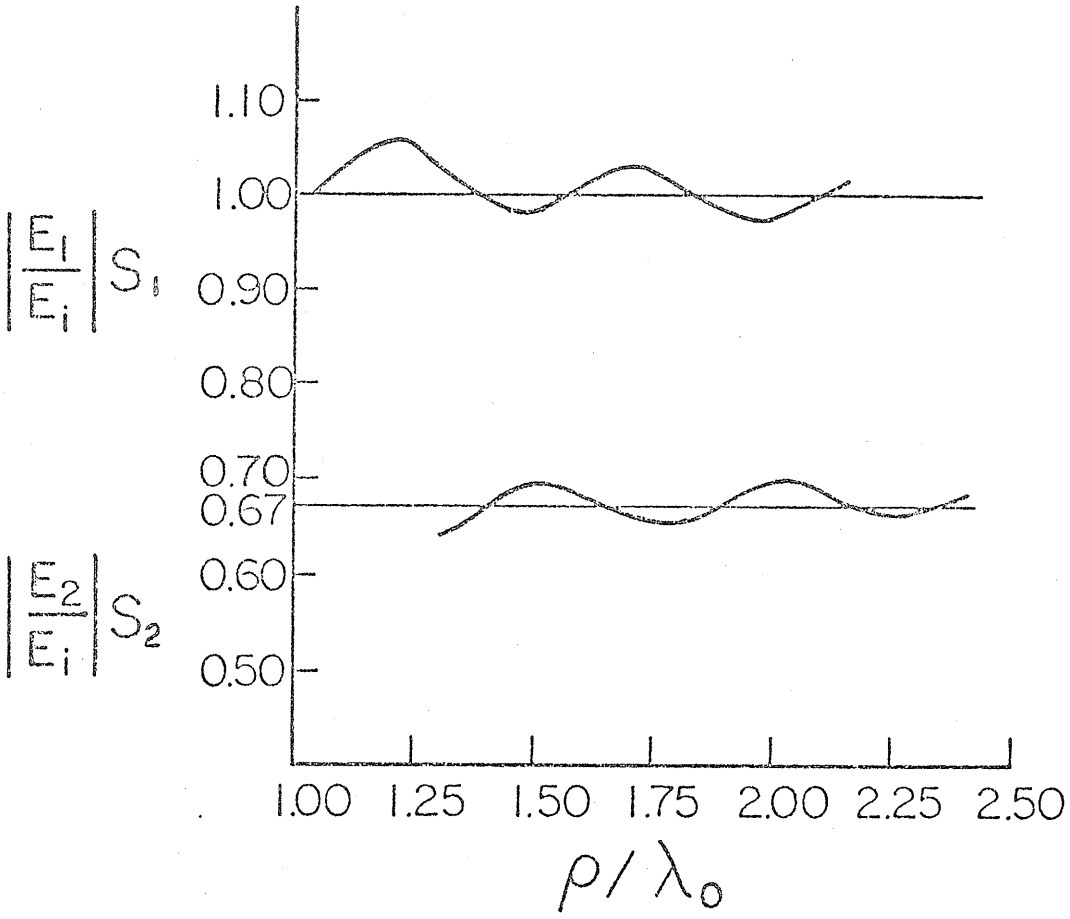

Figure 4.10: Weighted amplitude variation of the slot field of two coupled annular slots as a function of their average radii.

analyze the radiation characteristics of a sub-array formed by the first few members of the array under consideration. Even though the field distributions of these slots are not the same as those in a larger array, nevertheless, the information obtained in this manner provides the designer with useful *a priori* knowledge as to the selection of the initial values for the parameters of the antenna problem.

4.9 Radiation Characteristics of Annular Slot Array Antennas

Based on the theory presented earlier, the radiation patterns of radial waveguide fed annular slot array are studied and the results are presented in figures 4.11-4.14. The radiation pattern depicted by 4.11 is due to an array of four elements excited by a TM_{00} radial mode. For this particular mode of operation, the slot field is independent of ϕ and the pattern resembles that of a vertical dipole as far as the region $z \geq 0$ is concerned. It is interesting to note that even with four electrically narrow slots (slot width $\sim 0.02\lambda_o$) 99% of the total power is coupled out and a small fraction is transmitted through the waveguide region. Figure 4.12a illustrates the E and H plane radiation patterns of an array of eight elements, excited by a TM_{01} mode over an angular region equal to 20 degrees. As a measure to reduce the first side lobe level, the spacing between the sixth and seventh elements is doubled with respect to the other slots. The aperture efficiency compared to a circular aperture of the same diameter as the last slot and having uniform phase and amplitude distribution is about 70%. The gain of the antenna system with respect to an isotropic radiator is 29 dB. The half power beam width is lower than seven degrees and the first side lobe level is seven dB down the maximum value. The overall aperture diameter is about $11\lambda_o$. Figure 4.12b is the cross-polarized component of the

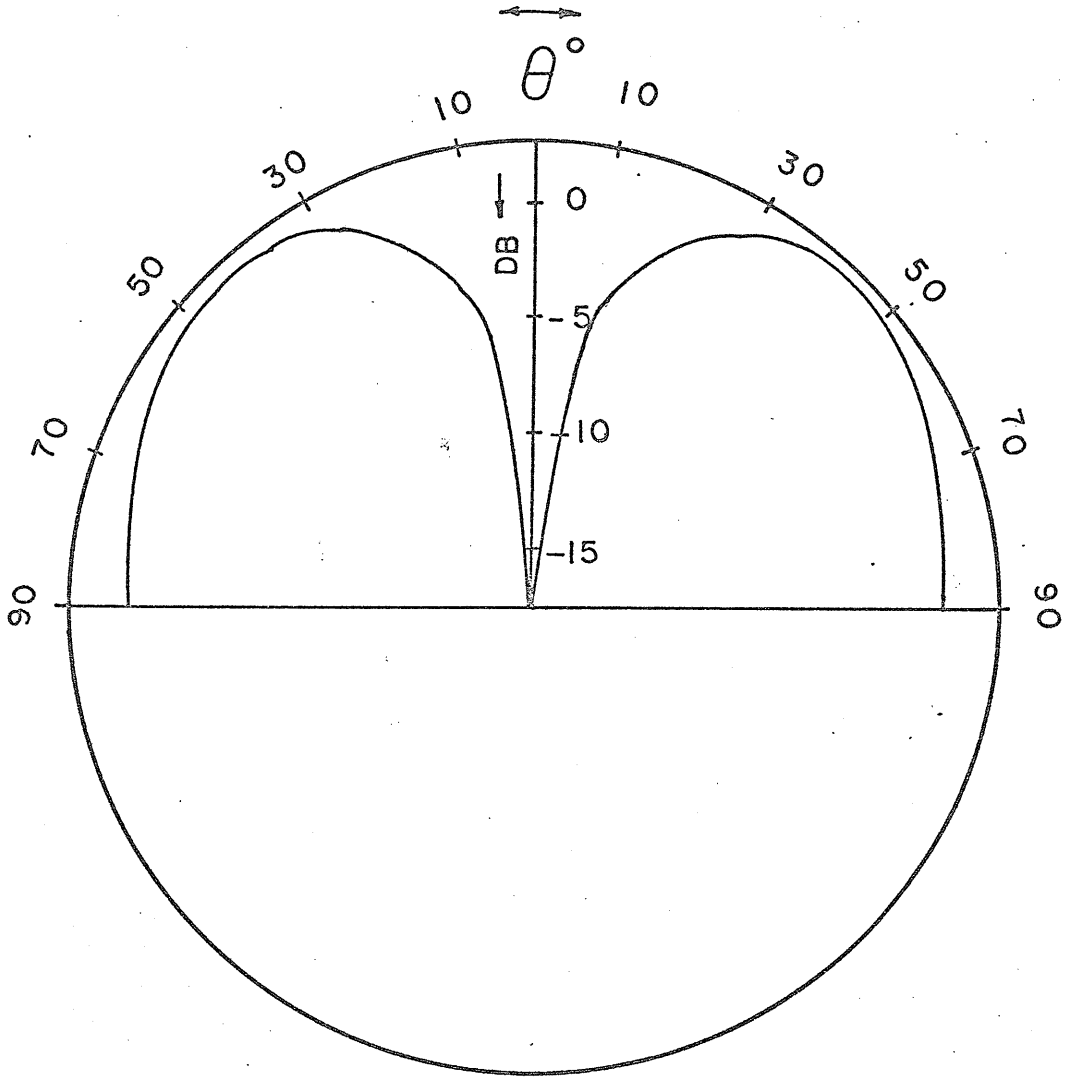

Figure 4.11: Radiation pattern of an annular slot array, TM_{00} excitation.

same antenna at $\phi = 45°$ cut-plane.

In order to have constant phase distribution over the entire array, using the result obtained earlier, the slot spacing for figure 4.13a is selected to be about 1λ (intrinsic wavelength of the guide region). To reduce the first side lobe level, the spacing between the slots was selected to be slightly more than 1λ (1.02λ). The waveguide thickness is about 0.16λ and a TM_{01} excitation is assumed. The side lobe level is down to -16 dB at the expense of wider H-plane beam width and lower gain and efficiency values. The radiated power is 95% of the total injected power by the source and the overall aperture diameter is about $10\lambda_o$. Figure 4.13b represents the cross-polarized field at $\phi = 45°$ cut-plane.

Figure 4.14 demonstrates the feasibility of designing annular slot arrays producing narrow beams with a high gain and efficiency with a total aperture size not exceeding $10\lambda_o$. The efficiency figure is about 90 per-cent and the gain is 29 dB. The half power beam width is about seven degrees and the first side lobe level is lower than 10 dB. For this array the radiated power is observed to be about 80 per-cent of the total power delivered by the source.

In conclusion, the theory presented in this chapter establishes a method of solution for the electromagnetic field set up by an array of concentric annular slots of finite width on a ground plane. The slots are assumed to be electrically thin enough as to suppress the azimuthal directed aperture electric field component. The field strength of the slots can be a general function of the azimuthal variable ϕ. One possible application of the method is in the design of annular slot array antennas capable of producing pencil beam radiation patterns of high efficiency and gain factors. The feeding assembly for the radiating slot array can be formed by either a radial waveguide or a cylindrical cavity which are also

used as the supporting structure for the array system. The forcing function generator is mounted in the central region of the radial waveguide or the cylindrical cavity. The part of radial waveguide annular slot arrays was discussed in Chapter III and IV. The cavity backed slot antenna which is closely related to the first case but is a more practical one is discussed in Chapter V.

In the previous sections, even though the analysis was presented for a general forcing function, the examples were all obtained by assuming single mode operation (TM_{00} or TM_{01}). A part of the next chapter is devoted to possible ways of generating these modes of radial waveguides. Another practical aspect of the problem which is not yet discussed is the effect of finiteness of the conducting baffle and the radial waveguide on the radiation field. This matter is also discussed in the next chapter.

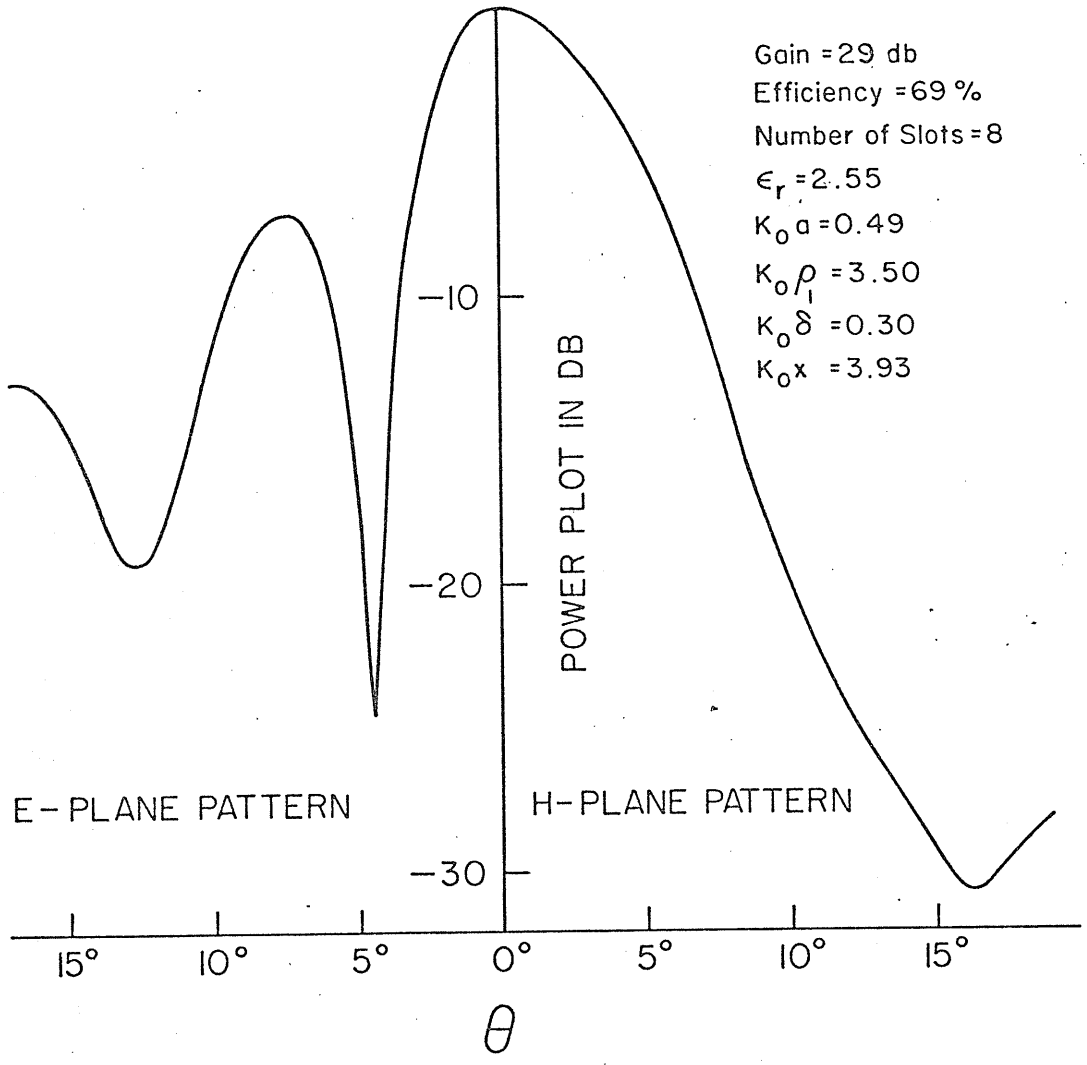

Figure 4.12a: Radiation patterns of an annular slot array, TM_{01} exciting mode.

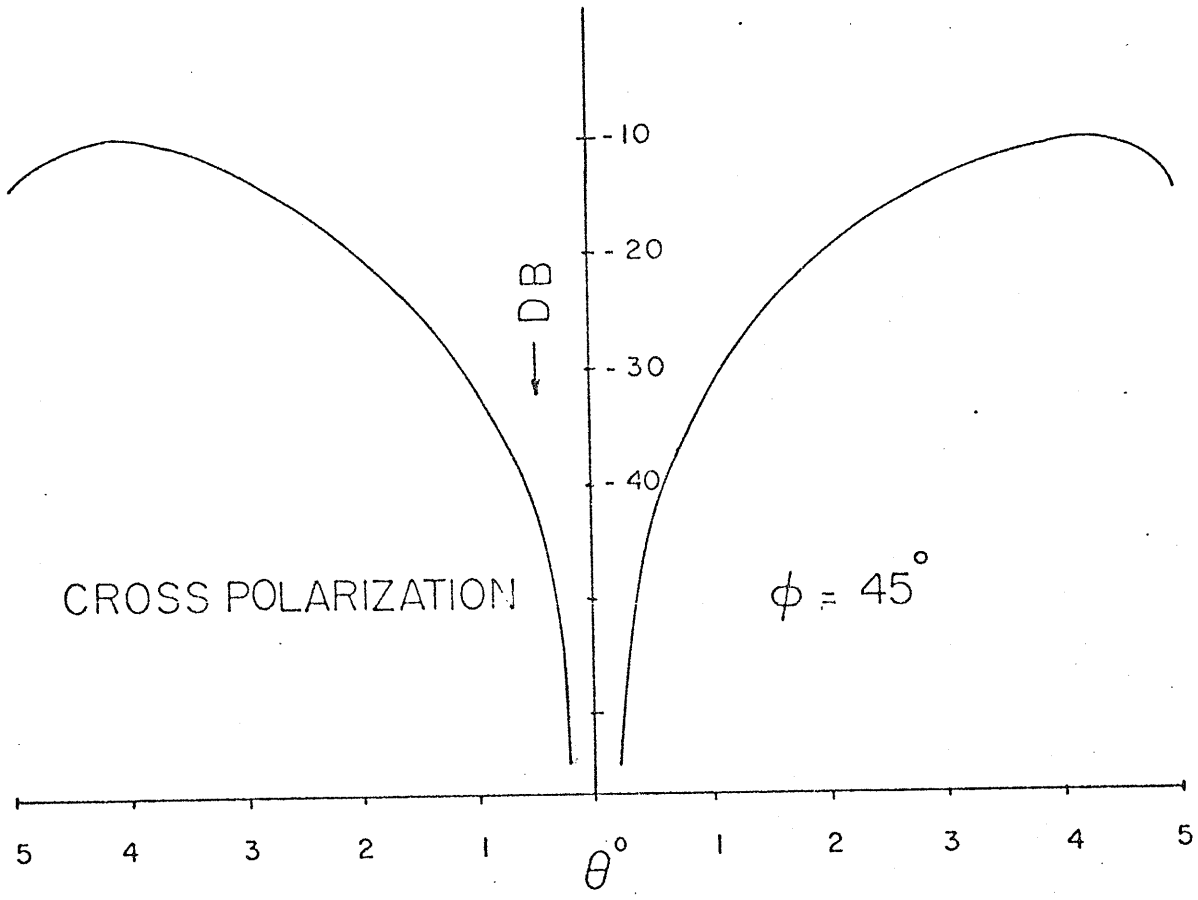

Figure 4.12b: Cross-polarized pattern at $\phi = 45°$ cut-plane.

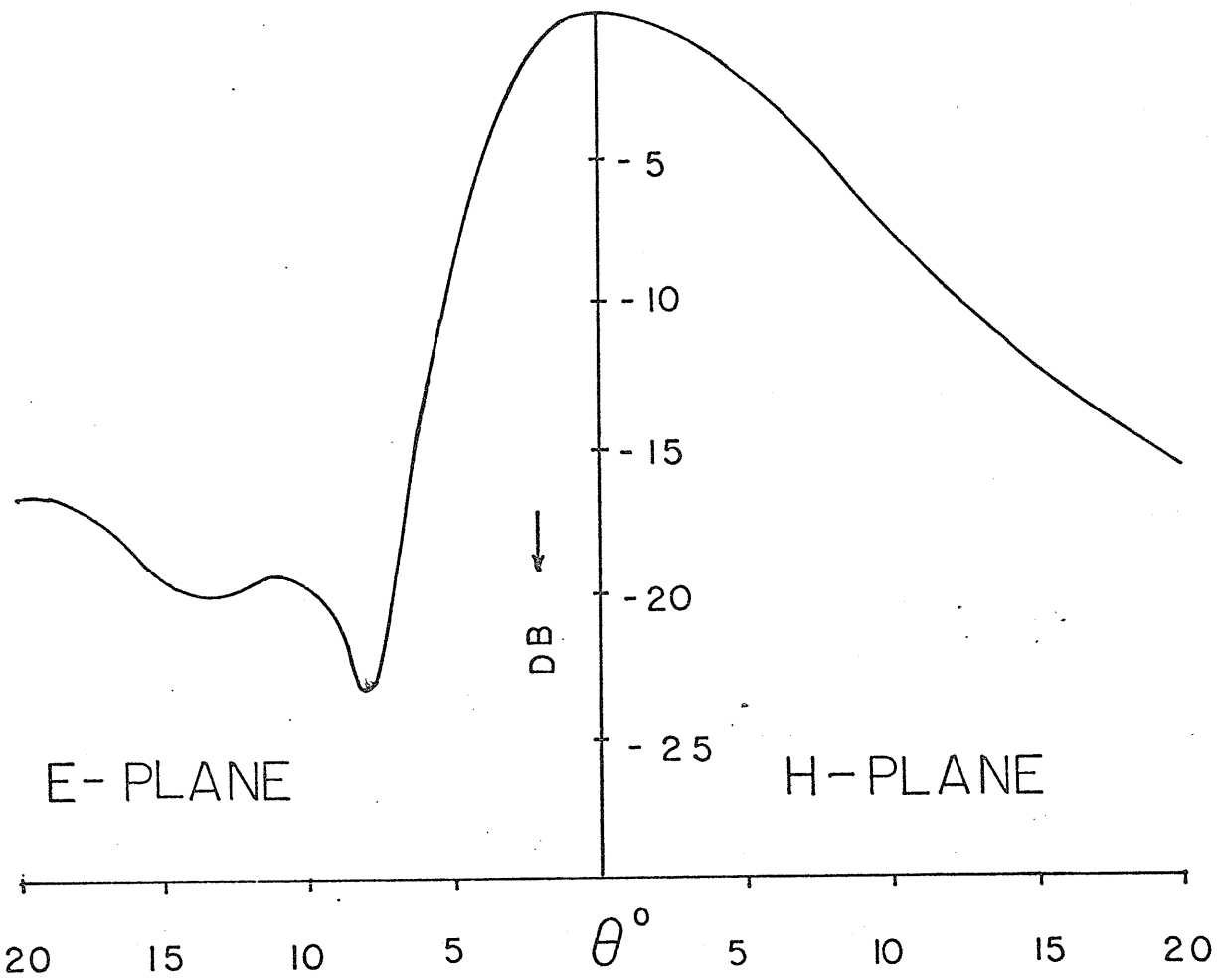

Figure 4.13a: Radiation patterns of an annular slot array, TM_{01} exciting mode. Gain = 23.22, Efficiency = 40%, Number of Slots = 8, $\varepsilon_r = 2.55$, $k_o a = 0.63$, $k_o \rho_1 = 4.28$, $k_o \delta = 0.20$, $k_o x = 4.01$.

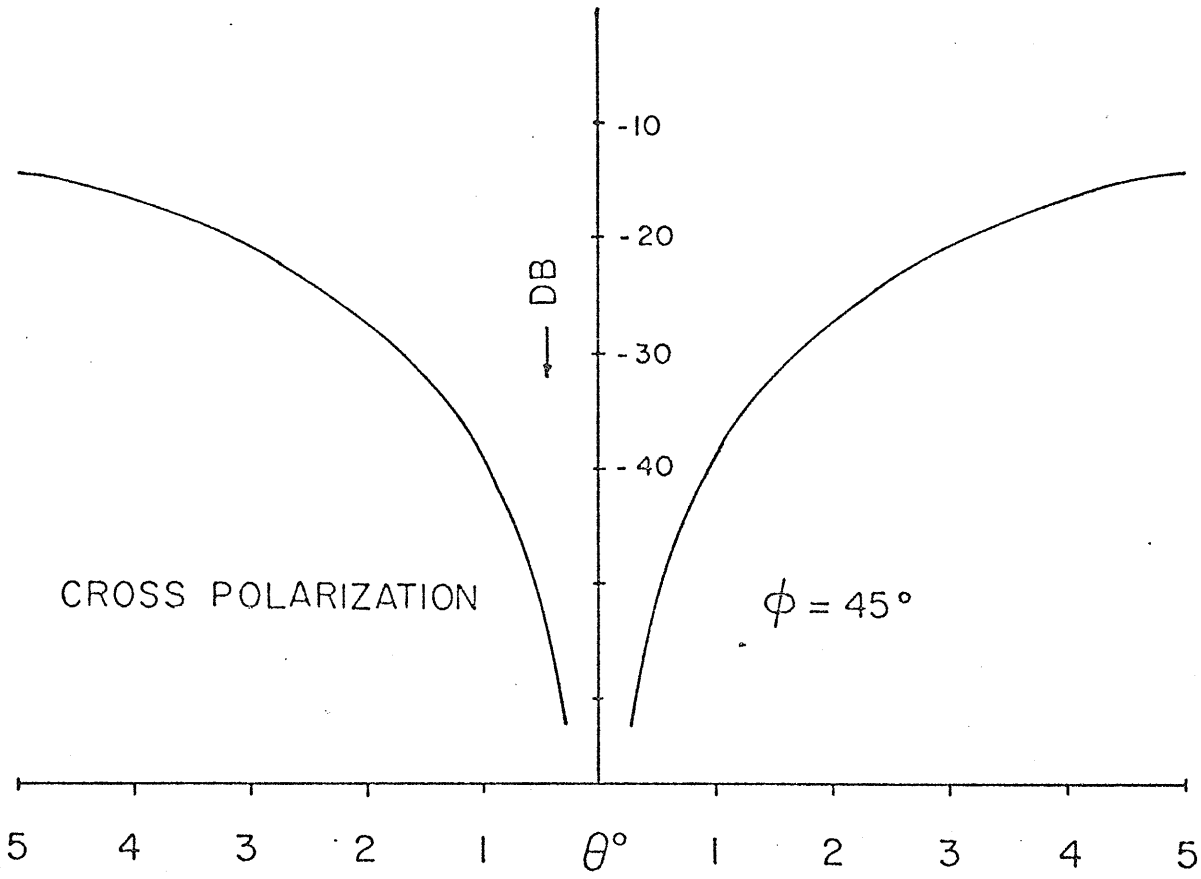

Figure 4.13b: Cross-polarized pattern at $\phi = 45°$ cut-plane.

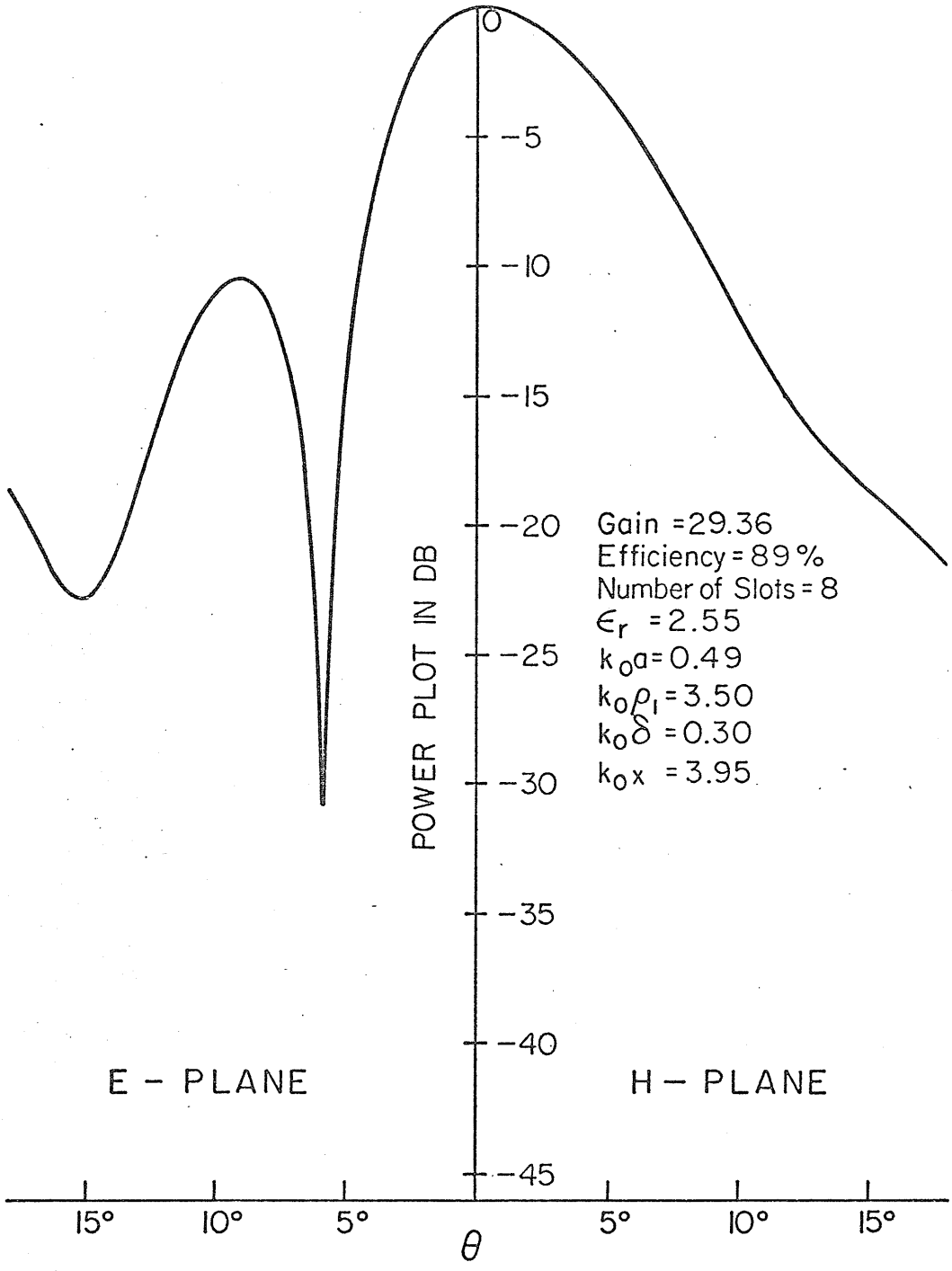

Figure 4.14a: Radiation patterns of an annular slot array, TM_{01} exciting mode.

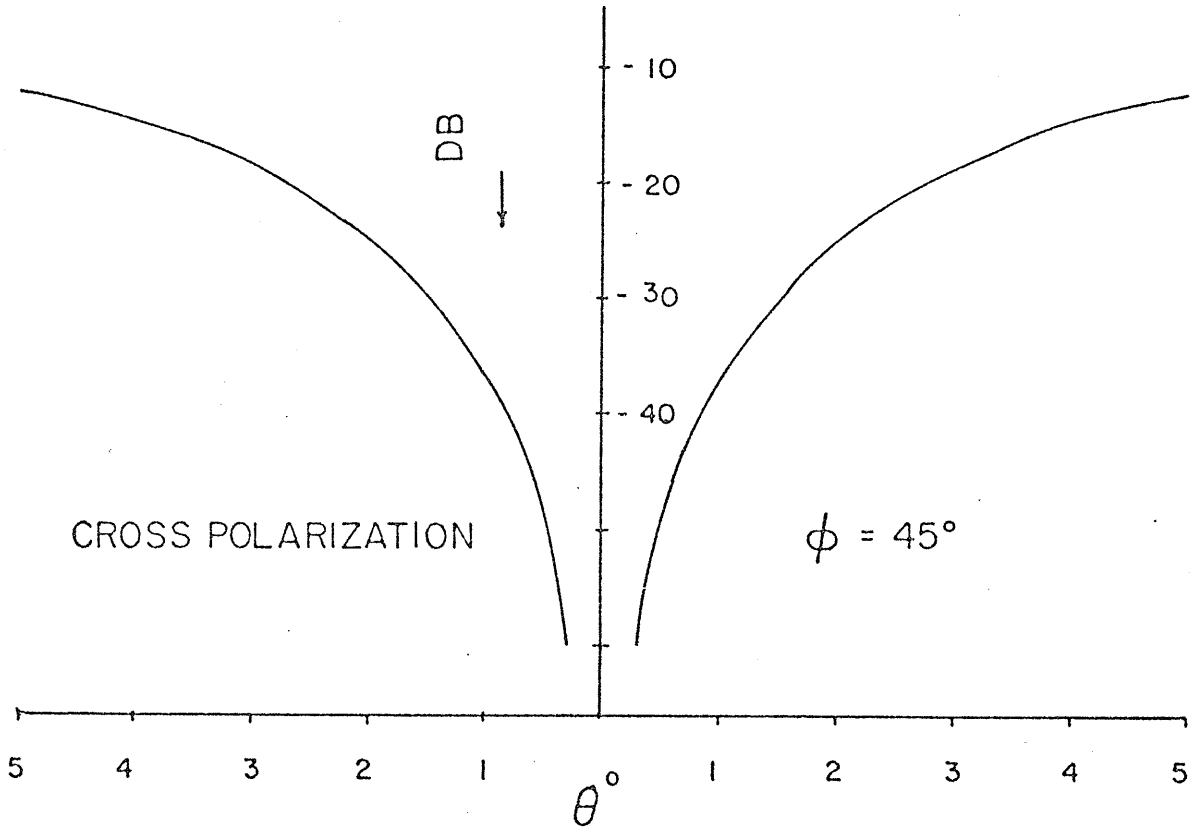

Figure 4.14b: Cross-polarized pattern at $\phi = 45°$ cut-plane.

CHAPTER V

FIELD SOLUTION FOR CAVITY BACKED ANNULAR SLOT ARRAYS

5.1 Introduction

For certain applications of waveguide fed slotted structures it is of interest to terminate the waveguide by placing a short circuit somewhere along the guiding region. Examples are airborne antennas where in addition to the size and weight restrictions, it is often desired to electrically isolate the antenna system from the electronic gear of the aircraft or the spacecraft. This is simply achieved by replacing the feeding waveguide by a cavity as the electromagnetic shielding device. Another advantage is the added mechanical rigidity produced by the conducting wall acting as the short circuit. The price to pay, however, is generally a reduction in bandwidth which in turn makes the antenna system more susceptible to the changes of the environment.

In the next section, the field solution for a cavity backed annular slot array antenna which is closely related to the waveguide fed case is derived. The geometry of the problem is obtained by introducing a cylindrical conducting surface at a radius $\rho = c$ in figure 4.1. The resulting structure is depicted in figure 5.1. Since the external region is not modified, the theory presented in Chapter IV related to the external region still applies. However, the field solution for the interior region needs the appropriate modifications. Here, we must impose the condition of vanishing tangential electric field on the conducting cylindrical wall at $\rho = c$.

Similar to Chapter IV, the solution is obtained by first constructing the appropriate Green's functions describing the impulse

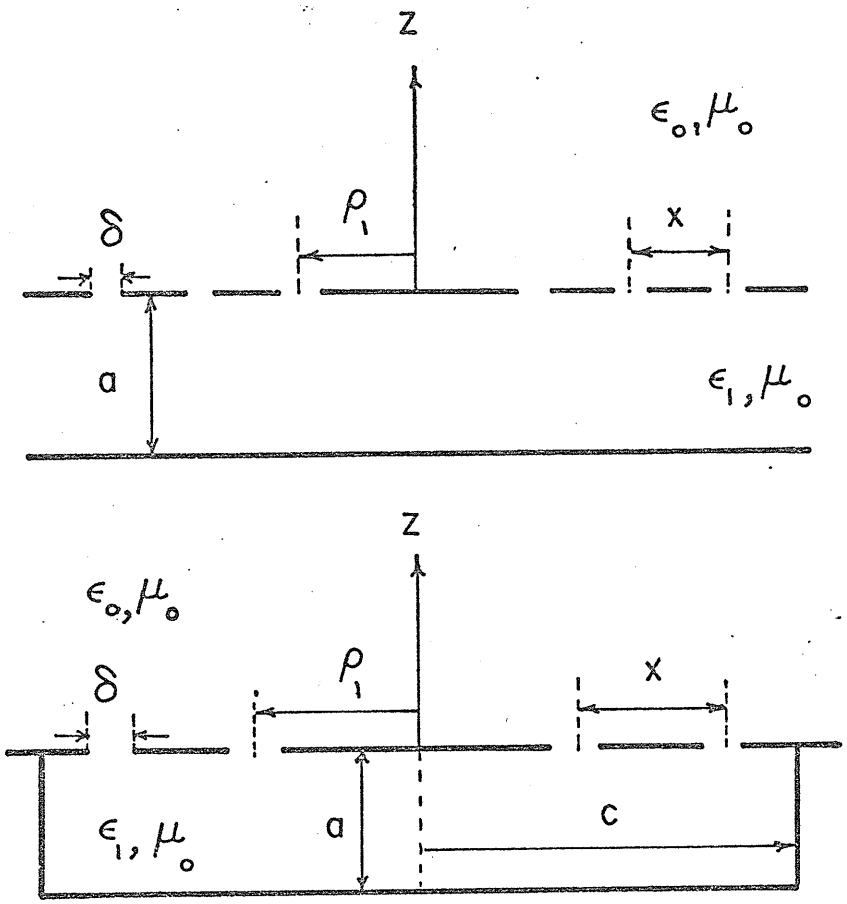

Figure 5.1: Typical cavity-backed annular slot array antenna.

response to a current filament of a general nature and then the final formulation is simply the integral of the impulse function over the aperture source distribution. However, as it will be described later, the impulse response exhibits a set of natural frequencies associated with the back-up cavity. The field coefficients are obtained in a similar manner as the two previous chapters by an application of the boundary condition on the magnetic field across the aperture. As before, the Green's functions due to an electric ring which is closely related to the former case are also derived. This would enable one to formulate the problems involving annular or cylindrical shaped scattering bodies in the cavity region in addition to the slots on the conducting walls.

5.2 Problem Formulation and Solution

5.2.1 Construction of the Appropriate Green's Functions, Magnetic Ring

Consider the geometry shown in figure 5.2, formed by a cylindrical cavity of thickness a and radius c. The constitutive parameters of the medium are ε and μ_o. The source is a magnetic filament of strength $I_m(\phi')$ characterized by equations (3.1,3.2). This problem is similar to the case of a radial waveguide which was treated in Chapter III, however, the existance of the conducting cylindrical wall at $\rho = c$ imposes the following conditions on the tangential electric field on the surface of the cylinder,

$$\begin{aligned} &\rho = c \\ E_z = E_\phi = 0 \qquad &0 \leq z \leq a \\ &0 \leq \phi \leq 2\pi \end{aligned} \tag{5.1}$$

Noting equations (3.3,3.4), the wave functions which satisfy the boundary conditions on the conducting planes at $z = -a, 0,$ can be

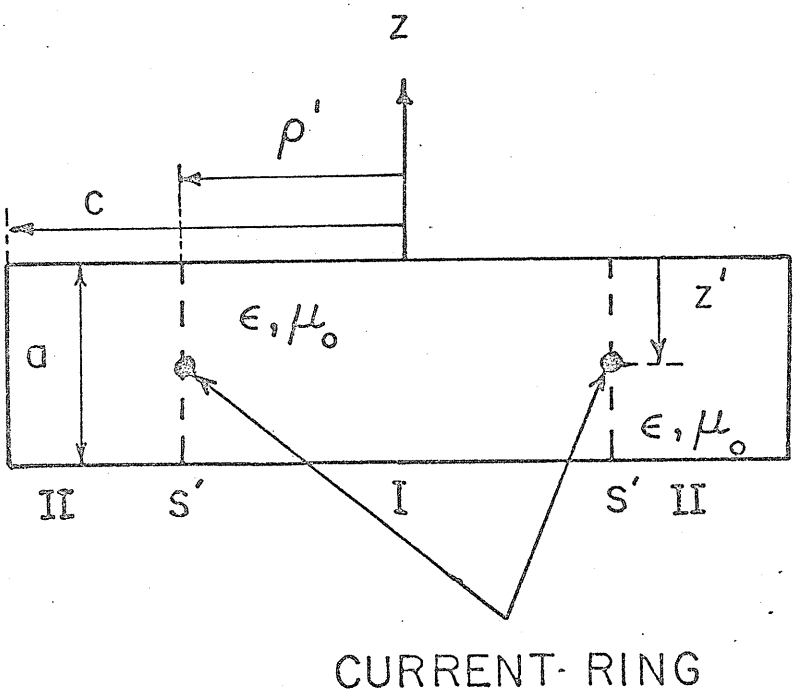

Figure 5.2: Current ring in a cylindrical cavity (impulse response).

expressed as

$$\psi^e = \sum_{n=0}^{\infty} \sum_{m=0}^{\infty} (a_n \cos n\phi + b_n \sin n\phi) \cos \frac{m\pi}{a} z$$

$$\begin{cases} u^e_{mn} J_n(k_{\rho m}\rho) & \rho < \rho' \\ [U^e_{mn} J_n(k_{\rho m}\rho) + V^e_{mn} N_n(k_{\rho m}\rho)] & \rho > \rho' \end{cases} \qquad (5.2a)$$

$$\psi^h = \sum_{n=0}^{\infty} \sum_{m=0}^{\infty} n(b_n \cos n\phi - a_n \sin n\phi) \sin \frac{m\pi}{a} z$$

$$\begin{cases} u^h_{mn} J_n(k_{\rho m}\rho) & \rho < \rho' \\ [U^h_{mn} J_n(k_{\rho m}\rho) + V^h_{mn} N_n(k_{\rho m}\rho)] & \rho > \rho' \end{cases} \qquad (5.2a)$$

where $k_{\rho m}$ is given by (3.5c). Note that due to the finiteness of the cavity, the most general form of the solution for the radial dependent part in region II has been selected. In order to determine the six unknown coefficients, we utilize the boundary conditions across the source surface as well as the cylindrical conducting wall, equation (5.1). The continuity of the tangential magnetic field across the surface $\rho = \rho'$ is ensured by satisfying the following relations

$$H^I_z - H^{II}_z = \frac{1}{j\omega\mu_o} \sum_{m=0}^{\infty} \sum_{n=0}^{\infty} n(b_n \cos n\phi - a_n \sin n\phi) k^2_{\rho m} \sin \frac{m\pi}{a} z$$

$$\Big|_{\substack{\rho = \rho' \\ 0 \le \phi \le 2\pi \\ -a \le z \le 0}} \cdot [(U^h_{mn} - u^h_{mn}) J_n(k_{\rho m}\rho') + V^h_{mn} N_n(k_{\rho m}\rho')] = 0 \qquad (5.3a)$$

$$H_{\phi}^{I} - H_{\phi}^{II} = \frac{\pi}{j\omega\mu_o\rho' a} \sum_{m=0}^{\infty}\sum_{n=0}^{\infty} mn^2 (a_n \cos n\phi + b_n \sin n\phi) \cos\frac{m\pi}{a} z$$

$$\Big|_{\substack{\rho = \rho' \\ 0 \le \phi \le 2\pi \\ -a \le z \le 0}} \quad [(U_{mn}^{h} - u_{mn}^{h}) J_n(k_{\rho m}\rho') + V_{mn}^{h} N_n(k_{\rho m}\rho')]$$

$$+ \sum_{m=0}^{\infty}\sum_{n=0}^{\infty} (a_n \cos n\phi + b_n \sin n\phi) k_{\rho m} \cos\frac{m\pi}{a} z$$

$$[(U_{mn}^{e} - u_{mn}^{e}) J_n'(k_{\rho m}\rho') + V_{mn}^{e} N_n'(k_{\rho m}\rho')] = 0 \qquad (5.3b)$$

Which upon utilizing the orthogonality property of sinusoidal functions over the range $-a \le z \le 0$ and $0 \le \phi \le 2\pi$ are reduced to

$$(U_{mn}^{h} - u_{mn}^{h}) J_n(k_{\rho m}\rho') + V_{mn}^{h} N_n(k_{\rho m}\rho') = 0 \qquad (5.4a)$$

$$(U_{mn}^{e} - u_{mn}^{e}) J_n'(k_{\rho m}\rho') + V_{mn}^{e} N_n'(k_{\rho m}\rho') = 0 \qquad (5.4b)$$

The continuity of E_{ϕ} can be stated as

$$E_{\phi}^{I} - E_{\phi}^{II} = \frac{\pi}{j\omega\varepsilon\rho' a} \sum_{m=0}^{\infty}\sum_{n=0}^{\infty} mn(b_n \cos n\phi - a_n \sin n\phi) \sin\frac{m\pi}{a} z$$

$$\Big|_{\substack{\rho = \rho' \\ 0 \le \phi \le 2 \\ -a \le z \le 0}} \quad [(U_{mn}^{e} - u_{mn}^{e}) J_n(k_{\rho m}\rho') + V_{mn}^{e} N_n(k_{\rho m}\rho')]$$

$$- \sum_{m=0}^{\infty}\sum_{n=0}^{\infty} n(b_n \cos n\phi - a_n \sin n\phi) k_{\rho m} \sin\frac{m\pi}{a} z$$

$$[(U_{mn}^{h} - u_{mn}^{h}) J_n'(k_{\rho m}\rho') + V_{mn}^{h} N_n'(k_{\rho m}\rho') = 0 \qquad (5.5a)$$

however, the axial component of the electric field is discontinuous across S' by an amount equal to the magnetic current density, that is

$$E_z^{I} - E_z^{II} = I_m(\phi')\,\delta(z - z') \qquad (5.5b)$$

Substituting the respective relations for E_z^I and E_z^{II} and using the properties of delta functions, the equations (5.5) yield

$$(U^e_{mn} - u^e_{mn})\, J_n(k_{\rho m}\rho') + V^e_{mn}\, N_n(k_{\rho m}\rho') = \frac{j\omega\,\varepsilon\,\varepsilon_m}{k^2_{\rho m}\, a} \cos\frac{m\pi}{a} z' \qquad (5.6a)$$

$$(U^h_{mn} - u^h_{mn})\, J_n(k_{\rho m}\rho') + V^h_{mn}\, N_n(k_{\rho m}\rho') = 0 \qquad (5.6b)$$

The presence of the conducting wall at $\rho = c$ requires,

$$U^h_{mn}\, J'_n(k_{\rho m}\, c) + V^h_{mn}\, N'_n(k_{\rho m}\, c) = 0 \qquad (5.7a)$$

$$U^e_{mn}\, J_n(k_{\rho m}\, c) + V^e_{mn}\, N_n(k_{\rho m}\, c) = 0 \qquad (5.7b)$$

where a use has been made of the condition (5.1) and the resulting relations are reduced by applying the orthogonality of sinusoidal functions. The set of equations (5.4), (5.6) and (5.7) can be solved for the coefficients and the final results are

$$U^e_{mn} = \frac{j\pi\omega\varepsilon\rho'\, N_n(k_{\rho m}\, c)}{2k_{\rho m}a\, J_n(k_{\rho m}\, c)}\, \varepsilon_m \cos\frac{m\pi}{a} z' J'_n(k_{\rho m}\,\rho')$$

$$V^e_{mn} = -\frac{j\pi\omega\varepsilon\rho'}{2k_{\rho m}a}\, \varepsilon_m \cos\frac{m\pi}{a} z' J'_n(k_{\rho m}\,\rho')$$

$$U^h_{mn} = -\frac{\pi^2 m\, N'_n(k_{\rho m}\, c)}{2(k_{\rho m}a)^2\, J'_n(k_{\rho m}\, c)}\, \varepsilon_m \cos\frac{m\pi}{a} z' J_n(k_{\rho m}\,\rho') \qquad (5.8)$$

$$V^h_{mn} = \frac{\pi^2 m}{2(k_{\rho m}a)^2}\, \varepsilon_m \cos\frac{m\pi}{a} z' J_n(k_{\rho m}\,\rho')$$

$$u^e_{mn} = -\frac{j\pi\omega\varepsilon\rho'}{2k_{\rho m}a}\, \varepsilon_m \cos\frac{m\pi}{a} z' \left[N'_n(k_{\rho m}\,\rho') - \frac{N_n(k_{\rho m}\, c)}{J_n(k_{\rho m}\, c)} J'_n(k_{\rho m}\,\rho')\right]$$

$$u^m_{mn} = \frac{\pi^2 m}{2(k_{\rho m}a)^2}\, \varepsilon_m \cos\frac{m\pi}{a} z' \left[N_n(k_{\rho m}\,\rho') - \frac{N'_n(k_{\rho m}\, c)}{J'_n(k_{\rho m}\, c)} J_n(k_{\rho m}\,\rho')\right]$$

Note that in (5.8), for $k_{\rho m}\, c$ equal to zeros of $J_n(z)$ and $J_n'(z)$, there is no steady-state solution to the problem. These values are associated with the TM and TE natural frequencies of the cavity, hence, existence of a source of the same frequency as any of the resonant frequencies of the cavity results in an unstable solution.

In view of equations (5.2) and (5.8), the Green's functions of a magnetic current filament characterized by (3.1,3.2) are as follows

$$\psi^e = -\frac{j\pi\omega\varepsilon\rho'}{2a} \sum_{m=0}^{\infty} \sum_{n=0}^{\infty} \frac{\varepsilon_m}{k_{\rho m}} (a_n \cos n\phi + b_n \sin n\phi) \cos \frac{m\pi}{a} z' \cos \frac{m\pi}{a} z$$

$$\cdot \begin{cases} \dfrac{J_n(k_{\rho m}c)\, N_n'(k_{\rho m}\rho') - N_n(k_{\rho m}c)\, J_n'(k_{\rho m}\rho')}{J_n(k_{\rho m}c)}\, J_n(k_{\rho m}\rho) & \rho < \rho' \\ \dfrac{J_n(k_{\rho m}c)\, N_n(k_{\rho m}\rho) - N_n(k_{\rho m}c)\, J_n(k_{\rho m}\rho)}{J_n(k_{\rho m}c)}\, J_n'(k_{\rho m}\rho') & \rho > \rho' \end{cases} \tag{5.9a}$$

$$\psi^h = \frac{\pi^2}{2a^2} \sum_{m=0}^{\infty} \sum_{n=0}^{\infty} \frac{\varepsilon_m\, m\, n}{k_{\rho m}^2} (b_n \cos n\phi - a_n \sin n\phi) \cos \frac{m\pi}{a} z' \sin \frac{m\pi}{a} z$$

$$\cdot \begin{cases} \dfrac{J_n'(k_{\rho m}c)\, N_n(k_{\rho m}\rho') - N_n'(k_{\rho m}c)\, J_n(k_{\rho m}\rho')}{J_n'(k_{\rho m}c)}\, J_n(k_{\rho m}\rho) & \rho < \rho' \\ \dfrac{J_n'(k_{\rho m}c)\, N_n(k_{\rho m}\rho) - N_n'(k_{\rho m}c)\, J_n(k_{\rho m}\rho)}{J_n'(k_{\rho m}c)}\, J_n(k_{\rho m}\rho') & \rho > \rho' \end{cases} \tag{5.9b}$$

5.2.2 Electric Ring

The derivation method for this case is similar to the previous case and the main differences together with the final results are presented here. Aside from the subscript m, the defining equations for

the current ring and its Fourier expansion are given by (3.1) and (3.2). The azimuthal dependence of the e and h modes are expressed by (3.13) which result in the following form for the required Green's functions

$$\psi^e = \sum_{m=0}^{\infty} \sum_{n=0}^{\infty} n(b_n \cos n\phi - a_n \sin n\phi) \cos \frac{m\pi}{a} z \begin{cases} u^e_{mn} J_n(k_{\rho m}\rho) & \rho < \rho' \\ [U^e_{mn} J_n(k_{\rho m}\rho) + V^e_{mn} N_n(k_{\rho m}\rho)] & \rho > \rho' \end{cases}$$

$$\psi^e = \sum_{m=0}^{\infty} \sum_{n=0}^{\infty} (a_n \cos n\phi + b_n \sin n\phi) \sin \frac{m\pi}{a} z \begin{cases} u^h_{mn} J_n(k_{\rho m}\rho) & \rho < \rho' \\ [U^h_{mn} J_n(k_{\rho m}\rho) + V^h_{mn} N_n(k_{\rho m}\rho)] & \rho > \rho' \end{cases}$$

(5.9b)

Now, in contrast to the previous case, the axial component of the electric field E_z is continuous across S' but the magnetic field is discontinuous by an amount equal to

$$H_z^I - H_z^{II} = I(\phi') \quad (z - z') \Big|_{\substack{\rho = \rho' \\ 0 \le \phi \le 2\pi \\ -a \le z \le 0}} \tag{5.10}$$

A similar approach as that of the magnetic case yields

$$U^e_{mn} = \frac{\pi^2 m \, N_n'(k_{\rho m} c)}{2(k_{\rho m} a)^2 \, J_n'(k_{\rho m} c)} \varepsilon_m \sin \frac{m\pi}{a} z' \, J_n(k_{\rho m}\rho')$$

$$V^e_{mn} = -\frac{\pi^2 m}{2(k_{\rho m} a)^2} \varepsilon_m \sin \frac{m\pi}{a} z' \, J_n(k_{\rho m}\rho')$$

$$U^h_{mn} = -\frac{j\pi\omega\mu_o\rho' N_n(k_{\rho m}c)}{2k_{\rho m}a\, J_n(k_{\rho m}c)}\,\varepsilon_m \sin\frac{m\pi}{a}z'\, J'_n(k_{\rho m}\rho')$$

$$V^h_{mn} = \frac{j\pi\omega\mu_o\rho'}{2k_{\rho m}a}\,\varepsilon_m \sin\frac{m\pi}{a}z'\, J'_n(k_{\rho m}\rho')$$

$$u^e_{mn} = -\frac{\pi^2 m}{2(k_{\rho m}a)^2}\,\varepsilon_m \sin\frac{m\pi}{a}z'\left[N_n(k_{\rho m}\rho') - \frac{N'_n(k_{\rho m}c)}{J'_n(k_{\rho m}c)}J_n(k_{\rho m}\rho')\right]$$

$$u^h_{mn} = \frac{j\pi\omega\mu_o\rho'}{2k_{\rho m}a}\,\varepsilon_m \sin\frac{m\pi}{a}z'\left[N'_n(k_{\rho m}\rho') - \frac{N_n(k_{\rho m}c)}{J_n(k_{\rho m}c)}J'_n(k_{\rho m}\rho')\right] \tag{5.11}$$

Note that as z' approaches $-a$ and zero (conducting boundaries) the field vanishes. This is similar to the result obtained in Section (3.2) and the same argument applies here.

In view of the above set of equations and (5.9), the Green's functions of an electric current filament are as follows

$$\psi^e = -\frac{\pi^2}{2a^2}\sum_{m=0}^{\infty}\sum_{n=0}^{\infty}\frac{\varepsilon_m\, m\, n}{k^2_{\rho m}}(b_n\cos n\phi - a_n\sin n\phi)\sin\frac{m\pi}{a}z'\cos\frac{m\pi}{a}z$$

$$\begin{cases}\dfrac{J'_n(k_{\rho m}c)\,N_n(k_{\rho m}\rho') - N'_n(k_{\rho m}c)\,J_n(k_{\rho m}\rho')}{J'_n(k_{\rho m}c)}\,J_n(k_{\rho m}\rho) & \rho < \rho' \\[2ex] \dfrac{J'_n(k_{\rho m}c)\,N_n(k_{\rho m}\rho) - N'_n(k_{\rho m}c)\,J_n(k_{\rho m}\rho)}{J'_n(k_{\rho m}c)}\,J_n(k_{\rho m}\rho') & \rho > \rho'\end{cases} \tag{5.12a}$$

$$\psi^h = \frac{j\pi\omega\mu_o\rho'}{2a}\sum_{m=0}^{\infty}\sum_{n=0}^{\infty}\frac{\varepsilon_m}{k_{\rho m}}(a_n\cos n\phi + b_n\sin n\phi)\sin\frac{m\pi}{a}z'\sin\frac{m\pi}{a}z$$

$$\begin{cases}\dfrac{J_n(k_{\rho m}c)\,N'_n(k_{\rho m}\rho') - N_n(k_{\rho m}c)\,J'_n(k_{\rho m}\rho')}{J_n(k_{\rho m}c)}\,J_n(k_{\rho m}\rho) & \rho < \rho' \\[2ex] \dfrac{J_n(k_{\rho m}c)\,N_n(k_{\rho m}\rho) - N_n(k_{\rho m}c)\,J_n(k_{\rho m}\rho)}{J_n(k_{\rho m}c)}\,J'_n(k_{\rho m}\rho') & \rho > \rho'\end{cases} \tag{5.12b}$$

5.3 Formulation of the Problem of a Cavity-Backed Annular Slot Array Antenna

Employing a similar approach as for the case of a radial waveguide fed annular slot antenna (Chapter IV), it is an easy matter to formulate the present problem, that is, the aperture field is expressed in terms of a finite sum of pulse functions with unknown coefficients. Then an application of the continuity condition of the azimuthal component of the total magnetic field across the coupling aperture determines the slots field coefficients E_i. Therefore, recalling equations (3.30), (3.31) and (3.2a,b) and the corresponding relations for the external region covered in Chapter IV, one obtains

$$
\begin{aligned}
Y_{ij} = {} & (j\omega\varepsilon_o) \cdot \frac{\rho_i}{\delta_j} \int_o^\infty [J_q(\alpha\rho_i)]_-^+ \cdot [J_q(\alpha\rho_j)]_-^+ \frac{d\alpha}{\alpha\gamma} \\
& + \frac{q^2}{(j\omega\mu_o)\rho_j\delta_j} \int_o^\infty [C_q(\alpha\rho_i)]_-^+ \cdot [C_q(\alpha\rho_j)]_-^+ \cdot \frac{\gamma}{\alpha}\, d\alpha \\
& - \frac{j\pi\omega\varepsilon\,\rho_i}{2a\,\delta_j} \sum_{m=0}^{\infty} \frac{\varepsilon_m}{k_{\rho m}^2} \frac{J_q(k_{\rho m}c) \begin{bmatrix} N_q(k_{\rho m}\rho_j) \\ N_q(k_{\rho m}\rho_i) \end{bmatrix}_-^+ - N_q(k_{\rho m}c) \begin{bmatrix} J_q(k_{\rho m}\rho_j) \\ J_q(k_{\rho m}\rho_i) \end{bmatrix}_-^+}{J_q(k_{\rho m}c)} \\
& \cdot \begin{bmatrix} J_q(k_{\rho m}\rho_i) \\ J_q(k_{\rho m}\rho_j) \end{bmatrix}_-^+ + \frac{\pi^3 q^2}{2(j\omega\mu_o)\rho_j a^3\delta_j} \sum_{m=0}^{\infty} \frac{m^2}{k_{\rho m}^2} \varepsilon_m \\
& \frac{J_q'(k_{\rho m}c) \begin{bmatrix} C_{qm}^N(\rho_j) \\ C_{qm}^N(\rho_i) \end{bmatrix}_-^+ - N_q'(k_{\rho m}c) \begin{bmatrix} C_{qm}^J(\rho_j) \\ C_{qm}^J(\rho_i) \end{bmatrix}_-^+}{J_q'(k_{\rho m}c)} \begin{bmatrix} C_{qm}^J(\rho_i) \\ C_{qm}^J(\rho_j) \end{bmatrix}_-^+
\end{aligned}
\tag{5.13a}
$$

where, $C_{qm}^{J,N}(\rho)$ is given by (3.32e) and $(+,-)$ corresponds to $(\overset{+}{\rho}, \bar{\rho})$, respectively. The incident field is assumed to be a TM_{pq} mode and its particulars are discussed later. For $i = j$ case, we have

$$Y_{ii} = (j\omega\varepsilon_o) \cdot \frac{\rho_i}{\delta_j} \int_o^\infty [J_q(\alpha\rho_i)]_-^+ \cdot [J_q(\alpha\rho_i)]_-^+ \frac{d\alpha}{\alpha\gamma}$$

$$+ \frac{q^2}{(j\omega\mu_o)\rho_i\delta_i} \int_o^\infty [C_q(\alpha\rho_i)]_-^+ \cdot [C_q(\alpha\rho_i)]_-^+ \cdot \frac{\gamma}{\alpha} d\alpha$$

$$- \frac{j\pi\omega\varepsilon\ \rho_i}{6a} \sum_{m=0}^{\infty} \frac{\varepsilon_m}{k_{\rho m}} \{ \frac{J_q(k_{\rho m}c)[N_q(k_{\rho m}\rho_i)]_-^+ - N_q(k_{\rho m}c)[J_q(k_{\rho m}\rho_i)]_-^+}{J_q(k_{\rho m}c)}$$

$$\cdot J_q'(k_{\rho m}\bar{\rho}_i) + \frac{J_q(k_{\rho m}c)N_q'(k_{\rho m}\overset{+}{\rho}_i) - N_q(k_{\rho m}c)J_q'(k_{\rho m}\overset{+}{\rho}_i)}{J_q(k_{\rho m}c)} [J_q(k_{\rho m}\rho_i)]_-^+$$

$$+ \frac{J_q(k_{\rho m}c)[N_q(k_{\rho m}\rho_i)]_{\rho_i}^+ - N_q(k_{\rho m}c)[J_q(k_{\rho m}\rho_i)]_{\rho_i}^+}{J_q(k_{\rho m}c)} J_q'(k_{\rho m}\rho_i)$$

$$+ \frac{J_q(k_{\rho m}c)\ N_q'(k_{\rho m}\rho_i) - N_q(k_{\rho m}c)\ J_q'(k_{\rho m}\rho_i)}{J_q(k_{\rho m}c)} [J_q(k_{\rho m}\rho_i)]_-^{\rho_i} \}$$

$$+ \frac{\pi^3 q^2}{6(j\omega\mu_o)\rho_i a^3} \sum_{m=0}^{\infty} \frac{m^2}{k_{\rho m}^2} \varepsilon_m \{ \frac{J_q'(k_{\rho m}c)[C_{qm}^N(\rho_i)]_-^+ - N_q'(k_{\rho m}c)[C_{qm}^J(\rho_i)]_-^+}{J_q'(k_{\rho m}c)}$$

$$\cdot J_q(k_{\rho m}\bar{\rho}_i) + \frac{J_q'(k_{\rho m}c)\ N_q(k_{\rho m}\overset{+}{\rho}_i) - N_q'(k_{\rho m}c)\ J_q(k_{\rho m}\overset{+}{\rho}_i)}{J_q'(k_{\rho m}c)} [C_{qm}^J(\rho_i)]_-^+$$

$$+ \frac{J_q'(k_{\rho m}c)[C_{qm}^N(\rho_i)]_{\rho_i}^+ - N_q'(k_{\rho m}c)[C_{qm}^J(\rho_i)]_{\rho_i}^+}{J_q'(k_{\rho m}c)} J_q(k_{\rho m}\rho_i)$$

$$+ \frac{J'_q(k_{\rho m}c)\, N_q(k_{\rho m}\rho_i) - N'_q(k_{\rho m}c)\, J_q(k_{\rho m}\rho_i)}{J'_q(k_{\rho m}c)} [C^J_{qm}(\rho_i)]^{\rho_i}_{-}\}$$

(5.13b)

Note that the case of $q = 0$ (ϕ symmetry) gives rise to a TM field and the field components are solely determined from ψ^e.

The incident field due to the feeding assembly placed in the central region of the cavity must also have $E_z^{inc} = E_\phi^{inc} = 0$ on the cylindrical conducting wall. Therefore, a suitable representation for the incident mode of a TM_{pq} type which satisfies the boundary conditions as well as the singularity of the source in the cavity region is as follows

$$\psi^{e\,inc}_{pq} = \cos\frac{p\pi}{a} z \cos q\phi \cdot \frac{J_q(k_{\rho p}c)\, N_q(k_{\rho p}\rho) - N_q(k_{\rho p}c)\, J_q(k_{\rho p}\rho)}{J_q(k_{\rho p}c)}$$

(5.14)

Hence, recalling (3.32a), we have

$$Y_j = -\frac{1}{\delta_j} \frac{J_q(k_{\rho p}c)\, [N_q(k_{\rho p}\rho_j)]^{+}_{-} - N_q(k_{\rho p}c)\, [J_q(k_{\rho p}\rho_j)]^{+}_{-}}{J_q(k_{\rho p}c)} \qquad (5.15)$$

Once the aperture field coefficients are determined from the matrix equation (3.32a) with elements given by (5.13) and (5.15), the other parameters of interest can easily be computed.

5.3.1 Expression for the Total Power

An examination of the physical nature of the problem reveals that there is no power transfer through the cavity region after the last slot. Therefore, the total power injected by the source system is coupled into the free space by means of the slot array. An application of equation (3.34) to an arbitrary cylindrical surface with a radius

smaller than the first slot results in an expression for the total power delivered by the source. As before, we assume the thickness of the cavity is smaller than $\lambda/2$, hence, only the TM_{01} modes contribute to the power transfer. The wave functions are expressed by

$$\psi^e = -\frac{j\pi\omega\varepsilon}{2a} \sum_{m=0}^{\infty} \sum_{n=0}^{\infty} \sum_{i=1}^{IC} \frac{\varepsilon_m \rho_i}{k_{\rho m}^2} E_{in} (a_n \cos n\phi + b_n \sin n\phi) \cos \frac{m\pi}{a} z$$

$$\frac{J_n(k_{\rho m}c)[N_n(k_{\rho m}\rho_i)]_-^+ - N_n(k_{\rho m}c)[J_n(k_{\rho m}\rho_i)]_-^+}{J_n(k_{\rho m}c)} J_n(k_{\rho m}\rho) \qquad \rho < \rho_i$$

$$\frac{J_n(k_{\rho m}c)\, N_n(k_{\rho m}\rho) - N_n(k_{\rho m}c)\, J_n(k_{\rho m}\rho)}{J_n(k_{\rho m}c)} [J_n(k_{\rho m}\rho_i)]_-^+ \qquad \rho > \rho_i$$

(5.16a)

$$\psi^h = \frac{\pi^2}{2a^2} \sum_{m=0}^{\infty} \sum_{n=0}^{\infty} \sum_{i=1}^{IC} \frac{\varepsilon_m m n}{k_{\rho m}} (a_n \cos n\phi + b_n \sin n\phi) \sin \frac{m\pi}{a} z$$

$$\frac{J_n'(k_{\rho m}c)\, [C_{nm}^N(\rho_i)]_-^+ - N_n'(k_{\rho m}c)\, [C_{nm}^J(\rho_i)]_-^+}{J_n'(k_{\rho m}c)} J_n(k_{\rho m}\rho) \qquad \rho < \rho_i$$

$$\frac{J_n'(k_{\rho m}c)\, N_n(k_{\rho m}\rho) - N_n'(k_{\rho m}c)\, J_n(k_{\rho m}\rho)}{J_n'(k_{\rho m}c)} [C_{nm}^J(\rho_i)]_-^+ \qquad \rho > \rho_i$$

(5.16b)

As before, the coefficients a_n and b_n entirely depend on the incident field. It can be shown that (Appendix G) the total power due to a general source of TM_{pq} type (combination of TM_{pq} modes) is given by

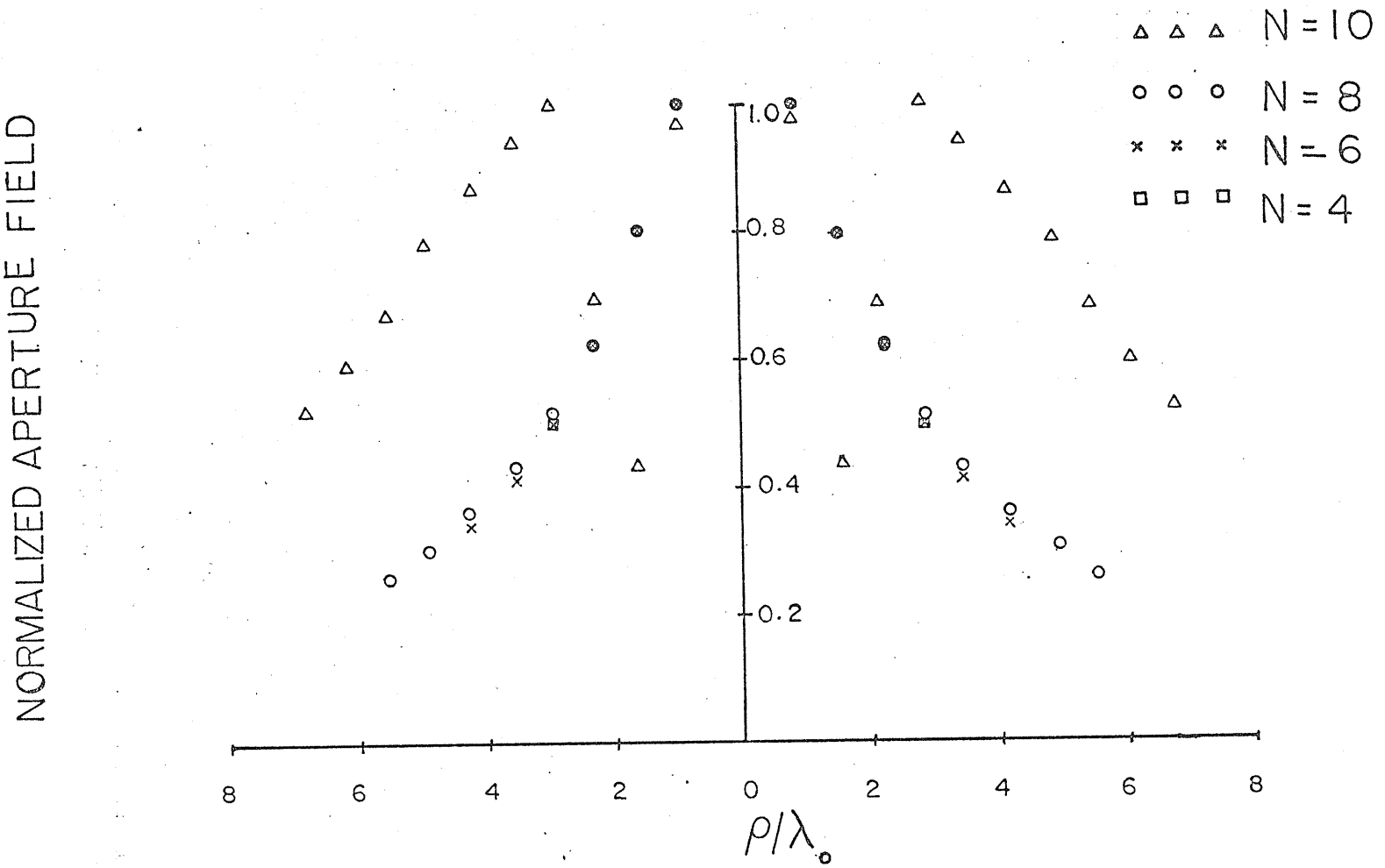

Figure 5.3: Array amplitude distribution. $\varepsilon_r = 2.32$, $k_o\delta = 0.30$, $k_o\rho_1 = 5.81$, $k_ox = 4.19$, $k_oa = 0.33$, $(k_oc - k_o\rho_N) = 0.82$, TM_{01} exciting mode.

$$P_{Total} = -2\pi \sum_{q=0}^{\infty} \sum_{i=1}^{IC} \frac{(a_q^2 + b_q^2)}{\varepsilon_q} \rho_i \mathrm{Re}(E_{iq}) \frac{J_q(kc)[N_q(k\rho_i)]^+ - N_q(kc)[J_q(k\rho_i)]^+}{J_q(kc)} \tag{5.17}$$

where a_q and b_q are the respective Fourier coefficients for the source function.

5.4 Radiation Characteristics of Cavity-Backed Annular Slot Arrays

Based on the theory presented in the earlier sections, the aperture field distribution and the radiation patterns of the cavity-backed annular slot arrays are studied for a number of cases. Figures 5.3 and 5.4 illustrate the amplitude and phase distributions among the elements of four arrays. Aside from the total number of elements forming the arrays (N), the antenna systems are identical. The slot spacing is selected about one λ to have constant phase distribution among the elements. It is interesting to note that as new slots are introduced to the initial array of four elements the amplitudes and phases of the previous slots are not affected appreciably, excluding the case of N = 10. The slot phases are almost constant and the amplitude distributions are similar to $\cos^p(\rho)$ distribution. The above results indicate that the mutual coupling between the slots is not strong for these cases. However, for N = 10, the system exhibits a resonant effect and the aperture fields of the first few slots are changed drastically. A higher order lobe is created at the center and the excitation levels of the slots with larger diameters are raised and the effective aperture diameter seems to be larger than that of the last slot. However, the decaying factor associated with the amplitude variation, with the exception

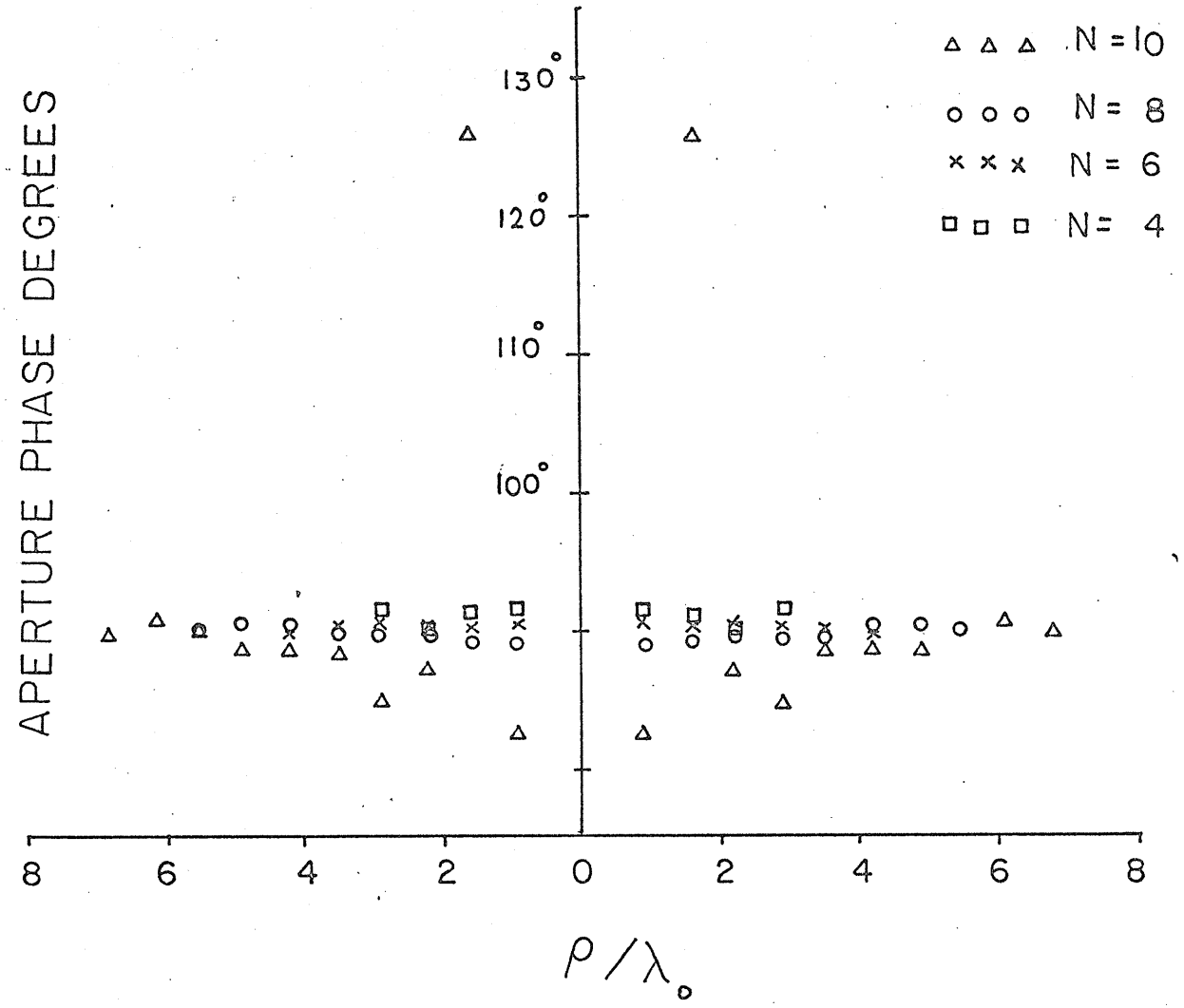

Figure 5.4: Array phase distribution.

of the first three slots, is similar to the previous cases.

It is generally desired to relate the antenna gain to its beam width by an approximate relation [52],[68],[69]. A formula based on experimental results is [52].

$$G = A_J/(\theta_E^\circ \cdot \theta_H^\circ) \qquad A_J = 27{,}000 \tag{5.18}$$

where θ_E° and θ_H° are the half-power beam widths corresponding to the two principal planes. The above formula is obtained for antennas with 65% aperture efficiency. In Table 5.1, the half-power beam width, gain and efficiency values for the cavity-backed annular slot arrays discussed earlier are tabulated. For these antenna systems A_J factor is calculated and the results are included in Table 5.1. The average value of the factor for cavity-backed antennas is observed to be $A_{average} = 39{,}536$. It is interesting to note that the ratio of the half-power beam widths remains fairly constant as the number of slots increases. Note that the efficiency values obtained are with respect to a circular aperture of constant phase and amplitude distribution and having a diameter equal to the largest slot. However, as it is clear from figure 5.3, the effective aperture of the cavity-backed annular slot array is larger than the radius of the last slot. This is due to the fact that the amplitude of the last slot has a non-zero value. Therefore, an efficiency value larger than 100 per-cent for the case which has a fairly constant phase distribution (N = 4) may be attributed to the respective amplitude distribution.

Table 5.2 compares the approximate formulas suggested by the references cited earlier. The predicted gain values by the first and the third approximate formulas, which are basically the same, agree well with the computed gain figures. However, the second formula [69] fails

N	θ°_{E}	θ°_{H}	θ_{H}/θ_{E}	Gain dB	Efficiency %	$A = \theta^{\circ}_{E} \cdot \theta^{\circ}_{H} \cdot G$
4	8.0	14.0	1.75	25.33	103	37,321
6	5.8	10.4	1.79	28.27	96	40,567
8	4.6	8.3	1.80	30.33	89	40,794
10	3.5	6.2	1.77	32.59	98	39,463

$A_{average} = 39,536$

$(\theta_{H}/\theta_{E})_{average} = 1.78$

Table 5.1: Beam width, gain and efficiency variation of cavity-backed annular slot arrays.

N	$G_{dB} \simeq 10\log(\frac{39,536}{\theta^{\circ}_{E} \cdot \theta^{\circ}_{H}})$	$G_{dB} \simeq 10\log[32\ell_{n}(\frac{6,566}{\theta^{\circ 2}_{H} + \theta^{\circ 2}_{H}})]$	$G_{dB} \simeq 10\log(\frac{41,253}{\theta^{\circ}_{E} \cdot \theta^{\circ}_{H}})$	G_{dB} (computed)
4	25.48	20.14	25.66	25.33
6	28.16	20.89	28.35	28.27
8	30.15	21.37	30.34	30.33
10	32.60	21.92	32.79	32.59

Table 5.2: Approximate formulas for the gain of the antenna in terms of the half-power beam widths in the two principal planes.

to yield results with reasonable accuracies for the present antenna model.

Figure 5.5 depicts the E and H plane patterns of a cavity-backed annular slot array with eight elements (N = 8). The thick line represents the cross-polarized component at $\phi = 45°$ cut plane. The first side lobe level is lower than 10 dB from the maximum value. The patterns are similar to those of radial waveguide fed annular slot arrays. However, for the present case, all the power injected by the source is coupled out due to the cavity wall.

5.5 Excitation of Radial Waveguides

5.5.1 Introduction

In any electromagnetic wave guiding system, the field must be generated by a suitable source. Throughout the analyses presented so far, a particular waveguide mode has always been assumed as the forcing function without mentioning the physical means of exciting such a mode. In this section attention is paid to a method for generating TM_{00} and TM_{01} which have been used throughout this work. These two modes are capable of producing radiation patterns with the main lobe in the direction of the z axis (TM_{01}) or a null in that direction (TM_{00}). Multi-mode operation which is generally aimed at reducing the cross-polarized component [61] for applications in Frequency-Reuse antenna systems [62]-[64] is presently under investigation by the author.

The polarization state of the antenna is determined basically by the feed assembly. For a small angular region about the antenna axis, linear, orthogonal and circular polarized radiation fields can be obtained. As it will be discussed later, a single feed located in the central region of the radial waveguide or cavity, gives rise to a linearly polarized field. However, a feed assembly formed by two orthogonally located

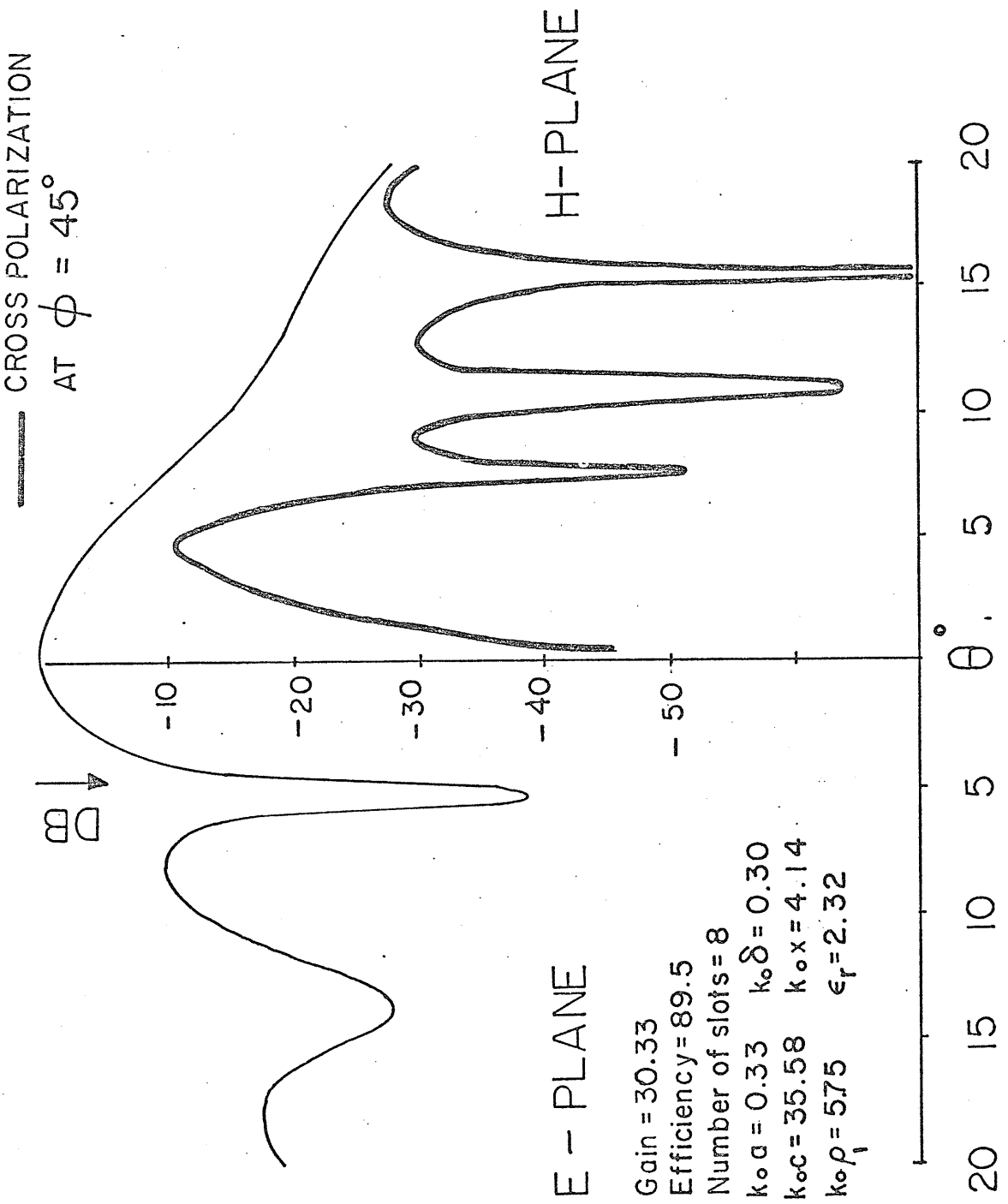

Figure 5.5: Radiation patterns of a cavity-backed annular slot slot array, cross-polarization at $\phi = 45°$. TM_{01} exciting mode.

feeds with respect to the azimuthal angle ϕ and operated with the same carrier frequency would produce orthogonal polarization. This mode of operation is particularly suited for frequency-reuse satellite communication systems. Such a system uses a given up-link and down-link frequency band twice, hence increasing the communication capacity of a single beam by a factor of two. However, single mode operation generates cross-polarization levels which for the off-axis region may create interference problems. For applications when a circularly polarized field is of interest, the annular slot array provides such polarization by operating the feeds in equal amplitude but in phase quadrature.

5.5.2 Method of Excitation of a TM_{00} Radial Mode

Among the simplest methods of excitation for waveguide structures, are the feed systems which employ posts, loops or small apertures [48]. However, for our purposes, a simple basic feeding element is considered, figure 5.6. It consists of a small coaxial line terminated at the center of the radial waveguide or a cavity with its center conductor extending a distance d in the guide region and its outer conductor connected to the lower plate of the waveguide. The height of the probe can be used as a matching parameter between the two waveguides for maximum power transfer. Note that in the analysis which follows we assume the radial structure is uninterrputed. Therefore, for an electrically thin coaxial line the problem is essentially that of a thin vertical current element in a radial waveguide or a cavity. However, the higher order modes created at the slot discontinuities are automatically taken care of in view of the solution developed earlier.

The method for finding the field inside a radial structure is generally based on integration of the appropriate dyadic Green's function

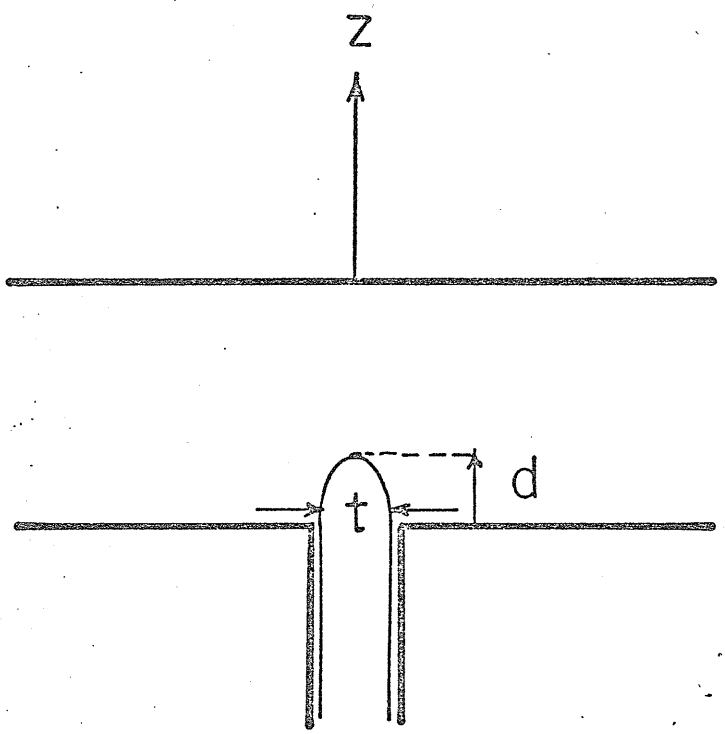

Figure 5.6: Coaxial line probe at the center of a radial waveguide.

corresponding to the electric field radiated by a unit dyadic source over the true source distribution [48]. This is the combination of the equivalent electric and magnetic currents associated with the probe and the small coaxial aperture. An exact solution is quite difficult, however; it has been shown that for a thin coaxial waveguide the effect of the aperture field on the input impedance of the probe is negligible [70]. Therefore, the current is mainly z-directed and its field can be obtained by using the Green's function of a vertically directed current source. The basic principle and the approximate methods for obtaining the input impedance is covered in the literature [48],[70]. However, for our purposes it suffices to say that the field generated by a z-directed electrically thin probe placed at the center of the radial waveguide, due to the ϕ symmetry of the structure, is TM to z and can be expressed as [49]

$$\psi^{e_{inc}}_{TM} = \sum_{m=0}^{\infty} A_m \cos \frac{m\pi}{a} z \, H_o^{(2)}(k_{\rho m}\rho) \tag{5.18}$$

where, $k_{\rho m}$ is given by (3.5c) and A_m can be obtained from a knowledge of the strength of the source. As was stated before, a practical value for a is generally less than $\lambda/2$, therefore, if the slots are sufficiently far from the probe, all the modes with $m > 0$ are evanescent and do not contribute to the travelling wave. However, these modes may have appreciable effects on the input impedance of the probe. Away from the source region, (5.18) can be approximated by

$$\psi^{e_{inc}}_{TM_{00}} = A_o \, H_o^{(2)}(k\rho) \tag{5.19}$$

which is the required TM_{00} mode of the radial waveguide. For a cavity-backed annular slot antenna, using a similar approach and noting the fact

that E_z must vanish at the cylindrical conducting wall placed at $\rho = c$, leads to

$$\psi^{e_{inc}}_{TM_{00}} \sim A_o \frac{J_o(kc)N_o(k\rho) - N_o(kc)J_o(k\rho)}{J_o(kc)} \tag{5.20}$$

The radiation field of a TM_{00} excited annular slot array is θ directed, equation (4.55).

5.5.3 Method of Excitation of a TM_{01} Radial Mode

For this mode of operation, the symmetry of the system with respect to the azimuth coordinate must be perturbed. To this end we consider the geometry shown in figure 5.7. Two identical probes are located symmetrically at a radius $\rho = \rho_s$. The probe currents are in opposite directions arranged by feeding the second probe through a 180° phase shifter. The groundplane is common with the outer conductors of the coaxial lines. The field inside the radial waveguide can be obtained from the following relation

$$\psi^{e_{inc}}_{TM} = \sum_{m=0}^{\infty} A_m \cos\frac{m\pi}{a} z \, H_o^{(2)}[k_{\rho m}|\vec{\rho} - \vec{\rho}_{s1}|] - \sum_{m=0}^{\infty} A_m \cos\frac{m\pi}{a} z \, H_o^{(2)}[k_{\rho m}|\vec{\rho} - \vec{\rho}_{s2}|] \tag{5.21}$$

where $\vec{\rho}_{s1}$ and $\vec{\rho}_{s2}$ are radial positional vectors of the sources and (5.21) merely represents the superposition of the fields contributed by the two sources. The minus sign is due to 180° phase shift and the coefficients are taken to be equal since identical sources are assumed. Note that any mutual interaction between the probes is assumed to be accounted for in A_m. Utilizing the addition theorem for Hankel functions, [49], we have

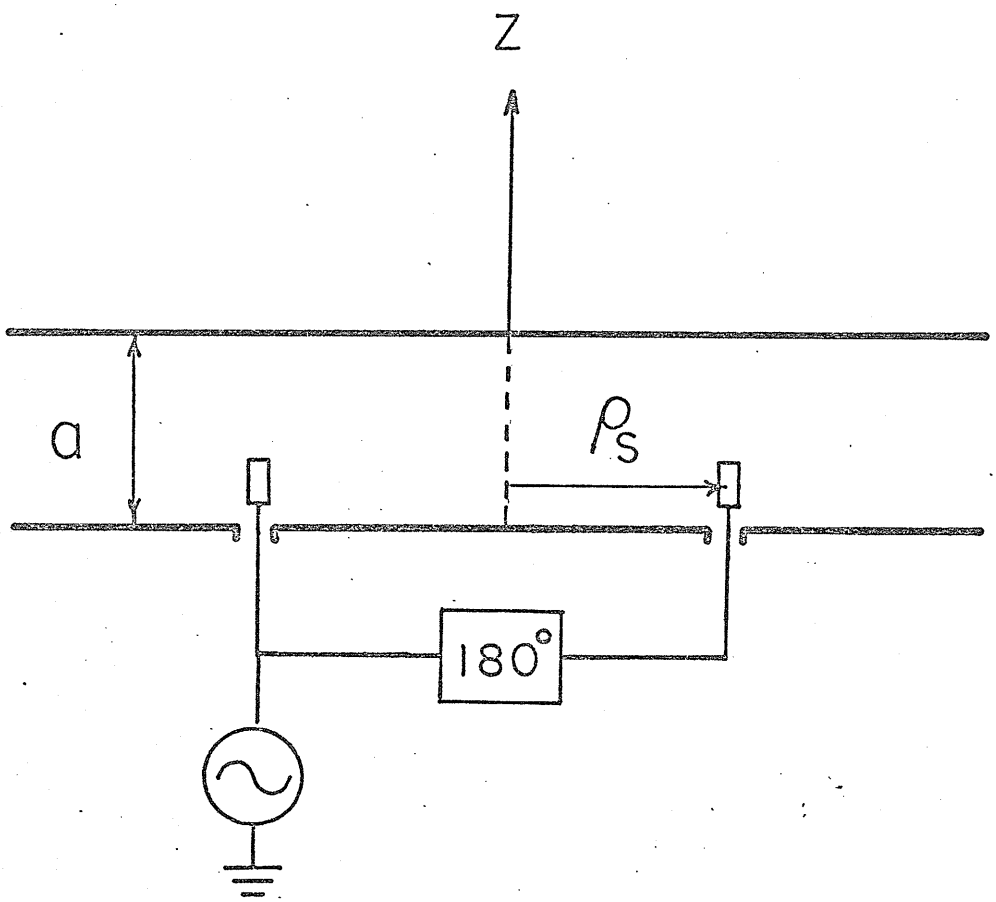

Figure 5.7: Two symmetrically oriented identical probes with a 180° phase difference.

$$H_o^{(2)}(k_{\rho m}|\vec{\rho} - \vec{\rho}_s|) = \begin{cases} \sum_{m=0}^{\infty} H_n^{(2)}(k_{\rho m}\rho_s)\, J_n(k_{\rho m}\rho)\, e^{jn(\phi - \phi_s)} & \rho < \rho_s \\ \sum_{m=-\infty}^{\infty} J_n(k_{\rho m}\rho_s)\, H_n^{(2)}(k_{\rho m}\rho)\, e^{jn(\phi - \phi_s)} & \rho > \rho_s \end{cases} \quad (5.22a)$$

(5.22b)

substituting (5.22a) in (5.21) and noting $\phi_{s2} = \pi + \phi_{s1}$, one obtains

$$\psi_{TM}^{e_{inc}} = \sum_{m=0}^{\infty} \sum_{n=-\infty}^{\infty} A_n \cos\frac{m\pi}{a} z\, J_n(k_{\rho m}\rho_s)\, H_n^{(2)}(k_{\rho m}\rho)\left[e^{jn(\phi-\phi_{s1})} - e^{jn(\phi-\phi_{s1}-\pi)}\right] \quad (5.23)$$

For even values of n, the term in the bracket vanishes, therefore,

$$\psi_{TM}^{e_{inc}} = 2\sum_{m=0}^{\infty} \sum_{n\ \text{odd}}^{\infty} A_m \cos\frac{m\pi}{a} z \cos n(\phi-\phi_{s1})\, J_n(k_{\rho m}\rho_s)\, H_n^{(2)}(k_{\rho m}\rho) \quad \rho > \rho_s \quad (5.24a)$$

where a use has been made of [58]

$$B_{-n}(z) = (-1)^n B_n(z) \quad (5.24b)$$

and $B_n(z)$ is any cylindrical function. Note that if the probes are orthogonally located ($\phi_{s2} = \pi/2 + \phi_{s1}$), odd modes will be eliminated. A consideration of the behaviour of the Bessel functions reveals that for arguments smaller than n, the wave impedances associated with the radial modes become predominantly reactive [49]. Therefore, if ρ_s is selected in such a way that $1 < k_{\rho s} < 3$, the modes with $n > 1$ are attenuated and the main propagating mode is due to $n = 1$. Furthermore, if the guide thickness is smaller than $\lambda/2$, the propagating mode

is given by

$$\psi^{e_{inc}}_{TM_{01}} \sim 2A_o J_1(k\rho_s) \cos(\phi-\phi_{s1}) H_1^{(2)}(k\rho) \qquad (5.25)$$

Taking $\phi_{s1} = 0$ the above relation is, within a multiplicative constant, the desired TM mode.

The radiation pattern for such a feed configuration, depending on the aperture phase distribution, may have a main lobe in the z-direction. As it is evident from equation (4.56), the electric field is x-directed for $\theta = 0$. Therefore, as far as the receiving antenna is concerned and for a small angular region about the z axis, the field may be assumed to be linearly polarized. Note that a 90 degrees rotation of the feed system in either direction about the z axis results in a y-polarized field in the front direction.

For communication links where circular polarized field is of interest, the above configuration does generate such a field by merely operating the two sets of orthogonally located probes in time-phase quadrature. Departure from ideal circular polarization is controlled by the differential phase and the relative magnitude of the excitation currents in the two sets of probes. It should be noted that the polarization is only pure for $\theta = 0$ direction.

5.6 Effects of a Finite Ground Plane on the Radiation Field

In problems associated with radiation from finite slotted structures, the configuration of slot antenna is such that an exact theoretical treatment, if not impossible, is quite complicated. A useful simplifying method is generally based on assuming the slotted front of the radiating antenna to be of infinite extend. This approach, for most

cases, provides results which closely match the measured values in the front direction provided that the edges of the finite ground plane are far from the slot array. However, for the back scattered field, the current induced on the rim of the baffle has the most contribution to the field in this region. Therefore, for geometries having substantial radiation in the plane of the conducting baffle, the excitation of the rim might be strong and the radiation pattern obtained for the infinite ground plane should be modified accordingly. A method for treating these cases is to superpose the infinite ground plane solution, the first order diffracted field and the axial caustic solution in their respective regions of validity by employing the geometrical theory of diffraction, [41]. Excellent results have been obtained and are compared against the measured radiation patterns. The differences between the computed and the measured values are attributed to the fact that aperture field distribution used for pattern computation is assumed to be the unperturbed field of the coaxial feeding guide.

Another method of treatment, which is closely related to the first approach and is presently under investigation by the author, is to replace the finite baffle by an equivalent current sheet. This current which is distributed over the finite plane is assumed to be given by the tangential magnetic field obtained for the infinite case. To take care of the geometrical discontinuity at the edge of the ground plane, a current filament of strength I_e is placed at this location which accounts for the difference between the assumed and the true currents of the rim [65]-[67]. The aperture fields are also affected by truncating the ground plane. The total effect on the radiation pattern can be lumped into a multiplicative complex constant associated with the

electric current distribution over the plane and the aperture. Now, if the aperture were in an infinite ground plane, the equivalent magnetic current associated with the aperture would produce the same radiation field as the equivalent electric current on the aperture and the induced current on the infinite ground plane. This results from the fact that the far field can be obtained from the tangential components of the fields over the plane $z = 0$. However, according to the equivalence principle and image theory, the radiated field is also equivalent to the one produced by an equivalent magnetic current $J_m = 2\ E_a \times \hat{n}$ over the aperture. Therefore, it would appear to be a good approximation to assume that the two sets of sources, for the case of finite ground plane, produce the same field (at least in the direction of the maximum field). This results in an equation in terms of the two newly introduced complex coefficients. We need one more equality to determine the radiation field. This is done by utilizing the principle of the conservation of power. Note that for a finite baffle, the total radiated power is obtained by integrating the poynting vector over a spherical surface enclosing the antenna system. In the above analysis, it is assumed that, for the case of radial waveguide fed antenna, the guide is terminated by a matched load (absorber) and the effects of the current induced on the back side of the antenna assembly on the radiation pattern are considered to be negligible. A quantitative study of the above theory is presently under investigation.

5.7 Experimental Results

In order to verify the validity of the theory presented earlier and investigate the effects of a finite ground plane on the radiation patterns, a small model of a cavity-backed annular slot array with four

elements is fabricated, figures 5.8-5.11. The designed pattern of slots is cut on one side of a two-sided copper-clad dielectric sheet (POLYGUIDE). The short circuit termination is achieved by using silver conducting paint on the rim of the structure. The feed system is designed to support TM_{01} of the cylindrical cavity region. The center conductors of two SMA connectors are used as the thin vertical probes by drilling two holes symmetrically about the center of the structure and separated by a distance equal to 13 mm. The tips of the probes are soldered to the copper-clad of the opposite face forming the annular slot array. To achieve 180° phase shift between the probes, a rectangular waveguide section is used. Two SMA terminals are mounted $\lambda g/2$ apart on the broad wall of the waveguide section. The guide is match terminated on one side and the crystal detector is placed at the other end for pattern measurements in the receiving mode, figure 5.9. Two identical high frequency coaxial lines are used for connecting the antenna terminals and the phase shifting device. A separate annular flange having an inner diameter equal to the aperture diameter of the annular slot array is also fabricated from aluminum. The ratio of the outer and inner diameters is selected to be equal to 2. The thickness of the aluminum sheet is equal to that of the two-sided copper-clad sheet to produce a smooth aperture surface. The latter conducting annular sheet is used to investigate the effects of the finite ground plane on the radiation pattern. The antenna assembly with the conducting flange is shown in figure 5.11.

The experimental investigation on both unflanged and flanged cavity backed annular slot array antenna is performed in the anechoic chamber of the Antenna Laboratory of the University of Manitoba, figure 5.12. Due to the interference levels of the antenna mount assembly and

the chamber itself, the receiving pattern measurements are carried out over an angular region $-100° \leq \theta \leq 100°$. Patterns are measured at $f = 10.11$ GHz, and the incident wave was launched by a horn antenna.

Figure 5.13 illustrates the E and H plane radiation patterns of the unflanged antenna. The computed patterns for the infinite ground plane are also included. As it is evident, the E-plane patterns have the same number of lobes and the main lobes have the same beam width. The first side lobe levels, which in addition to the main lobe, carry the major part of the radiated power are close to each other. However, the off-axis lobes of the finite antenna have larger values compared to the infinite case. This is expected, since, due to a sudden geometrical interruption at the rim location edge diffraction, which increases the off-axis side lobe levels, occurs. The H-plane patterns also have the same general trend. Note that at $\theta = 27°$ the computed pattern shows the generation of a new side lobe which corresponds to the first side lobe level of the measured pattern. For θ greater than 32 degrees, the side lobe levels of the computed patterns are smaller than -40 dB and are not shown.

In order to investigate the effects of a finite ground plane on the radiation patterns, the aluminum annular flange was added to the aperture surface of the antenna assembly. Hence, the aperture diameter for this case is increased by a factor of two compared to the previous case and the aperture current distribution is expected to have a more tapered behaviour. The measured E and H plane receiving patterns for this case are depicted in figure 5.14. The beam width of the patterns are not altered. However, the off-axis side lobe levels are slightly decreased, due to a smoother edge transition, at the expense of a lower

efficiency factor.

The gain of the finite cavity-backed antenna was also measured. As a measure to broaden the operating frequency band of the feed system, the feed assembly shown in figure 5.15 was used. The 180 degrees phase shifting device for this case was formed by a Magic-T, having its symmetry arm match terminated (port 3). A standard pyramidal horn was used as a reference aperture antenna for gain measurements. The loss components associated with the feed assembly are tabulated in Table 5.3. The gain of the standard horn, the measured relative gain and the computed gain (infinite ground plane) are also included. The difference value of 0.6 dB between the theoretical and measured gains accounts for the effects of a finite ground plane, mismatch loss and the measurement errors.

The reflection coefficient at the feeding arm of the magic-T was also measured by a Network Analyzer. The result over the X-Band is presented in figure 5.16. The operating point for gain and radiation pattern measurements is also shown (f = 10.11 GHZ). Figure 5.17 shows the effects of a slide-screw tuner on the reflection cofficient of the feed and antenna systems. The results obtained for a short as well as a matched termination are also included.

It is,therefore concluded that the infinite ground plane solution yields reasonably accurate results for the radiation field of a finite aperture antenna. The edge scattered field which raises the off-axis side lobe levels can be reduced by introduction of an annular conducting rim.

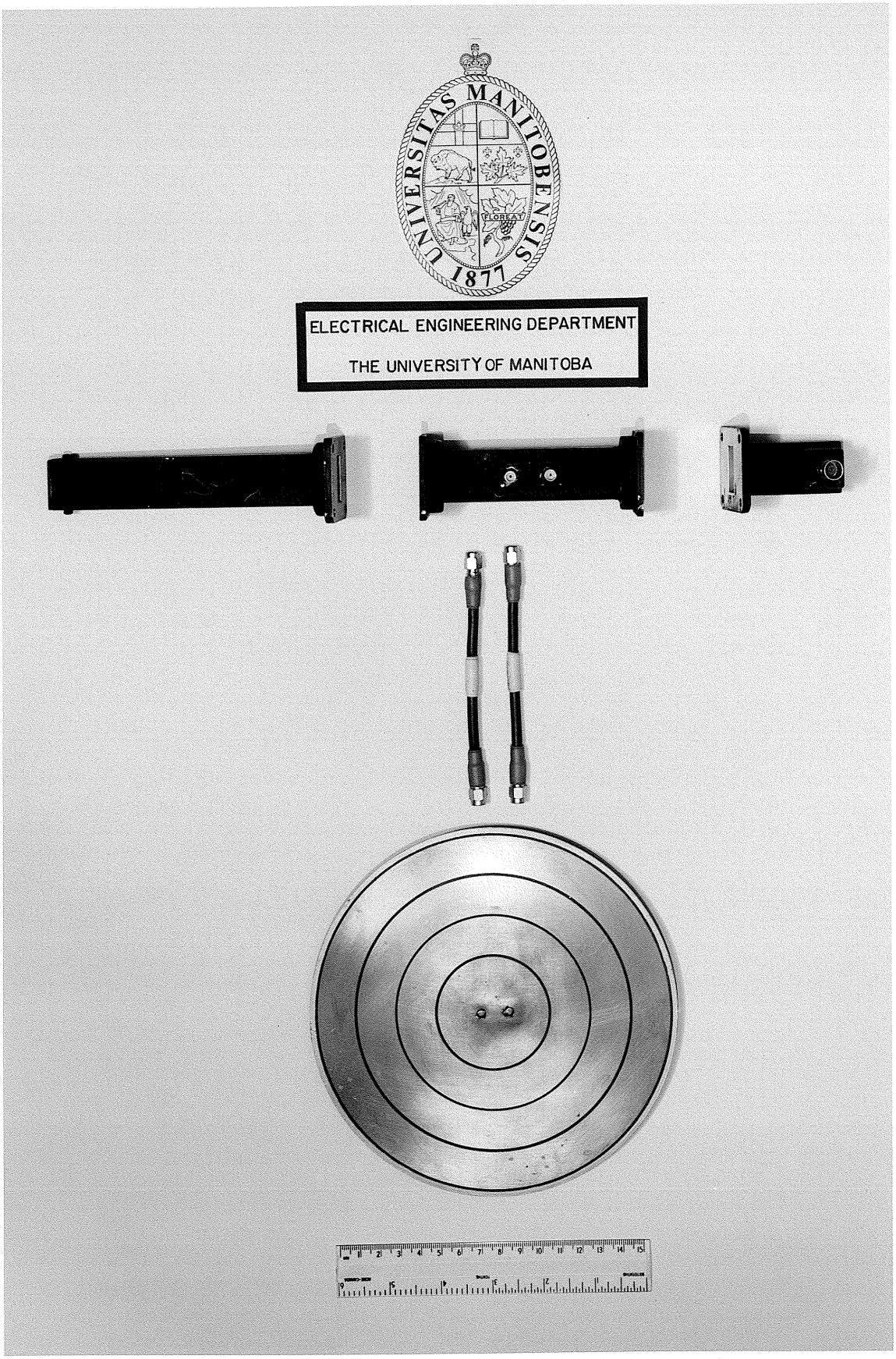

Fig. 5.8: Cavity-backed annular slot array antenna and the feed system, TM_{01} excitation.

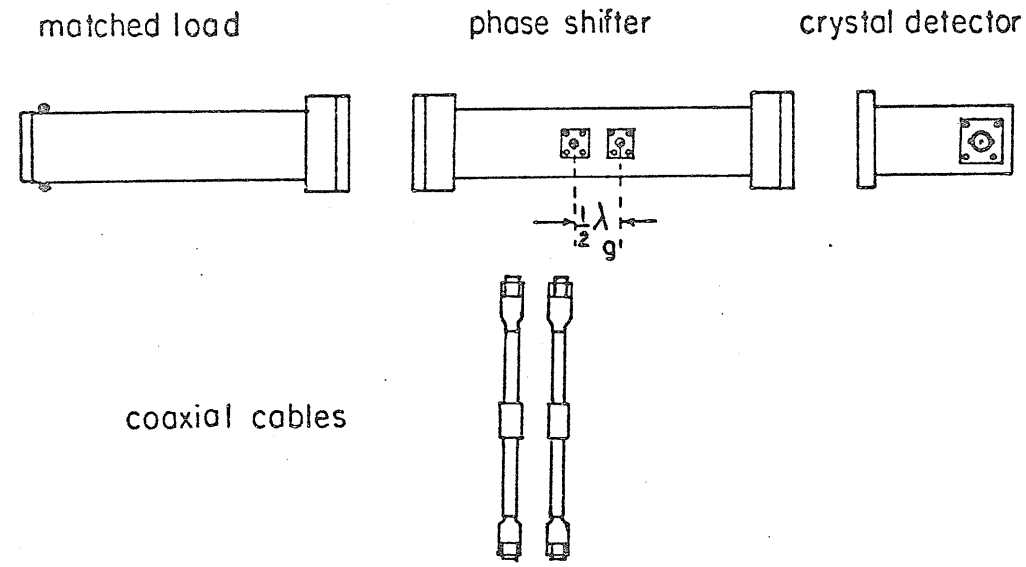

number of slots = 4

$\epsilon_r = 2.32$

$\delta = 1.5$ mm

$\rho_1 = 27.8$ mm

$X = 20.0$ mm

$C - \rho_4 = 3.9$ mm

$a = 1.6$ mm

$f = 10.11$ GHZ

probes separation = 13.0 mm

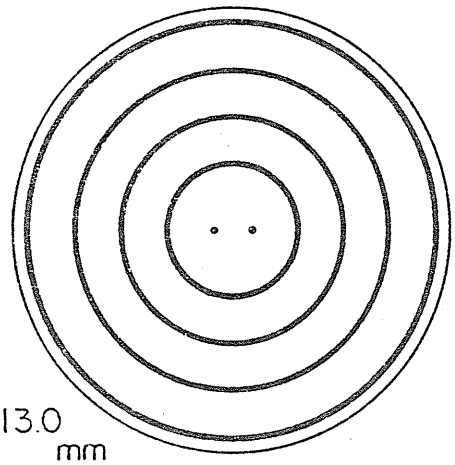

Figure 5.9: Geometry of the antenna and the feed system.

Figure 5.10: Feed terminals, conducting flange and the mounting fixture.

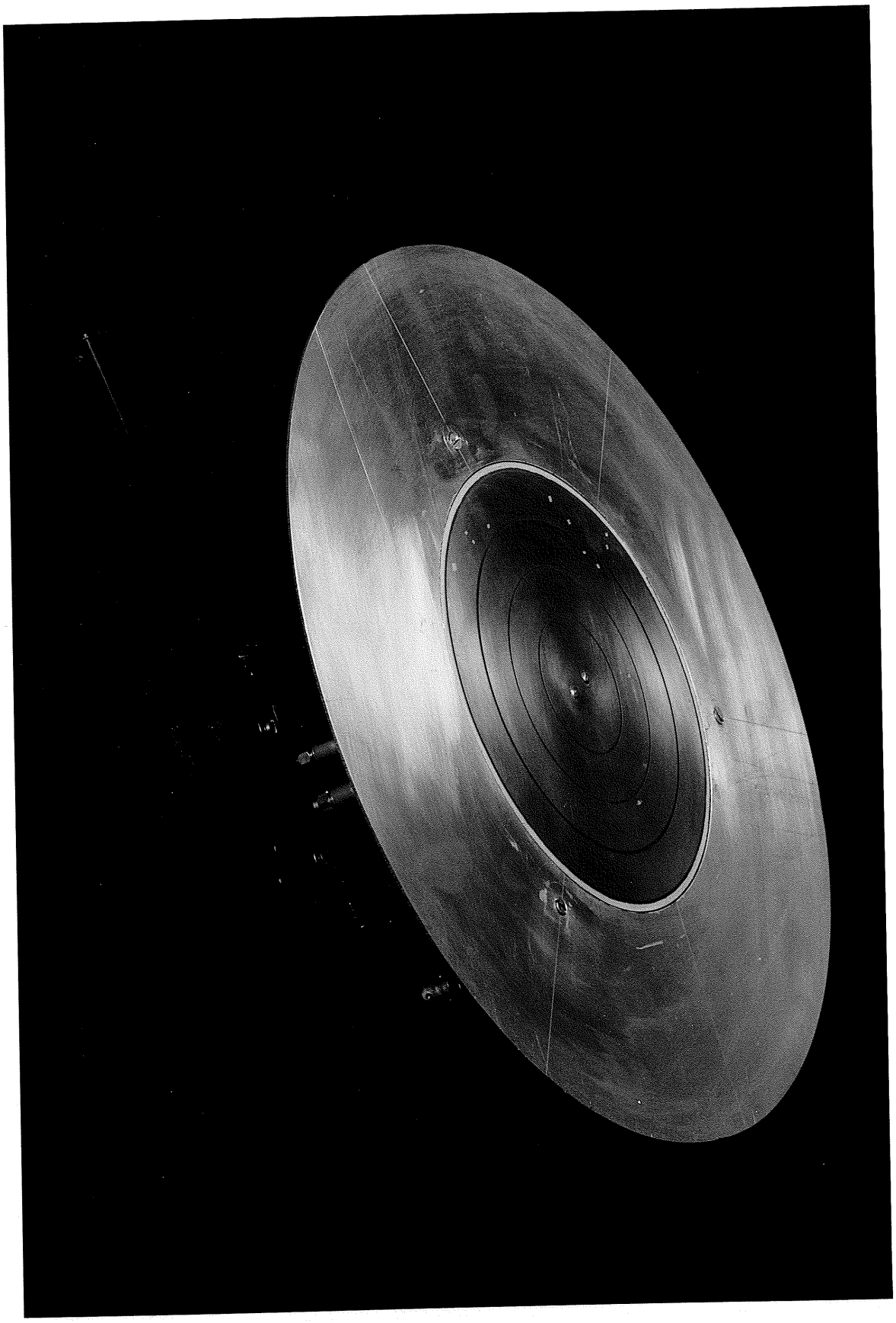

Fig. 5.11: Assembled annular slot array antenna with the conducting flange.

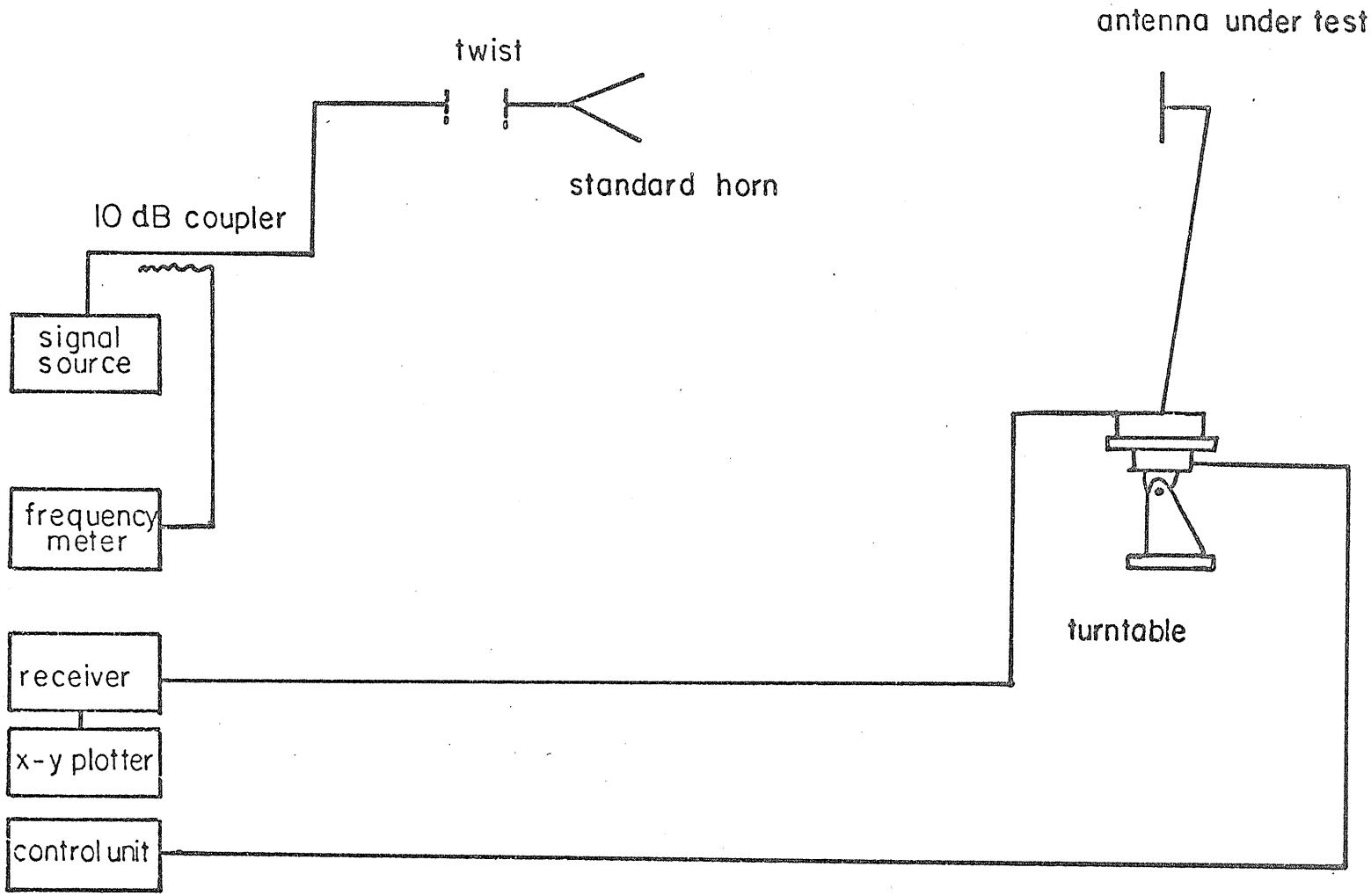

Figure 5.12: Experimental set-up for pattern measurements.

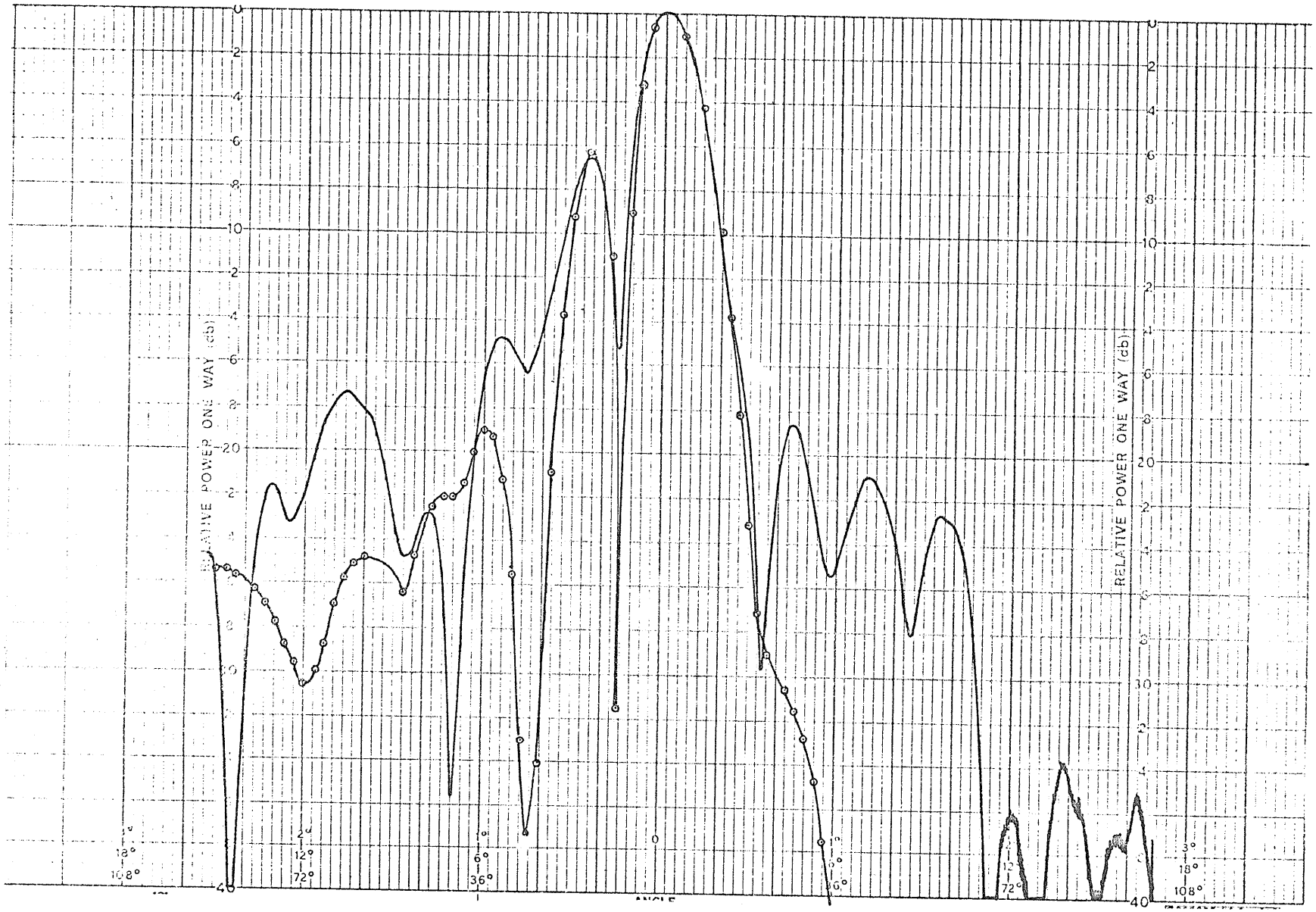

Figure 5.13: E and H plane radiation patterns of a cavity-backed annular slot antenna. ———— measured, -0-0-0- calculated.

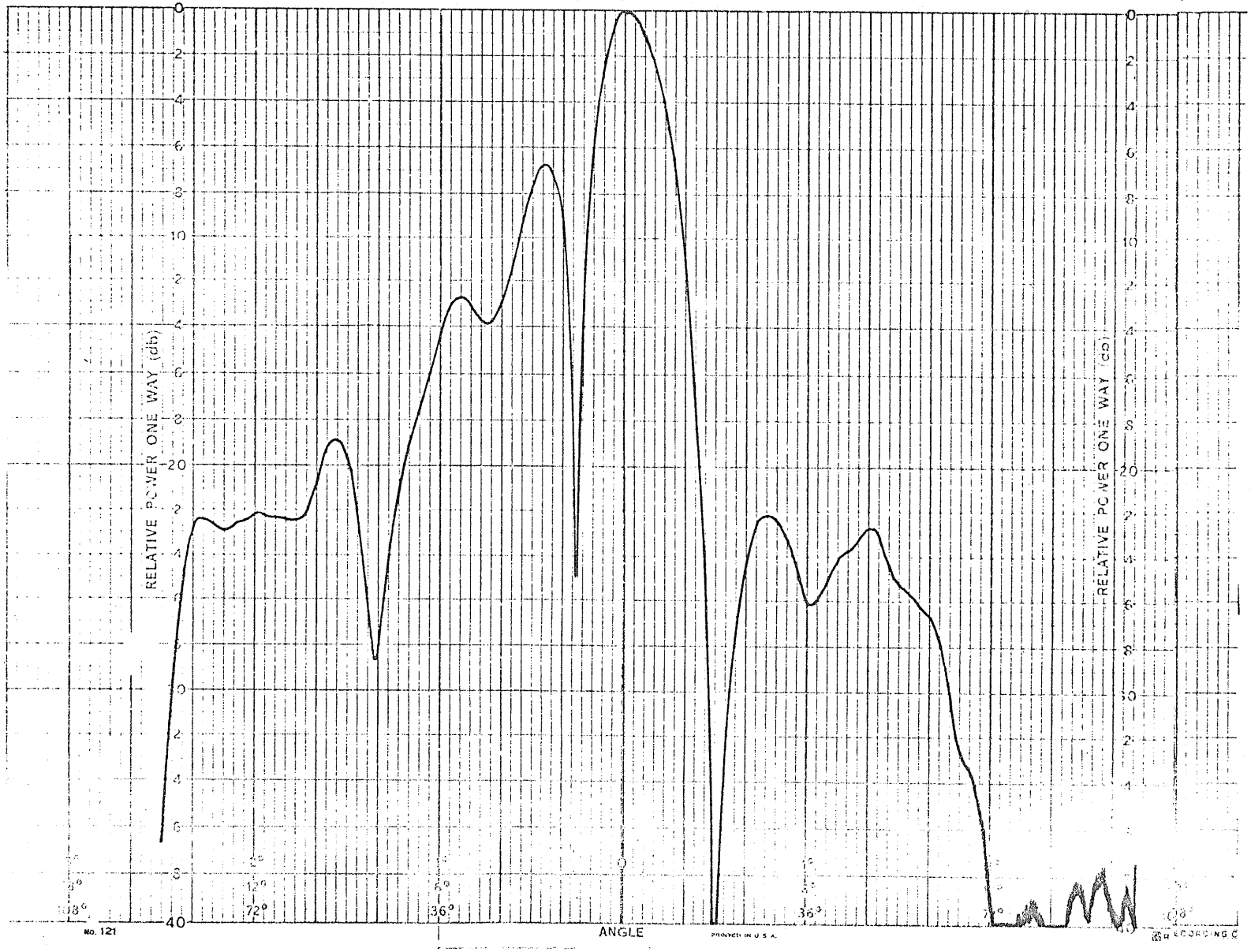

Figure 5.14: Measured E and H plane radiation patterns of the antenna system with the conducting flange.

A Matched Load

B Magic - T (arms 1, 2, 3 are H - Plane ports)

C Detector, Source or Network Analyzer

D Coaxial Cables

E Male - Type Connectors

F Annular Slot Antenna

G SMA - Waveguide Transitions

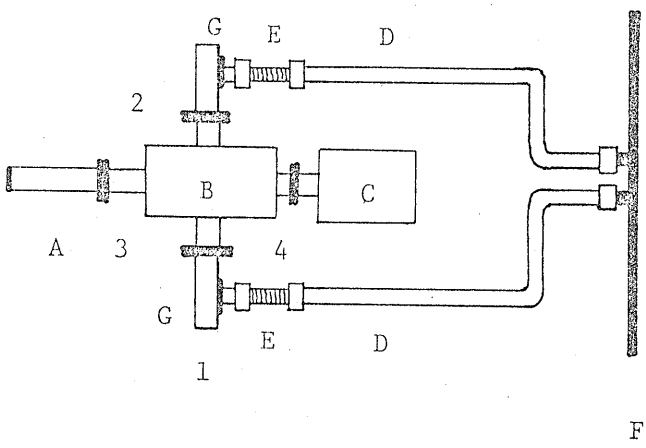

Figure 5.15: Feed assembly used for gain and reflection measurements.

Table 5.3: Details of Gain Measurements

Loss Components dB	Gain of Standard Horn at f = 10.11 GHZ dB	Measured relative Gain dB (w.r.t. Horn)	Annular Slot Aperture Gain dB
Coaxial Cable 2 x 2.7	22.3	- 4.5	24.7
Waveguide- SMA Transition 2 x 0.2			
Male-Type SMA Connector 2 x 0.1			
Magic T 0.9			
Total = 6.9			

Computed Aperture Gain (infinite case) = 25.2 dB

Measured Aperture Gain (finite case) = 22.3 - 4.5 + 6.9 = 24.7 dB

Difference = 25.2 - 24.7 = 0.6 dB

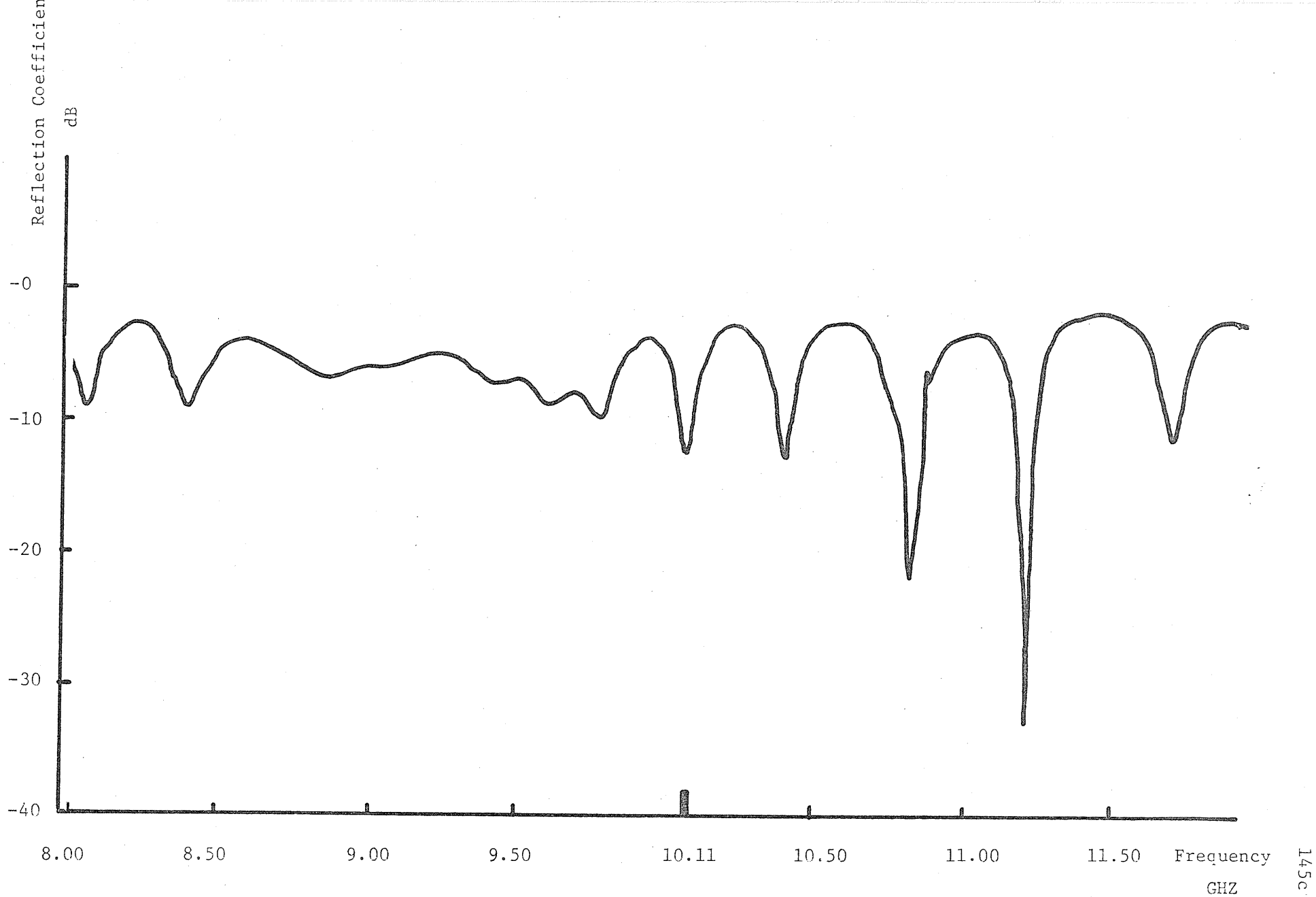

Figure 5.16: Magnitude of the reflection coefficient at the feeding arm as a function of frequency.

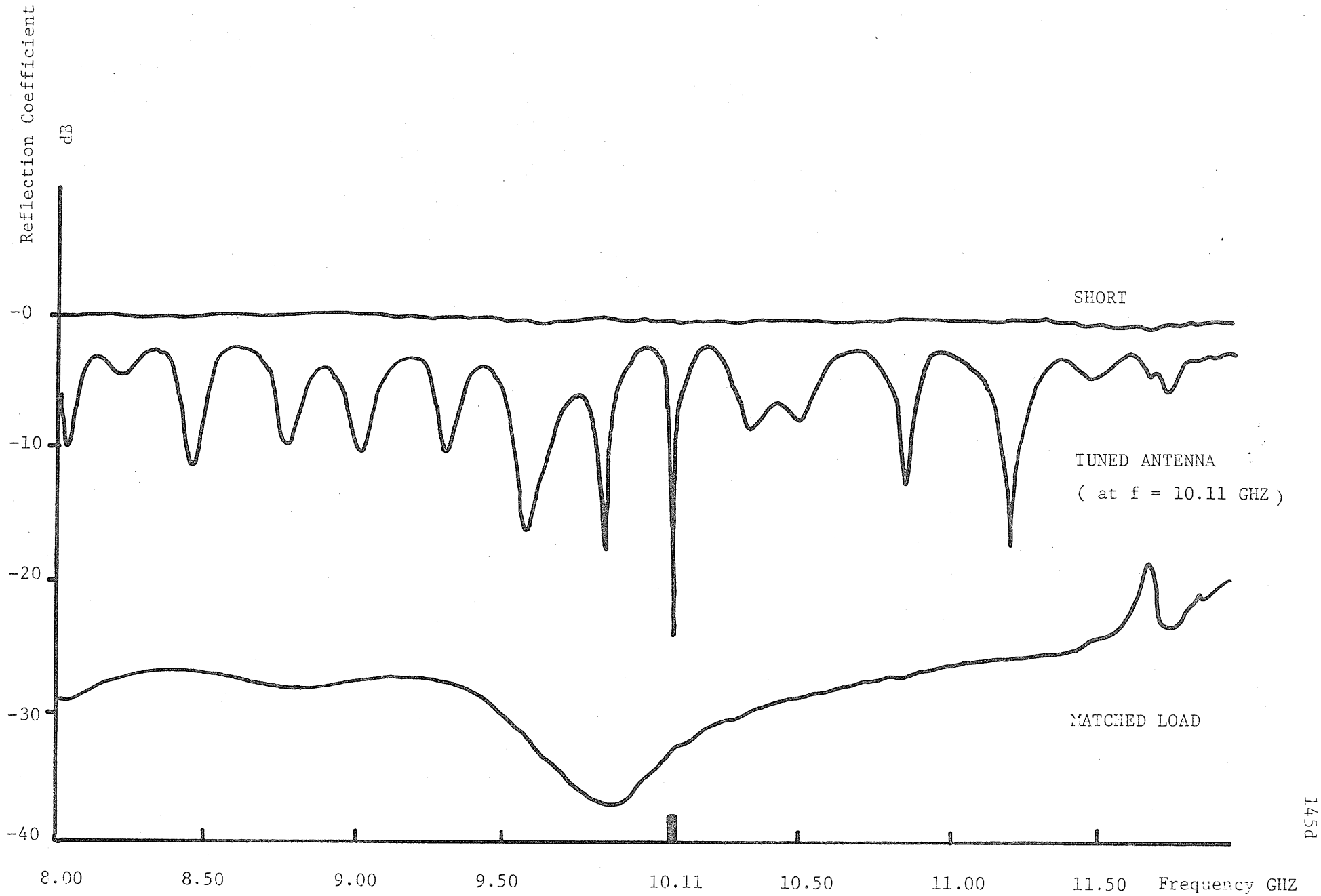

Figure 5.17: Effects of a Slide-Screw tuner on the reflection coefficient.

CHAPTER VI

DISCUSSION AND CONCLUSION

The problem of electromagnetic scattering by concentric arrays of annular type geometrical discontinuities inside or on the common boundaries of radial waveguides was studied throughout this thesis. The cases of electromagnetic penetration into half-space as well as cylindrical cavity regions are also treated. The method employed for obtaining field solutions in the respective regions utilized a boundary value treatment. The appropriate Green's functions of e and h types representing the response of the system to a ϕ directed current ring of arbitrary excitation were obtained. Both electric and magnetic current distributions were assumed in order to extend the range of applicability of the analyses to aperture coupling problems. The final formulation was carried out by an integration of the impulse response over the induced current distribution on the surface of the geometrical discontinuities. The induced source function was then expanded into a finite series of basis functions with complex coefficients (for the examples provided in this thesis, pulse functions were assumed). These constants were later obtained by an application of the boundary conditions over the discontinuity surfaces. The analysis was mainly oriented toward investigating the scattering characteristics of arrays of electrically thin elements. Therefore, the contribution from the second component of the induced surface current with respect to the azimuthal directed one was assumed to be negligible. However, for problems where this contribution is expected to be appreciable, a similar method can be utilized to find another set of equations describing the contribution of the second component to the total field. The electromagnetic

coupling between these two sets of fields is then ensured by a simultaneous evaluation of the constant coefficients of the two sets, using the appropriate boundary conditions on the surfaces of the scattering bodies.

The method was then applied to three different geometries, namely,

a) Two radial waveguides coupled by an array of concentric annular slots of finite width on the common boundaries for applications as band-pass, band-stop filtering devices.

b) Radial waveguide fed annular slot array antenna for applications as highly directive antenna systems of low profile and low cost for use in high frequency communication links.

c) Cylindrical cavity-backed annular slot array antenna for applications as flush-mounted antenna systems of high gain, for use in communication satellites and aircrafts.

For a source placed at the central region of the feeding waveguide, expressions for the total power, power coupled out through the slot array and the transmitted part through the waveguide region were obtained for each case. As a check on the accuracy of the numerical results the balance of power between the supplied, coupled and transmitted powers was examined for all cases and excellent results were obtained. The radiation field of an annular slot array was also obtained for a general excitation by an application of equivalence theorem and the image theory. The special case of TM_{00} as well as TM_{01} exciting mode were chosen for numerical examples. The thickness of the guides were selected smaller than half a wavelength to suppress the propagation of modes other than the dominant mode.

As an equivalent principal mode circuit representation, an admittance expression associated with each slot was defined. For the case

of two coupled radial waveguides it was observed that for most applications the dominant mode representation, such as that in the transmission line theory for waveguide applications, adequately describes the slot admittance. However, the accuracy of the results, especially for slots where $k\rho$ is small, is not satisfactory. As a further check on the dominant mode approximation, the field distribution over the slot was also calculated. The result indicated that the higher order modes excited by the slot discontinuities have significant contribution to the slot field amplitude only in the vicinity of the slot edges. Their contribution to the slot field decreases as the distance from the edges increases. On the other hand, the dominant mode theory failed to describe the phase of the aperture field. The actual phase of the slot field which was calculated by including higher order modes was observed to be virtually constant over the slot. Whereas, the result due to the dominant mode showed an oscillatory behaviour.

For the case of a radial waveguide fed annular slot antenna, a similar trend was generally observed. However, the phase distribution over the slot obtained by dominant mode approximation closely resembled that of the actual field. The dominant mode result, however, was obtained by only suppressing the higher order modes of the waveguide region. Whereas, the continuous spectrum of the modes associated with the semi-infinite region was included in the numerical results computed for the admittance and aperture field.

The admittance variation of the annular slot antenna as a function of its radius was compared against the available theoretical as well as experimental data for a coaxial radiator of the same aperture size. It was observed that for electrically thin slots, the admittance of the slot approaches that of an infinitely thin annular slot driven by a delta-function

generator. This indicates that the admittance for this case is mainly determined by the external region. However, for wider slots, the admittance values of a radial waveguide fed annular slot antenna are generally smaller than those of the coaxial fed slot.

In order to study the degree of coupling between two radial waveguides, the coupled power contributed by each slot was computed for an array of annular slots on the common boundary of the two regions. It was observed that depending on the arrangement of the slots and the other parameters involved, the coupling could be so strong as to redirect back part of the power coupled by a number of slots; to the region including the exciting source system. An equivalent transmission line representation for this case would then be a negative slot conductance (a source) associated with the respective slots.

In application of the previous geometry for the design of microwave filtering devices with band-pass characteristics suitable for printed circuit strip-line fabrication techniques, a number of cases were considered. It was observed that by a proper arrangement of the array structure, wide band was well as highly selective filtering responses with sharp cut-off characteristics are realizable. That is, over the frequency band, the array of slots effectively coupled a major part of the total power to the external region.

The phase and amplitude variation of slots (isolated as well as coupled case) were studied for the purpose of array antenna designs. The results obtained for the case of annular slot antenna indicated that, for thin slots, the determining factor for the phase of the aperture field is normally the waveguide region. The nonlinear phase variation as a function of slot radius, showed a periodicity of one λ (intrinsic wavelength

of the guide region). The field magnitude was observed to decay as the radius increased, however, the decaying factor (asymptotic value) obtained for several cases seemed to be proportional to the square root of the slot radius. These results suggested that, knowing an initial value for the slot field at a certain radius, the field magnitude for the slot of different radii can be predicted, within a few percent error, by noting that $|E| \cdot \sqrt{\rho}$ oscillates about a constant level. For two coupled slots, the same conclusion holds and the relative position of the two constant levels associated with each slot is an indication of the magnitude of the transmission coefficient at the first slot location. For the case of coupled slots, the phase variation had a similar behaviour as the isolated case, however, the second slot was observed to experience a phase shift related to the slot spacing. The array field distribution for a cavity backed slot antenna also exhibited a periodicity of one λ. However, for a particular arrangement of the slots, the system showed a resonant effect, figures 5.3 and 5.4. So far, a satisfactory explanation of the result has not been found.

In application of the theory in design of directive beam antennas as well as uniform radiation fields, several cases were presented. Efficiencies of the order of 100 per-cent and gains of about 32 dB was shown to be easily obtainable with aperture diameters not exceeding $12\lambda_o$. Since the directivity of an antenna is proportional to the electrical area of the radiating aperture, it seems quite possible to achieve pencil beam radiation patterns by fabricating a fine pattern of slots over a moderately sized aperture. Thus, operating the antenna system at high frequencies, results in an electrically large aperture capable of launching beams of very narrow beam widths.

A method was proposed to realize simple feed systems capable of producing the desired mode or modes of the feeding waveguide. The feed assembly essentially consisted of isolated single or double vertical probes in a particular configuration. In order to verify the validity of the theory presented and also to investigate the effects of the finite ground plane on the radiation patterns, an experiment was performed. It was observed that the effects of a finite aperture on the radiation field of the infinite ground plane case is small and mainly of the edge diffraction form. Introduction of a conducting flange reduced the edge diffracted lobes at the expense of a lower efficiency value.

We, therefore, conclude that due to the inherent high frequency capability of the waveguide structures and the simplicity and ease of fabrication of the suggested radiating models, such structures can be utilized for applications as filtering devices, as well as efficient and highly directive low profile array antennas for operation in communication links at high frequency bands.

6.1 Suggestions for Future Research

During the course of the present work, several topics have stemmed from the practical point of view of the subject matter which requires more detailed attention. The first and most related problem is to investigate the possibility of circuit modeling of the slotted structure for synthesis purposes. The models must account for the higher order modes excited by the discontinuities. Closed form approximate expressions for the circuit elements, which closely follow the actual results, should be obtained to facilitate the design and synthesis process. This requires a thorough study of the slot's hybrid admittances and their relation to the characteristic dimensions of the structure. The result would be a simpler routine for

optimizing the desired electrical characteristic as the needs arise. A study of ohmic loss of the structure is required to substanciate the practicality of the design as an efficient filtering device or antenna system.

The applicability of annular slot antennas for use as a pencil beam launcher requires detailed analysis of aperture efficiency in conjunction with the beam width and side lobe characteristics. The fact that side lobe levels and the beam width are intimately related to the dependence of gain on the electrical size of the aperture and its field distribution makes it necessary to seek for a systematic way for compromising between these factors in order to fulfill the design objectives.

A study of the effects of a finite ground plane on the solution of an infinite one is in order. Even though the finiteness of the conducting baffle is observed to have a negligible effect in the front direction, as long as the radiating slots concentrate the energy in that direction, nevertheless, the back-scattered field can only be accounted for by utilizing the existing techniques such as geometrical theory of diffraction. A method of solution for this case was qualitatively presented in the last chapter and a quantitative study is underway.

APPENDIX A

DERIVATION OF EQUATIONS (3.8) USING LORENTZ RECIPROCITY

Noting that the auxiliary wave functions defined by (3.7) are source free in the volume V, by setting J = 0 in (3.6a), the reciprocity relation reduces to

$$\oint_S (\vec{E}_a^{\pm} \times \vec{H} - \vec{E} \times \vec{H}_a^{\pm}) \cdot \hat{n} ds = - \int_V \vec{H}_a \cdot \vec{J}_m \, dv \qquad (A.1)$$

where (+) and (-) signs represent (3.7a) and (3.7b), respectively. Since the tangential components of $\vec{E}_a^{+}$, $\vec{E}_a^{-}$ and $\vec{E}$ vanish on the conducting walls, equation (A.1) can be transformed to

$$\rho_1 \int_0^a \int_0^{2\pi} (E_{za}^{\pm} \cdot H_\phi + E_\phi \cdot H_{za}^{\pm} - E_z \cdot H_{\phi a}^{\pm} - E_{\phi a}^{\pm} \cdot H_z) d\phi dz$$

$$- \rho_2 \int_0^a \int_0^{2\pi} (E_{za}^{\pm} \cdot H_\phi + E_\phi \cdot H_{za}^{\pm} - E_z \cdot H_{\phi a}^{\pm} - E_{\phi a}^{\pm} \cdot H_z) d\phi dz$$

$$= - \int_0^{2\pi} \int_{\rho_1}^{\rho_2} \int_0^a H_{\phi a}^{\pm} \cdot I_m(\phi) \, \delta(\rho-\rho') \, \delta(z-z') \rho d\phi dz d\rho \qquad (A.2)$$

The second surface integral in (A.2) vanishes for (+) fields and the first surface integral vanishes for (-) fields. Using the Wronskian relation for Bessel functions [50] in the form of

$$J_\ell(z) \, H_\ell^{(2)\prime}(z) - H_\ell^{(2)}(z) \, J_\ell'(z) = - \frac{2j}{\pi z} \qquad (A.3)$$

and employing the orthogonality property of the sinusoidal functions, one obtains the following result for (+) fields

$$\ell^2 \varepsilon U_{\rho\ell}^h - \mu U_{\rho\ell}^e = - \frac{\pi\omega\varepsilon\mu\varepsilon_p}{2k_{\rho p}^2 a} \cos \frac{p\pi}{a} z' [k_{\rho p}\rho' \, J_\ell'(k_{\rho p}\rho') - \ell^2 \frac{p\pi}{j\omega\mu a} J_\ell(k_{\rho p}\rho')] \qquad (A.4)$$

where a use has been made of the property of the delta function. A similar mathematical routine for the case of (-) fields leads to

$$\ell^2 \varepsilon u^h_{\rho\ell} - \mu u^e_{p\ell} = -\frac{\pi\omega\varepsilon\mu\varepsilon_p}{2k^2_{\rho p}a} \cos\frac{p\pi}{a} z' [k_{\rho p}\rho' \, H^{(2)'}_{\ell}(k_{\rho p}\rho') - \ell^2 \frac{p\pi}{j\omega\mu a} H^{(2)}_{\ell}[k_{\rho p}\rho')] \qquad (A.5)$$

APPENDIX B

DERIVATION OF EQUATIONS (3.35) FOR THE TOTAL, COUPLED AND TRANSMITTED POWERS

A practical thickness for a radial waveguide is generally smaller than one-half of the intrinsic wavelength. Therefore, expressions derived here are for cases in which the propagating mode (or modes) are of ψ_{oq} type. That is, higher order modes for $m > 0$ have a complex propagation constant $k_{\rho m}$ and are attenuated rapidly, hence, these modes do not contribute to power transfer. Therefore, power expressions can be obtained only by retaining the propagating mode and an application of equation (3.34) to respective surfaces (Section 3.3.2). Considering the coefficients given by equations (3.12) reveals that due to the existance of the integer m in the coefficients for h modes, the contribution from TE modes to the power flow is zero. Therefore, for power flow calculations, we only take the field components contributed by TM_{oq} modes.

The total power is obtained by an application of (3.34) to a circular cylindrical surface which surrounds the feeding system in the lower waveguide and has an arbitrary radius ρ_p smaller than the radius of the leading edge of the first slot (Section 3.3.2). Equation (3.34) for this surface transforms to

$$P = \rho_p \, \mathrm{Re} \int_0^{2\pi} \int_{-b}^{0} [E_\phi \cdot H_z^* - E_z \cdot H_\phi^*] d\phi dz \qquad (B.1)$$

Note that E_ϕ and H_z are zero for TM_{oq} modes (equations 3.3b). The other components are

$$E_z = -j\frac{\pi}{2b}\sum_{i=1}^{IC}\rho_i E_{iq}\cos q\phi\,[H_q^{(2)}(k_1\rho_i)]_-^+ J_q(k_1\rho) - j\omega\mu_o\cos q\phi\, H_q^{(2)}(k_1\rho)$$

$$H_\phi = -\frac{\pi}{2b}\left(\frac{\varepsilon_1}{\mu_o}\right)^{\frac{1}{2}}\sum_{i=1}^{IC}\rho_i E_{iq}\cos q\phi\,[H_q^{(2)}(k_1\rho_i)]_-^+ J_q'(k_1\rho)$$

$$- k_1\cos q\phi\, H_q^{(2)\prime}(k_1\rho) \qquad \text{(B.2)}$$

The contribution of the first terms of (B.2) to $E_z \cdot H_\phi^*$ is purely imaginary. This is due to the fact that this product is only determined by the slot fields. Since the contribution of the slot induced sources to the total field in the central region of the guides is of standing wave type, this product is purely imaginary. Upon substituting (B.2) in (B.1), performing the integration and taking the real part, one obtains

$$P_{Total} = \frac{480}{\varepsilon_q}\pi k_o b + \frac{2\pi}{\varepsilon_q}\cdot\sum_{i=1}^{IC}\rho_i\,\mathrm{Re}[E_{iq}H_q^{(2)}(k_1\rho_i]_-^+ \qquad \text{(B.3)}$$

The transmitted power can be obtained by applying the same method to a cylindrical surface in the lower waveguide having a radius ρ_p greater than the last slot. We, therefore, assume ρ_p approaches infinity, hence, we may use the asymptotic relations for Bessel functions which facilitate the derivation of the final result. For the field components we have,

$$E_z = -j\frac{\pi}{2b}\sum_{i=1}^{IC}\rho_i E_{iq}\cos q\phi\,[J_q(k_1\rho_i)]_-^+ H_q^{(2)}(k_1\rho) - j\omega\mu_o\cos q\phi\, H_q^{(2)}(k_1\rho)$$

$$H_\phi = -\frac{\pi}{2b}\left(\frac{\varepsilon_1}{\mu_o}\right)^{\frac{1}{2}}\sum_{i=1}^{IC}\rho_i E_{iq}\cos q\phi\,[J_q(k_1\rho_i)]_-^+ H_q^{(2)\prime}(k_1\rho)$$

$$- k_1\cos q\phi\, H_q^{(2)\prime}(k_1\rho) \qquad \text{(B.4)}$$

Substituting (B.4) in (B.1) and using the principal asymptotic forms of Bessel functions [50]

$$H_q^{(2)}(z) \sim \sqrt{\frac{2}{\pi z}}\, e^{-j(z - \frac{q}{2}\pi - \frac{\pi}{4})}$$

for z large (B.5)

$$H_q^{(2)\prime}(z) \sim H_{q-1}^{(2)\prime}(z)$$

one obtains

$$P_{Transmitted} = \frac{480}{\varepsilon_q}\pi k_o b + \frac{4}{\varepsilon_q}\pi \sum_{i=1}^{IC} \rho_i \, Re(E_{iq})[J_q(k_1\rho_i)]_-^+$$

$$+ \frac{\pi}{120\varepsilon_q k_o b} \sum_{i=1}^{IC}\sum_{j=1}^{IC} \rho_i \cdot \rho_j \, Re(E_{iq} \cdot E_{jq}^*)[J_q(k_1\rho_i)]_-^+ \quad (B.6)$$

The same method when applied to a similar surface in the upper waveguide leads to,

$$E_z = j\frac{\pi}{2a}\sum_{i=1}^{IC} \rho_i \, E_{iq} \cos q\phi [J_q(k_2\rho_i)]_-^+ H_q^{(2)}(k_2\rho)$$

(B.7)

$$H_\phi = -\frac{\pi}{2a}\left(\frac{\varepsilon_2}{\mu_o}\right)^{\frac{1}{2}} \sum_{i=1}^{IC} \rho_i \, E_{iq} \cos q\phi [J_q(k_2\rho_i)]_-^+ H_q^{(2)\prime}(k_2\rho)$$

The relation for the power is now

$$P = -\rho_p \, Re\left[\int_0^{2\pi}\int_0^a E_z \cdot H_\phi^* \, d\phi dz\right] \quad (B.8)$$

which upon substituting (B.7) in the above relation leads to

$$P_{Coupled} = \frac{\pi}{120\varepsilon_q k_o a}\sum_{i=1}^{IC}\sum_{j=1}^{IC} \rho_i \cdot \rho_j \cdot Re(E_{iq} \cdot E_{jq}^*)[J_q(k_2\rho_i)]_-^+ \quad (B.9)$$

Note that the above relations are derived for single mode operation. However, formulation for a general case is simply obtained by including an infinite summation on q, that is

$$P_{Total} = \sum_{q=0}^{\infty} \frac{(a_q^2 + b_q^2)}{\varepsilon_q} \{480\pi k_o b + 2\pi \sum_{i=1}^{IC} \rho_i \, Re[E_{iq} H_q^{(2)}(k_1\rho_i)]_-^+\} \tag{B.10}$$

$$P_{Transmitted} = \sum_{q=0}^{\infty} \frac{(a_q^2 + b_q^2)}{\varepsilon_q} \{480\pi k_o b + 4\pi \sum_{i=1}^{IC} \rho_i \, Re(E_{iq}) [J_q(k_1\rho_i)]_-^+$$

$$+ \frac{\pi}{120\, k_o b} \sum_{i=1}^{IC} \sum_{j=1}^{IC} \rho_i \cdot \rho_j \cdot Re(E_{iq} \cdot E_{jq}^*) [J_q(k_1\rho_i)]_-^+\} \tag{B.11}$$

$$P_{Coupled} = \sum_{q=0}^{\infty} \frac{(a_q^2 + b_q^2)\pi}{120\varepsilon_q\, k_o a} \sum_{i=1}^{IC} \sum_{j=1}^{IC} \rho_i \cdot \rho_j \cdot Re(E_{iq} \cdot E_{jq}^*) [J_q(k_2\rho_i)]_-^+ \tag{B.12}$$

APPENDIX C

PROOF OF THE IDENTITIES (4.14)

In the course of constructing the appropriate Green's functions for describing the field generated by an annular slit of strength $V(\phi)$ on a conducting infinite plane, two types of infinite integrals involving Bessel functions and their derivatives were encountered. These integrals in their present forms are not tabulated in common mathematical tables and the proof of the resulting identities requires showing

$$\rho' \int_0^\infty J_\nu(\alpha\rho) J'_\nu(\alpha\rho')\,d\alpha + \rho \int_0^\infty J'_\nu(\alpha\rho)\, J_\nu(\alpha\rho') = 0 \qquad \text{(C.1)}$$

$$\text{for all } \rho,\ \mathrm{Re}\ \nu \geq 0$$

$$\rho' \int_0^\infty J'_\nu(\alpha\rho) J'_\nu(\alpha\rho')\alpha\,d\alpha + \frac{\nu^2}{\rho} \int_0^\infty \frac{1}{\alpha} J_\nu(\alpha\rho) J_\nu(\alpha\rho')\,d\alpha = \delta(\rho-\rho') \qquad \text{(C.2)}$$

Derivation of (C.1) is fairly straightforward. Using the following relation for Bessel functions [50]

$$J'_\nu(z) = J_{\nu-1}(z) - J_{\nu+1}(z) \qquad \text{(C.3)}$$

the identity (C.1) is modified to

$$\rho' \left[\int_0^\infty J_\nu(\alpha\rho)\, J_{\nu-1}(\alpha\rho')\,d\alpha - \int_0^\infty J_\nu(\alpha\rho)\, J_{\nu+1}(\alpha\rho')\,d\alpha\right] + \rho \left[\int_0^\nu J_{\nu-1}(\alpha\rho)\, J_\nu(\alpha\rho')\,d\alpha - \int_0^\infty J_{\nu+1}(\alpha\rho)\, J_\nu(\alpha\rho')\,d\alpha\right] = 0 \qquad \text{(C.4)}$$

The above four infinite integrals are in the form of discontinuous integrals of Bessel functions represented by [50]

$$\int_0^\infty J_\mu(x\beta)\, J_{\mu-1}(y\beta)\,d\beta = \begin{cases} \dfrac{(y)^{\mu-1}}{x^\mu} & y < x \\ \dfrac{1}{2y} & y = x \\ 0 & y > x \end{cases} \qquad \mathrm{Re}\ \mu > 0 \qquad \text{(C.5)}$$

For $\rho' > \rho$, after replacing the integrals by their respective values given by (C.5) one obtains

$$\rho'\left(0 - \frac{\rho^{\nu}}{\rho'^{\nu+1}} + \rho\left(\frac{\rho^{\nu-1}}{\rho'^{\nu}} - 0\right)\right) = 0 \qquad \text{(C.6)}$$

which is an obvious identity. For $\rho' < \rho$ we have

$$\rho'\left(\frac{\rho'^{\nu-1}}{\rho^{\nu}} - 0\right) + \rho\left(0 - \frac{\rho'^{\nu}}{\rho^{\nu+1}}\right) = 0 \qquad \text{(C.7)}$$

and the proof for $\rho' = \rho$ is trivial.

Derivation of (C.2) is somewhat more complicated. We start by forming

$$J'_{\nu}(\alpha\rho)\, J'_{\nu}(\alpha\rho) = \left[\frac{\nu}{\alpha\rho} J_{\nu}(\alpha\rho) - J_{\nu+1}(\alpha\rho)\right]\left[-\frac{\nu}{\alpha\rho'} J_{\nu}(\alpha\rho') + J_{\nu-1}(\alpha\rho')\right] \qquad \text{(C.8)}$$

where a use has been made of (4.12c). Substitution of (C.8) in the first integrand of (C.2) results in

$$\frac{\nu\rho'}{\rho}\int_0^{\infty} J_{\nu}(\alpha\rho)\, J_{\nu-1}(\alpha\rho')\,d\alpha + \nu\int_0^{\infty} J_{\nu+1}(\alpha\rho)\, J_{\nu}(\alpha\rho')\,d\alpha$$

$$- \rho'\int_0^{\infty} J_{\nu+1}(\alpha\rho)\, J_{\nu-1}(\alpha\rho')\,\alpha\,d\alpha = \delta(\rho-\rho') \qquad \text{(C.9)}$$

It can be shown that

$$\rho'\int_0^{\infty} J_{\nu+1}(\alpha\rho)\, J_{\nu-1}(\alpha\rho')\,\alpha\,d\alpha = \nu\int_0^{\infty} J_{\nu+1}(\alpha\rho)\, J_{\nu}(\alpha\rho')\,d\alpha$$

$$+ \frac{\nu\rho'}{\rho}\int_0^{\infty} J_{\nu}(\alpha\rho)\, J_{\nu-1}(\alpha\rho')\,d\alpha$$

$$- \frac{\rho'}{2}\left[\int_0^{\infty} J_{\nu+1}(\alpha\rho)\, J_{\nu+1}(\alpha\rho')\,\alpha\,d\alpha\right.$$

$$\left. - \int_0^{\infty} J_{\nu-1}(\alpha\rho)\, J_{\nu-1}(\alpha\rho')\,\alpha\,d\alpha\right] \qquad \text{(C.10a)}$$

where a use has been made of

$$\frac{2\nu}{z} J_{\nu}(z) = J_{\nu-1}(z) + J_{\nu+1}(z) \qquad \text{(C.10b)}$$

substituting (C.10a) in (C.9) results in

$$\frac{\rho'}{2} \left[\int_o^{\infty} J_{\nu+1}(\alpha\rho)\, J_{\nu+1}(\alpha\rho')\alpha d\alpha + \int_o^{\infty} J_{\nu-1}(\alpha\rho)\, J_{\nu-1}(\alpha\rho')\alpha d\alpha\right] = \delta(\rho-\rho') \qquad \text{(C.11)}$$

According to the definition of delta function in terms of infinite integrals of Bessel function we have [57]

$$\delta(r - r') = r' \int_o^{\infty} J_{\mu}(\beta r)\, J_{\mu}(\beta r')\beta d\beta \quad \text{for all } \mu \qquad \text{(C.12)}$$

Finally, an application of (C.12) to (C.11) proves the identity.

APPENDIX D

DERIVATION OF $Re(I^e)$

First we establish the following identity

$$J_1(z) = -\frac{2z}{\pi}\frac{d}{dz}\left[\frac{1}{z}\int_1^\infty \frac{\sin(zt)\,dt}{t^2(t^2-1)^{1/2}}\right] \tag{D.1}$$

To this task, we represent the right-hand side by $f(z)$ and take the derivative of the both sides with respect to z, that is

$$\frac{df}{dz} = \frac{2}{\pi}\frac{d}{dz}\left[\frac{1}{z}\int_1^\infty \frac{\sin(zt)\,dt}{t^2(t^2-1)^{1/2}}\right] + \frac{2}{\pi}\int_1 \frac{\sin(zt)\,dt}{(t^2-1)^{1/2}} \tag{D.2}$$

The first term in (D.2) can be identified as $-\frac{1}{z}f$ and the second term is the integral representation of $J_o(z)$ [50], therefore, one obtains

$$z\frac{df}{dz} + f = -z\,J_o(z) \tag{D.3}$$

or equivalently

$$\frac{d(zf)}{dz} = \frac{d}{dz}[z\,J_1(z)] \tag{D.4}$$

which immediately proves equation (D.1). From (D.1) it follows that

$$\left[\frac{1}{z'}\int_1^\infty \frac{\sin(z't)\,dt}{t^2(t^2-1)^{1/2}}\right]_o^z = -\frac{\pi}{2}\int_o^z \frac{J_1(z')}{z'}\,dz' \quad \text{for all } z \tag{D.5}$$

hence

$$\frac{1}{z}\int_o^\infty \frac{\sin(zt)\,dt}{t^2(t^2-1)^{1/2}} = -\frac{\pi}{2}\int_o^z \frac{J_1(z')}{z'}\,dz' + \int_1^\infty \frac{dt}{t\,(t^2-1)^{1/2}} \tag{D.6}$$

The second term on the right-hand side is a known integral equal to $\frac{\pi}{2}$, therefore,

$$\int_1^\infty \frac{\sin(zt)\,dt}{t^2(t^2-1)^{1/2}} = \frac{\pi z}{2}\left[1 - \int_o^z \frac{J_1(z')}{z'}\,dz'\right] \tag{D.7}$$

By a similar process, it can be shown that

$$N_1(z) = \frac{2z}{\pi}\frac{d}{dz}\left[\frac{1}{z}\int_1^\infty \frac{\cos(zt)\,dt}{t^2(t^2-1)^{1/2}}\right] \tag{D.8}$$

which leads to

$$\left[\frac{1}{z'}\int_1^\infty \frac{\cos(z't)\,dt}{t^2(t^2-1)^{1/2}}\right]_o^z = \frac{\pi}{2}\int_o^\infty \frac{N_1(z')}{z'}\,dz' \quad \text{for all } z \tag{D.9}$$

substituting

$$\frac{N_1(z)}{z} = N_o(z) - \frac{d}{dz}N_1(z)$$

yields

$$\int_1^\infty \frac{\cos(zt)\,dt}{t^2(t^2-1)^{1/2}} = \frac{z\pi}{2}\left[\int_o^z N_o(z')\,dz' - N_1(z)\right] \tag{D.10}$$

where a use has been made of the following relation

$$\lim_{z\to o} N_1(z) = -\frac{2}{\pi}\lim_{z\to o}\int_1^\infty \frac{\cos(zt)\,dt}{zt^2(t^2-1)^{1/2}} \tag{D.11}$$

By substituting (D.7) and (D.10) in equation (4.39) the desired relation for $\mathrm{Re}(I^e)$, as expressed by (4.41), is obtained.

APPENDIX E

DERIVATION OF $RE(I^h)$

The infinite integrals on the right-hand side of (4.43a) and (4.43b) can be evaluated using the following known integrals [50]

$$\int \frac{\cos t}{t^{2n+1}}\,dt = \frac{(-1)^{n+1}}{(2n)!\,t}\left\{\sum_{p=0}^{n-1}\frac{(-1)^{p+1}(2p+1)!}{t^{2p+1}}\right.\left.[\cos t - (2p+1)t\sin t]\right\} + \frac{(-1)^n}{(2n)!}\,Ci(t) \tag{E.1}$$

$$\int \frac{\sin t}{t^{2n+1}}\,dt = \frac{(-1)^{n+1}}{(2n)!\,t}\left\{\sum_{p=0}^{n-1}\frac{(-1)^{p+1}(2p)!}{t^{2p+1}}\right.\left.[t\cos t + (2p+1)\sin t]\right\} + \frac{(-1)^n}{(2n)!}\,Si(t) \tag{E.2}$$

Using a change of variable in the form

$$t = z\beta \tag{E.4}$$

transforms (4.43a) and (4.43b) into suitable forms to be evaluated by (E.1) and (E.2). The resulting integrals are then evaluated for the limits $z \leq t < \infty$, with the aid of limiting forms for $Si(\infty)$, $Ci(\infty)$, [50]. The final results are of the following forms

$$\int_1^\infty \cos[k_o(x-y)\beta]\left(\frac{1}{\beta^3} - \frac{1}{2\beta^5}\right)d\beta = \frac{1}{48}\left[(z_1^2+18)\cos z_1 - z_1(z^2+22)\sin z_1 + z_1^2(z_1^2+24)Ci(z_1)\right] \tag{E.5}$$

$$\int_1^\infty \sin[k_o(x+y)\beta]\left(\frac{1}{\beta^3} - \frac{1}{2\beta^5}\right)d\beta = \frac{1}{48}\left[z_2(z_2^2+22)\cos z_2 + (z_2^2+18)\sin z_2 + z_2^2(z_2^2+24)Si(z_2)\right] \tag{E.6}$$

where

$$z_1 = k_o |x - y|$$

$$z_2 = k_o |x - y|$$

substituting (E.5) and (E.6) in (4.40) results in (4.44a)

APPENDIX F

DERIVATION OF THE EQUATION (4.50)

Using the addition formulas for sinusoidal functions, the integral part of (4.49) on u is transformed to

$$U = \int_{-\pi}^{\pi} [a_n \cos n\phi + b_n \sin n\phi) \cos nu \cos u + (b_n \cos n\phi - a_n \sin n\phi) \sin nu \cos u] \cdot \exp(jk_o\rho' \sin\theta \cos u)\hat{\theta}\, du - \sin\theta \int_{-\pi}^{\pi} [(a_n \cos n\phi + b_n \sin n\phi) \cos nu \sin u + (b_n \cos n\phi - a_n \sin n\phi) \sin nu \sin u] \exp(jk_o\rho' \sin\theta \cos u)\hat{\phi}\, du \qquad (F.1)$$

The second term of $\hat{\theta}$ component and the first term of $\hat{\phi}$ are odd functions of u, hence, do not contribute to the integral U. Therefore,

$$U = 2\int_{o}^{\pi} [(a_n \cos n\phi + b_n \sin n\phi) \cos nu \cos u\, \hat{\theta} - \sin\theta (b_n \cos n\phi - a_n \sin n\phi) \cdot \sin nu \sin u\, \hat{\phi}] \exp(jk_o\rho' \sin\theta \cos u)\, du \qquad (F.2)$$

A use of the following identities

$$\begin{aligned} 2 \cos nu \cos u &= \cos(n-1)u + \cos(n+1)u \\ 2 \sin nu \sin u &= \cos(n-1)u - \cos(n+1)u \end{aligned} \qquad (F.3)$$

in (F.2) results in the desired relation, equation (4.50).

APPENDIX G

DERIVATION OF EQUATION (5.17) FOR THE TOTAL POWER

The total power is obtained by an application of (3.34) to a circular cylinder which surrounds the feeding system and has a radius ρ_p smaller than that of the first slot. For a cavity of a thickness smaller than $\frac{\lambda}{2}$ only TM_{oq} modes contribute to the power transfer. This leads to

$$P = -\rho_p \, \mathrm{Re}\left[\int_0^{2\pi} \int_{-a}^{o} E_z \cdot H_\phi^* \, d\phi dz\right] \tag{G.1}$$

Using (3.3b), (5.14) and assuming an incident field of the type

$$\psi^{e}_{in} = \sum_{p=0}^{\infty} \sum_{q=0}^{\infty} (a_q \cos q\phi + b_q \sin q\phi) \cos \frac{p\pi}{a} z \, \frac{J_q(k_{\rho p} c) N_q(k_{\rho p} \rho) - N_q(k_{\rho p} c) J_q(k_{\rho p} \rho)}{J_q(k_{\rho p} c)} \tag{G.2}$$

leads to

$$E_z = -j\omega\mu_o \cdot \sum_{q=0}^{\infty} (a_q \cos q\phi + b_q \cos q\phi) \cdot \frac{J_q(k\,c) N_q(k\,\rho) - N_q(k\,c) J_q(k\,\rho)}{J_q(k\,c)}$$

$$- \frac{\pi\sqrt{\varepsilon_r}}{2a} \sum_{q=0}^{\infty} \sum_{i=1}^{IC} k_o \rho_i \, E_{iq} (a_q \cos q\phi + b_q \sin q\phi)$$

$$\cdot \frac{J_q(k\,c)\,[N_q(k\rho_i)]_-^+ - N_q(k\,c)\,[J_q(k\rho_i)]_-^+}{J_q(k\,c)} \, J_q(k\,\rho) \tag{G.3}$$

$$H_\phi = -k \sum_{q=0}^{\infty} (a_q \cos q\phi + b_q \sin q\phi) \, \frac{J_q(k\,c) N_q'(k\,\rho) - N_q(k\,c)\, J_q'(k\,\rho)}{J_q(k\,c)}$$

$$- \frac{j\pi\,\omega\sqrt{\varepsilon_r}}{2a} \sum_{q=0}^{\infty} \sum_{i=1}^{IC} k_o \rho_i \, E_{iq} (a_q \cos q\phi + b_q \sin q\phi)$$

$$\frac{J_q(k\,c)\,[N_q(k\rho_i)]_-^+ - N_q(k\,c)\,[J_q(k\rho_i)]_-^+}{J_q(k\,c)} \, J_q'(k\rho) \tag{G.4}$$

where E_z and H_ϕ denote to TM_{oq} modes only. An application of (G.1) then results in

$$P_{Total} = -2\pi \sum_{q=0}^{\infty} \sum_{i=1}^{IC} \frac{(a_q^2 + b_q^2)}{q} \rho_i \mathrm{Re}(E_{iq}) \frac{J_q(kc)\,[N_q(k\rho_i)]_-^+ - N_q(kc)\,[J_q(k\rho_i)]_-^+}{J_q(kc)} \tag{G.5}$$

REFERENCES

1. KAMPINSKY, A,, et al., "ATS-F Spacecraft: An EMC challenge", 16th. Electromagnetic Compatibility Symposium, San Francisco, CA., July, 1974.

2. JAKSTYS, V.J., et al., "Composite ATS-F4G Satellite Antenna Feed", 7th. IEE Ann. Conf. Communications, Montreal, Canada, June 1971.

3. BANGERT, J.T., et al., "The Spacecraft Antennas", Bell. Syst. Tech. J., July 1963.

4. ASSALY, R.N., et al., "Switched Beam Antenna Systems for LES-1 and LES-2", Tech. Rep. 409, Lincoln Laboratory, M.I.T., Dec. 16, 1965.

5. RANKIN, J.B., et al., "Multifunction Single Package Antenna System for Spin-Stabilized Near-Synchronous Satellite", IEEE Trans. Antennas and Propagation, Vol. AP-17, July 1969, pp. 435-442.

6. ROSENTHAL, M.L., et al., "VHF Antenna Systems for a Spin-Stabilized Satellite", IEEE Trans. Antennas and Propagation, Vol. AP-17, July 1969, pp. 443-451.

7. CROSWELL, W.F., et al, "An Omnidirectional Microwave Antenna for use on Spacecraft", IEEE Trans. Antennas and Propagation, Vol. AP-17, July 1969, pp. 459-466.

8. DONNELLY, E.E., et al., "The Design of a Mechanically Despun Antenna for Intelsat - III Communications Satellite", IEEE Trans. Antennas and Propagation, Vol. AP-17, July 1969, pp. 407-414.

9. BLAISDELL, L., "ATS Mechanically Despun Communications Satellite Antenna", IEEE Trans. Antennas and Propagation, Vol. AP-17, July 1969, pp. 415-427.

10. AZARBAR, B., "Coupling of Electromagnetic Fields Between Two Regions by Annular Slots on the Common Boundary", Ph.D. Candidacy Paper, Electrical Engineering Department, The University of Manitoba, Winnipeg, Manitoba, R3T 2N2, November, 1977.

11. BUTLER, C.M., "Electromagnetic Penetration Through Apertures in Conducting Surfaces", IEEE Trans. Antennas and Propagation, Vol. AP-26, January 1978, pp. 82-93.

12. STRATTON, J.A., "Electromagnetic Theory", McGraw-Hill Book Company, 1941, Chapter 8.

13. STRATTON, J.A., CHU, L.J., "Diffraction Theory of Electromagnetic Waves", The Physical Review, Vol. 56, 1939, pp. 99-

14. LORD RALEIGH , "On the Incidence of Aerial and Electric Waves on Small Obstacles in the Form of Ellipsoids or Elliptic Cylinders, on the Passage of Electric Waves Through a Circular Aperture in a Conducting Screen", The Philosophical Magazine, Vol. 44, 1897, pp. 28-52.

15. BATEMAN, H., "The Mathematical Analysis of Electrical and Optical Wave Motion", Cambridge, 1915, pp. 90-

16. BETHE, H.A., "Theory of Diffraction by Small Holes", The Physical Review, Vol. 66, Oct. 1944, pp. 163-182.

17. BOUWKAMP, C.J., "Theoretical and Numerical Treatment of Diffraction Through a Circular Aperture", IEEE Trans. Antennas and Propagation, Vol. AP-18, March 1970, pp. 152-176.

18. MEIXNER, J., "The Behavior of Electromagnetic Fields at Edges", Inst. Math. Sci. Res. EM-72, New York University, New York, N.Y., Dec. 1954.

19. LEVINE, H., SCHWINGER, J., "On the Theory of Electromagnetic Wave Diffraction by an Aperture in an Infinite Plane Conducting Screen", Communications on Pure and Applied Mathematics, Vol. 3, Dec. 1950, pp. 355-391.

20. LEVINE, H., PAPAS, C.H., "Theory of the Circular Diffraction Antenna", Journal of Applied Physics, Vol. 22, No. 1, Jan. 1951, pp. 29-43.

21. NOMURA, Y., KATSURA, S., "Diffraction of Electromagnetic Waves by Circular Plate and Circular Hole", Journal of Physical Society of Japan, Vol. 10, No. 4, April 1955, pp. 285-304.

22. NOMURA, Y., KATSURA, S., "Diffraction of Electromagnetic Wave by Ribbon and Slit", Journal of Phyiscal Society of Japan, Vol. 12, No. 2, Feb. 1957, pp. 190-200.

23. BUTLER, C.M., "Formulation of Integral Equations for an Electrically Small Aperture in a Conducting Screen", IEEE International Symposium on Antennas and Propagation, Atlanta, GA, June 1974.

24. RAHMAT-SAMII, Y., MITTRA, R., "Electromagnetic Coupling Through Small Apertures in a Conducting Screen", IEEE Trans. Antennas and Propagation, Vol. AP-25, March 1977, pp. 180-187.

25. KELLER, J.B., "Geometrical Theory of Diffraction", Journal of Applied Physics, Vol. 28, 1962, pp. 426-444.

26. KOUYOUMJIAN, R.K., PATHAK, P.H., "A Uniform Geometrical Theory of Diffraction for an Edge in a Perfectly Conducting Surface", Proc. IEEE, Vol. 62, 1974, pp. 1448-1461.

27. RAHMAT-SAMII, Y., MITTRA, R., "A Spectral Domain Interpretation of High Frequency Diffraction Phenomena", IEEE Trans. Antenna and Propagation, Vol. AP-25, September 1977, pp. 676-687.

28. WAIT, J.R., "A Low Frequency Annular-Slot Antenna", Journal of Research of the National Bureau of Standards, Vol. 60, No. 1, Jan. 1958, pp. 59-64.

29. GALEJS, J., THOMPSON, W.T., "Admittance of a Cavity-Backed Annular Slot Antenna", IRE Trans. Antennas and Propagation, Vol. AP-10, Nov. 1962, pp. 671-678.

30. HARRISON, C.W., Jr., CHANG, C.W., "Theory of Annular-Slot Antenna Based on Duality", IEEE Trans. Electromagnetic Compatibility, Vol. EMC-13, No. 1, Feb. 1971, pp. 8-14.

31. TSAI, L.L., "A Numerical Solution for the Near and Far Fields of an Annular Ring of Magnetic Current", IEEE Trans. Antennas and Propagation, Vol. AP-20, Sept. 1972, pp. 569-576.

32. CHANG, D.C., "Input Admittance and Complete Near-Field Distribution of an Annular Aperture Antenna Driven by a Coaxial Line", IEEE Trans. Antennas and Propagation, Vol. AP-18, Sept. 1970, pp. 610-616.

33. IRZINSKI, E.P., "The Admittance of a TEM excited Annular-Slot Antenna", IEEE Trans. Antennas and Propagation, Vol. AP-23, Nov. 1975, pp. 829-834.

34. KELLY, K.C., GOEBELS, F.J., Jr., "Annular Slot Monopulse Antenna Arrays", IEEE Trans. Antennas and Propagation, Vol. AP-12, July 1964, pp. 391-403.

35. BUGNOLO, D.S., "A Quasi'Isotropic' Antenna in the Microwave Spectrum", IRE Trans. Antennas and Propagation, Vol. AP-10, July 1962, pp. 377-383.

36. CROSWELL, W.F., COCKRELL, C.R., "An Omnidirectional Microwave Antenna for use on Spacecraft", IEEE Trans. Antennas and Propagation, Vol. AP-17, July 1969, pp. 459-466.

37. HOLST, D.W., "Radiation Patterns of Radial Waveguides with TM Mode Excitation", IEEE Trans. Antennas and Propagation, Vol. AP-21, March 1973, pp. 238-241.

38. TROUGHTON, P., "High Q Factor Resonators in Microstrip", Electronics Letters, Vol. 4, No. 24, Nov. 1968, pp. 520-522.

39. TROUGHTON, P., "Measurement Techniques in Microstrip", Electronics Letters, Vol. 5, No. 2, Jan. 1969, pp. 25-56.

40. WATKINS, J., "Circular Resonant Structures in Microstrip", Electronics Letters, Vol. 5, No. 21, Oct. 1969, pp. 524-525.

41. COCKRELL, C.R., PATHAK, P.H., "Diffraction Theory Techniques Applied to Aperture Antennas on Finite Circular and Square Ground Planes", IEEE Trans. Antennas and Propagation, Vol. AP-22, May 1974, pp. 443-448.

42. KIEBURTZ, R.B., ISHIMARU, A., "Scattering by a Periodically Apertured Conducting Screen", IRE Trans. Antennas and Propagation, Vol. AP-9, pp. 506-514, Nov. 1961.

43. OTT, R.H., KOUYOUMJIAN, R.G., PETERS, L., "Scattering by a Two-Dimensional Periodic Array of Narrow Plates", Radio Science, Vol. 2, pp. 1347-1349, Nov. 1967.

44. CHEN, C.C., "Transmission Through a Conducting Screen Perforated Periodically With Apertures", IEEE Trans. Microwave Theory Tech., Vol. MTT18, No. 9, pp. 627-632, Sept. 1970.

45. MATTHAEI, G.L., YOUNG, L., JONES, E.M.T., "Microwave Filters, Impedance-Matching Networks, and Coupling Structures", McGraw-Hill Book Company, 1964, Chapter 9.

46. WAIT, J.R., HILL, D.A., "On the Electromagnetic Fields of a Dielectric Coated Coaxial Cable", IEEE Trans. Antennas and Propagation", Vol. AP-23, pp. 470-479, July 1975.

47. WAIT, J.R., HILL, D.A., "Electromagnetic Fields of a Dielectric Coated Coaxial Cable with Interrupted Shield-Quasi-Static Approach", IEEE Trans. Antennas and Propagation, Vol. AP-23, pp. 679-682, Sept.

48. COLLIN, R.E., "Field Theory of Guided Waves", McGraw-Hill Book Company, 1960, Chapter 5, 7.

49. HARRINGTON, R.F., "Time-Harmonic Electromagnetic Fields", McGraw-Hill Book Company, Chapter 3-5, 1961.

50. GRADSHTEYN, I.S., RYZHIK, I.M., "Table of Integrals, Series and Products", Academic Press, 1973.

51. SHAFAI, L., "Currents induced on a conducting strip", Canadian Journal of Physics, Vol. 49, No. 4, pp. 495-498, 1971.

52. JASIK, H.J., "Antenna Engineering Handbook", McGraw-Hill Book Company, 1961, 12.12, 27.6.

53. PISTOLKORS, A.A., "Theory of the Circular Diffraction Antenna", Proc. IRE, Vol. 36, January 1948, pp. 56-60.

54. HARRISON, C.W., Jr., CHANG, D.C., "Theory of the Annular Slot Antenna Based on Duality", IEEE Trans. Electromagnetic Compatibility, Vol. EMC-13, February 1971, pp. 8-14.

55. SNEDDON, I.N., "Fourier Transforms", McGraw-Hill Book Company, Chapter 2, 1951.

56. MITTRA, R., LEE, S.W., "Analytical Techniques in the Theory of Guided Waves", The MacMillan Book Company, Chapter 1, 1971.

57. TYRAS, G., "Radiation and Propagation of Electromagnetic Waves", Academic Press, 1969, Chapter 5, 8.

58. ABRAMOWITS, M., SEGUN, I.A., "Handbook of Mathematical Functions", Dover Publications, Inc., New York, 1968, Chapters 11, 12.

59. COLLIN, R.E., ZUCKER, F.J., "Antenna Theory Part 1", McGraw-Hill Book Comapny, 1969, Chapters 2, 3.

60. AZARBAR, B., SHAFAI, L., "Filter Characteristics of Radial Waveguides Coupled by Annular Slots", 1978 IEEE-MTT-S International Microwave Symposium, Ottawa, Canada, June 1978.

61. POTTER, P.D., "A New Horn Antenna with Suppressed Sidelobes and Equal Beamwidths", The Microwave Journal, June 1963, pp. 71-78.

62. LUDWIG, A., "The Definition of Cross Polarization", IEEE Trans. Antennas and Propagation, Vol. AP-21, Jan. 1973, pp. 116-119.

63. KREUTEL, R.W., et al., "Antenna Technology for Frequency Reuse Satellite Communications", IEEE Proc., Vol. 65, No. 3, March 1977, pp. 370-378.

64. GHOBRIAL, S.I., "Cross Polarization in Satellite and Earth-Station Antennas", IEEE Proc., Vol. 65, No. 3, March 1977, pp. 378-386.

65. AZARBAR, B., "Scattering by Cylindrical Reflectors and the Effects of Dielectric Loading", M.Sc. Thesis, Elec. Eng. Dept., The University of Manitoba, Winnipeg, Manitoba, Canada, R3T 2N2, May 1975.

66. AZARBAR, B., SHAFAI, L., "Application of Moment Method to Large Reflector Antennas", 1975 IEEE-AP-S International Antennas and Propagation Symposium, Urbana, IL., U.S.A.

67. AZARBAR, B., SHAFAI, L., "Application of Moment Method to Large Cylindrical Reflector Antennas", IEEE Trans. Antennas and Propagation, Vol. AP-26, May 1978, pp. 500-502.

68. KRAUS, J.D., "Antennas", McGraw-Hill Book Company, 1950, p. 25.

69. TAI, C.T., PEREIRA, C.S., "An Approximate Formula for Calculating the Directivity of an Antenna", IEEE Trans. Antennas and Propagation, Vol. AP-24, March 1976, pp. 235-236.

70. KING, R.W.P., "The Theory of Linear Antennas", Harvard University Press, Cambridge, Mass., 1956, Sec. II.38.